HAL
open science

Étude de l'érosion des berges et du transport de sédiments d'une micro-rivière à chenal droit

Lawrence Armstrong

▶ To cite this version:

Lawrence Armstrong. Étude de l'érosion des berges et du transport de sédiments d'une micro-rivière à chenal droit. Géomorphologie. Université Paris-Diderot - Paris VII, 2003. Français. NNT : . tel-00130323

HAL Id: tel-00130323
https://theses.hal.science/tel-00130323

Submitted on 11 Feb 2007

HAL is a multi-disciplinary open access archive for the deposit and dissemination of scientific research documents, whether they are published or not. The documents may come from teaching and research institutions in France or abroad, or from public or private research centers.

L'archive ouverte pluridisciplinaire **HAL**, est destinée au dépôt et à la diffusion de documents scientifiques de niveau recherche, publiés ou non, émanant des établissements d'enseignement et de recherche français ou étrangers, des laboratoires publics ou privés.

THÈSE de DOCTORAT
de l'UNIVERSITÉ PARIS 7 – DENIS DIDEROT

Spécialité: GÉOPHYSIQUE INTERNE

présentée par

Lawrence ARMSTRONG

pour obtenir le titre de
DOCTEUR DE L'UNIVERSITÉ PARIS 7 – DENIS DIDEROT

Sujet de la thèse :

Étude de l'érosion des berges et du transport de sédiments d'une micro-rivière à chenal droit (Bank erosion and sediment transport in a microscale straight river)

Soutenue le 10 septembre 2003, devant le jury composé de

Monsieur François MÉTIVIER (IPGP) ..... Co-Directeur de Thèse
Monsieur Claude JAUPART (IPGP) ..... Co-Directeur de Thèse
Monsieur Jean-Philippe AVOUAC (Caltech, USA) ..... Rapporteur
Monsieur Gary PARKER (University of Minnesota, USA) ..... Rapporteur
Monsieur Didier RICHARD (CEMAGREF) ..... Examinateur

Laboratoire de Dynamique des Systèmes Géologiques
Institut de Physique du Globe de Paris
4, place Jussieu - 75252 Paris cedex 05

Remerciements

Ce travail n'aurait pas pu voir le jour sans l'aide de nombreuses personnes qui m'ont aidé et soutenu tout au long de cette thèse. Grâce à elles, j'ai beaucoup appris sur les plans scientifique et personnel. Je tiens ici à les remercier.

Tout d'abord, un grand merci à François Métivier qui m'a initié à la géomorphologie et m'a ainsi fait découvrir que la surface de la Terre était un système très dynamique notamment au travers des rivières. François m'a offert un sujet passionnant et je le remercie pour la confiance et la grande liberté qu'il m'a accordées notamment en me permettant de participer activement à la création du laboratoire expérimental de Géomorphologie. Pendant toute la durée de la thèse, François, en me donnant tous les moyens nécessaires à la réussite de ce travail, a su encadrer mon travail et notamment éviter que je me perde trop dans les méandres de mes reflexions (je le rappelle, ce travail concernait uniquement les rivières à chenal droit !).

Je remercie également Claude Jaupart qui a suivi mon travail de plus loin mais avec qui j'ai eu de nombreuses discussions fortes intéressantes sur des sujets très variés allant de la philosophie de la recherche au jazz (c'est pour l'instant la seule personne que j'ai rencontré qui connaisse Danny Gatton !) : je retiendrais sa vision claire et juste de nombreux aspects de la vie. Je remercie également Claude en tant que directeur de l'IPGP, pour toutes les aides financières qu'il a su me trouver.

Je tiens à remercier tous les membres du jury : Jean-Philippe Avouac, Gary Parker et Didier Richard qui m'ont fait l'honneur de bien vouloir examiner mon travail. Leur travail rigoureux a permis d'apporter des améliorations significatives à ce travail.

Je remercie également Gérard Bienfait qui m'a accueilli dans son magnifique et grand bureau à Saint Maur. J'ai été très touché par sa gentilesse.

J'associe tout l'atelier de Saint Maur : Yves Gamblin (merci pour les pommes !), Antonio Viera et Karim Mahiouz à la réussite du montage de l'expérience. Leur aide a été précieuse pour rendre la manip efficace et je les en remercie.

Je remercie tout particulierement Patrick Meunier pour toutes les discussions que nous avons eu dans la cabane au fond du bois et pour son soutien lorsque j'étais sur la dernière ligne droite. Un grand merci aussi à Éric Lajeunesse qui occupe désormais la cabane où la première micro-rivière a coulé et dont les conseils sont toujours réfléchis et judicieux. Je remercie également Lydie Denis qui a participé à la deuxième session de manips.

Ce travail s'est effectué en partie à Jussieu et à Saint Maur. Je tiens donc à remercier les parisiens et les saint-mauriens qui m'ont soutenu tout au long de cette thèse et avec qui j'ai passé de très bons moments. Les parisiens : Tout particulièrement Stéphanie N'D., Catherine C., Sylvie V. et Geneviève B. ainsi que Anne D., Cinzia F., Neil R., Steve T., Damien J., Chloé M., Henri S., Jules B., Claire P., Virginie P. et Michael L.. Les saint-mauriens : Michel C., Maxime L., Hugues C., Giovanni O., Laurent B. et Olivier D..

Un merci aux zozos ipgpiens : Manu M., Nordin F., Cricra C., Julie C., Xavier Q., Laurence A., Olivier H., Edouard K., Anne S., David A., Claire M., Stephane L., Cécile L. Un merci à mes amis de longue date : Yannick C., Gilles D., Benjamin M., Céline L., Omar O. et à tous les autres...

Enfin, je remercie toute ma famille qui m'a supporté et encouragé tout au long de cette thèse. Je pense tout particulièrement à ma grand-mère. Je leur dédie cette thèse.

L. A.

Résumé

Ce travail porte sur l'étude de l'interaction entre la tectonique et la morphologie d'une rivière. Nous nous sommes intéressés à la réponse d'une rivière à un décalage horizontal de son chenal afin d'essayer d'apporter des contraintes aux tectoniciens qui utilisent les décalages des terrasses de rivières pour dater et estimer d'anciens rejets de failles. L'approche de ce problème est faite au moyen d'un modèle réduit de rivière d'échelle métrique (micro-rivière). Nous montrons essentiellement (1) que les micro-rivières sont un bon moyen pour étudier la dynamique des rivières, (2) que la rivière, dans son évolution à chenal droit, montre un découplage entre l'évolution en temps de sa morphologie et de son transport de sédiments et (3) que la réponse du chenal au décalage se caractérise par la propagation d'un front d'érosion sur le bord exposé à l'écoulement de type onde cinématique, permettant ainsi au chenal de retrouver une morphologie d'équilibre.

Abstract

This work dealed with the study of the interactions between tectonics and river morphology. We got interested into the river response to a lateral offset of its channel in order to bring some constraints to the tectonicians that uses terraces offsets to estimate lateral slip rate. This problem was addressed with the use of a laboratory river model of metric size (microscale river). It is shown essentially that (1) experimental microscale channels can be used to study river dynamics, (2) the microscale river, while evolving with a straight channel, denotes a decoupling between the time evolution of its morphology and its sediment transport and (3) the channel response to a lateral offset is characterised by a propagation of an erosion front on the bank exposed to flow that can be described by a kinematic wave, allowing for the channel to return to a stable straight configuration.

Table des matières

Introduction **13**

1 État de l'art et problématique **16**

1.1 Introduction 16

1.2 Description physique de l'écoulement et du transport 17

1.2.1 Écoulement dans les rivières 20

1.2.2 Érosion et transport de sédiments 22

1.3 Concept d'équilibre des rivières alluviales 25

1.3.1 Variables indépendantes ou dépendante et échelles de temps 25

1.3.2 Rivières à pente graduellement décroissante 26

1.3.3 Géométrie hydraulique 28

1.4 Approche expérimentale et mise à l'échelle 30

1.5 Conclusion 34

Bibliographie 35

2 Protocole expérimental **41**

2.1 Introduction 41

2.2 Une micro-rivière expérimentale 42

2.2.1 Cuve à lit mobile 42

2.2.2 Billes de verre comme materiel alluvial 45

2.2.3 Alimentation en eau 48

2.2.4 Modularité de l'expérience 50

2.2.5 Préparation et déroulement des expériences 51
2.3 Mesures des variables de l'expérience 52
2.3.1 Acquisition de la géométrie des bords 53
2.3.2 Mesure continue du flux de masse de sédiments 57
2.3.3 La pente comme paramètre 61
2.4 Conclusion 61

3 Equilibrium Width and Scaling of the Microscale Rivers 63
3.1 Introduction 63
3.2 Equilibrium width and scaling of the microscale river 64

4 Time Evolution of a Straight River Channel 95
4.1 Time evolution of a straight river channel 95
4.2 Discussion on the sediment budgets from the banks and the bed 118
4.3 Conclusion 120

5 Channel Offset of a Stable Straight River 127
5.1 Introduction 127
5.2 Experimental setup and observations 130
5.2.1 Apparatus and procedure 130
5.2.2 Evolution of the experiment during a run 132
5.3 Results 138
5.3.1 Local angle of the bank and bank velocities 138
5.3.2 Derivation of the kinematic equation and implication on the bedload transport 144
5.4 Offsets of natural rivers in Turkey 147
5.4.1 Tectonic setting and measurments 147
5.4.2 River response 149
5.5 Conclusion 150

6 Conclusion and perspectives **157**

A The Sediment Digester **159**

A.0.1 Hydraulics 159

A.0.2 Bedload transport 162

A.0.3 Sediment continuity 163

A.0.4 Width variation equation 167

B Variables and physical parameters **173**

Bibliographie **177**

Introduction

Les rivières sont les écoulements chenalisés de l'eau à la surface des continents et résultent des processus d'interaction entre le fluide et son environnement. Si les rivières sont essentielles, du point de vue du géomorphologue, car participant à l'échelle continentale aux transferts de matière depuis les chaines de montagnes, zone principale de production de sédiments, vers l'océan, elles offrent aux hydrauliciens le problème complexe d'un écoulement modifiant lui-même ses frontières. Tout en étant sujet aux forcages climatique et tectonique, les rivières témoignent néanmoins d'un équilibre dynamique dans lequel (1) sur le long terme (typiquement sur plusieurs milliers d'années), le profil en long du chenal développe une forme concave permettant d'optimiser le transport de sédiments de sorte que la rivière n'est ni en érosion ni en déposition et (2) à l'échelle de l'année, la géométrie de la section de chenal est au premier ordre contrôlée par le débit liquide moyenné sur l'année.

La physique décrivant les interactions entre fluide et particules pour prédir les processus élémentaires d'érosion, de transport et déposition n'étant décrite actuellement que de façon semi-empirique, plusieurs approches ont été developpées pour la compréhension de la dynamique des rivières. Parmi elles, l'approche basée sur l'analyse dimensionnelle ou bien encore l'approche par les méthodes de minimisation d'un critère énergétique ont abordé le problème de l'équilibre de la section du chenal. Néanmoins, la validité de ces modèles physiques est difficile à vérifier dans le cas des rivières naturelles car leur évolution en temps est suffisament lente de sorte qu'elle suppose un suivi à long terme avec des mesures fastidueuses. Il existe par exemple très peu de mesures portant sur le transport de

sédiments et notamment son évolution en temps ou le long de la rivière. La modélisation analogique de rivières est donc apparue très vite comme un moyen d'étudier la dynamique des rivières en permettant de réduire les temps d'observations. Avec elles, apparait le problème de la mise aux dimensions notamment relié au fait que la mise aux dimensions de l'écoulement de l'eau est impossible sans relâcher l'un des deux nombres sans dimensions le caractérisant : la plupart des rivières expérimentales sont alors faites en respectant le nombre de Froude.

Un deuxième aspect dans l'étude de la dynamique des rivières est celui qui consiste à savoir comment elles répondent à une perturbation de leur écoulement. Par exemple, de nombreuses études à l'échelle du réseau hydrographique ont porté sur la réponse du profil en long de la rivière à la subsidence. À une échelle spatiale plus petite, il existe à notre connaissance peu de travaux portant sur la réponse d'une rivière à une faille modifiant son chenal. Ce sujet est pourtant fondamental du point de vue des tectoniciens qui ont besoin de contraintes pour leurs estimations de rejets de failles à partir de la mesure des décalages des terrasses.

Nous avons conduit ce travail avec deux objectifs en tête : (1) caractériser l'equilibre des rivières alluviales, aussi bien chenal que transport. L'utilisation d'une micro-rivière nous a permis de réduire considérablement le temps des manipulations. Ce travail permet aussi de valider une telle reduction d'echelle. (2) Dans un deuxieme temps nous avons caracterisé la réponse d'une rivière à un décalage horizontal de son chenal afin de voir comment la rivière réagit dans une telle configuration. Cette modélisation a pour objectif de nous apporter des contraintes sur la dynamique de l'érosion des berges et sur les hypothèses faites en tectonique.

Ce travail est organisé en 6 chapitres :

Nous présentons dans un premier temps les points nécessaires pour comprendre les méthodes employées et pour cerner la problématique de notre travail en géomorphologie fluviale. Cette présentation se limite au cas des rivières alluviales à chenal droit qui ont été l'objet de notre étude. Elle nous permet également de poser clairement les échelles de

temps et d'espace auxquelles se rapporte notre travail et de discuter de notre approche par la modélisation de micro-rivières concernant deux aspects : le régime d'équilibre des rivières alluviales à chenal droit et la réponse à un décalage horizontal d'une rivière à l'équilibre.

Le dispositif expérimental que nous avons développé est ensuite décrit. Nous discutons en particulier des mesures qui ont été effectuées lors du déroulement des expériences.

Les résultats de la modélisation expérimentale de rivière à chenal droit portant sur la morphologie du chenal et sur l'écoulement sont ensuite présentés. Une discussion sur la mise à échelle nous permet de valider notre approche. Une loi d'échelle pour l'écoulement est obtenue qui permet de s'affranchir des problèmes de tensions de surface.

Nous présentons alors les résultats portant sur le régime transitoire des expériences de micro-rivières. Un régime d'équilibre pour le flux de sédiment est mis en évidence. Son découplage avec l'évolution du chenal nous permet de discuter du transport de sédiments le long du chenal.

Les résultats concernant la modélisation expérimentale de décalage de rivières sont ensuite présentés. Un comportement de l'érosion des bords en onde cinématique est mis en évidence et une équation pour l'évolution du bord est obtenue.

Enfin, dans un dernier chapitre, nous synthétisons et discutons les résultats.

Chapitre 1

État de l'art et problématique

1.1 Introduction

Il existe fondamentalement deux types de rivières, les rivières alluviales (Fig. 1.1a) et les rivières à fond rocheux (Fig. 1.1b) qui se distinguent par la nature de leur lit. Contrairement aux rivières à fond rocheux dont l'écoulement est fortement contraint par des murs et un lit difficilement érodables, les rivières alluviales s'écoulent sur un lit composé de leur propres sédiments ce qui leur permet d'être très dynamiques car pouvant adapter très rapidement la morphologie de leur chenal suite à des modifications de leur écoulement. Ces rivières possèdent donc un chenal formé par l'écoulement et dont la forme est déterminée par les processus d'érosion et de transport de sédiments.

Une rivière alluviale peut prendre deux formes en plan : à méandres (Fig. 1.2b) et en tresses (Fig. 1.2b). Les rivières en tresses sont certainement les rivières les plus dynamiques car elles possèdent un réseau hydrographique instable de sorte qu'un équilibre de forme ou de morphologie à l'échelle du chenal n'est jamais atteint. Néanmoins, ces rivières peuvent, à l'échelle de leur réseau, atteindre un équilibre en terme de quantité de sédiments transportés (Meunier et Métivier, 2000; Métivier et Meunier, 2003). Nous nous sommes intéressés dans ce travail aux rivières à chenal droit qui sont une forme limite des rivières à méandres quand la sinuosité, égale au rapport de la longueur de la rivière sur

(a) (b)

FIG. 1.1 – *(a) Rivière sableuse (Yampa River, Colorado, USA). (b) Rivière à fond rocheux (Oregon, USA). Photos d'Alan Howard (http://erode.evsc.virginia.edu).*

la longueur dans la direction moyenne, tend vers 1.

Nous commençons par un bref rappel des concepts physiques utilisés couramment pour décrire les rivières. La dynamique des rivières alluviales et plus particulièrement l'existence d'un état d'équilibre est ensuite discutée. Nous présentons une revue des différents outils de la géomorphologie quantitative qui permet de justifier nos choix méthodologiques. À partir des points précédents, nous définissons précisément les questions scientifiques qui ont été à la base de ce travail.

1.2 Description physique de l'écoulement et du transport

La forme du chenal des rivières alluviales est la conséquence de l'interaction de l'écoulement avec une frontière déformable. Conceptuellement, cette interaction peut être séparée en trois processus généraux (Fig. 1.3). L'écoulement dans un chenal s'adapte à la topographie du chenal (courbure du chenal, irrégularités des berges, ondulation du lit,

(a) (b)

FIG. 1.2 – *(a) Rivière à méandres (Alaska, USA), photo de C. Northon (http://geoimages.berkeley.edu). (b) Rivière en tresse (Alaska, Denali National Park, USA), photo de A. Howard (http://erode.evsc.virginia.edu).*

dunes, nature des sédiments) et génère un cisaillement à la base du lit et des berges qui contrôle l'érosion et le transport de sédiments.

Afin de pouvoir comprendre, quantifier et prédire le comportement et la morphologie du chenal, les interactions dans la Fig. 1.3 doivent être examinées théoriquement. Les équations générales qui décrivent ce système sont les équations de la quantité de mouvement pour le fluide,

$$\rho \frac{d\mathbf{u}}{dt} = -\nabla p + \nabla \cdot \tau - \rho \mathbf{g}, \tag{1.1}$$

les équations de continuité pour le fluide et les sédiments,

$$\nabla \cdot \mathbf{u} = 0, \tag{1.2}$$

$$\nabla \cdot \mathbf{Q_s} = -(1-\phi)\frac{\partial z_b}{\partial t}, \tag{1.3}$$

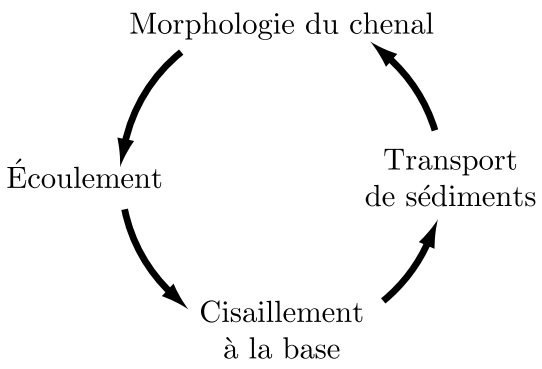

FIG. 1.3 – *Processus contrôlant la morphologie de la rivière. Ne sont pas indiqués les couplages existant entre le transport de sédiment, l'écoulement et le cisaillement à la base (d'après Dietrich et Gallinatti, 1991).*

une équation reliant les conditions d'écoulement au cisaillement à la base,

$$\tau_b = f\left(\frac{\partial \mathbf{u}}{\partial z}\right), \tag{1.4}$$

une équation enfin décrivant la dynamique du transport,

$$\mathbf{Q_s} = h\left(\tau_b, d, \ldots\right). \tag{1.5}$$

Ici, $\mathbf{u}$ est le champ de vitesse, ρ représente la densité du fluide, p est la pression, τ est le tenseur des contraintes, g est l'accélération de la gravité, $\mathbf{Q_s}$ est le transport de sédiment, ϕ est la porosité des sédiments, z_b est l'élevation du lit, τ_b est le cisaillement à la base et d est la taille des particules. La solution de ces équations est extrêmement compliquée voire impossible à obtenir dans le cas des rivières naturelles car (1) l'écoulement est turbulent et sa résolution par l'équation (1.1) n'est pas possible analytiquement, (2) car les équations (1.4) et (1.5), ne sont connues que de façon semi-empirique et doivent prendre en compte une grande diversité de paramètres dans les rivières naturelles comme notamment la cohésion des sédiments, l'influence de la végétation. Certaines simplifications sont néanmoins possibles et permettent d'avancer pour la compréhension de la dynamique des rivières. Une multitude de relations, le plus souvent empiriques, ont été proposées tant pour l'écoulement que pour les relations à l'interface Eqs. (1.4) et (1.5). Nous en

présentons les plus courantes ayant un fondement physique ainsi que les nombres sans dimensions caractéristiques que nous avons utilisés dans notre travail.

1.2.1 Écoulement dans les rivières

1.2.1.1 Nombres sans dimension

L'écoulement dans les rivières est fondamentalement turbulent. Le nombre de Reynolds qui caractérise l'effet inertiel par rapport à l'effet visqueux dans l'équation (1.1),

$$\mathrm{Re} = \frac{\rho u h}{\mu}, \tag{1.6}$$

où μ est la viscosité du fluide et h est la hauteur de l'écoulement, est en effet souvent largement supérieur à 10^5. Cette observation permet de négliger le terme visqueux dans l'équation de la quantité de mouvement, Eq. (1.1).

Un deuxième nombre important permettant de décrire l'état énergétique de l'écoulement est le nombre de Froude qui estime l'énergie cinétique de l'écoulement relativement à son énergie potentielle. Ce nombre obtenu à partir de l'équation de Bernouilli retranscrit le fait que l'énergie mécanique de l'écoulement, composée de l'énergie cinétique et de l'énergie potentielle, est conservée (voir par exemple Chow, 1959). Le nombre de Froude s'exprime selon

$$\mathrm{Fr} = \frac{u}{\sqrt{gh}}. \tag{1.7}$$

Ce nombre traduit la dualité de l'écoulement à surface libre et dans quel régime se trouve lécoulement : lorsque $\mathrm{Fr} < 1$, l'écoulement est dit fluvial ou sous-critique et lorsque $\mathrm{Fr} > 1$, l'écoulement est dit torrentiel ou sur-critique. À débit liquide et pente identiques pour les deux régimes, le régime fluvial est caractérisé par une vitesse d'écoulement faible et une grande hauteur d'eau alors que le régime torrentiel est caractérisé par une vitesse plus grande distribuée sur une plus faible hauteur d'eau.

1.2.1.2 Profil de vitesse et vitesse moyenne d'un écoulement uniforme

Le profil de vitesse mesuré selon la hauteur de l'écoulement turbulent peut s'ajuster par une courbe logarithmique mettant en évidence l'effet de la friction sur le fond du lit. Ce profil peut être obtenu théoriquement (voir par exemple Hinze, 1975) et s'écrit selon,

$$\frac{u}{u_*} = \frac{1}{\kappa} \ln z + C, \tag{1.8}$$

où z est la hauteur dans l'eau, C est une constante déterminée par la condition au limite, κ est la constante de Von Kármán ($\kappa \approx 0.4$) et u_* est la vitesse de cisaillement. Cette vitesse est la vitesse dans la couche limite à la base de l'écoulement et peut s'écrire dans le cas d'un écoulement uniforme selon

$$u_* = \sqrt{ghS}, \tag{1.9}$$

où S est la pente de l'écoulement. Le coefficient de friction de l'écoulement à sa base est défini comme le rapport de la vitesse moyennée sur la hauteur sur la vitesse de cisaillement :

$$c = \frac{\overline{u}}{u_*}. \tag{1.10}$$

Ce coefficient dépend de la rugosité, de la forme du lit et de nombreuses relations semi-empiriques ont été proposées. Parmi elles, retenons celle de Keulegan (Chang, 1988),

$$c = 2.5 \ln \left(11 \frac{h}{k_s} \right) \tag{1.11}$$

et celle de Manning-Strickler (Chang, 1988),

$$c = 8.1 \left(\frac{h}{k_s} \right)^{1/6} \tag{1.12}$$

où k_s est la rugosité dépendant de la taille des particules.

1.2.1.3 Vitesse moyenne d'un écoulement uniforme

Des formules pour la vitesse moyenne ont été établies pour les rivières ayant un profil de vitesse ne variant pas ou peu le long du chenal : lécoulement dans ce cas est dit

uniforme. La première est la formule de Chézy qui s'exprime selon (Chow, 1959)

$$\overline{u} = c\sqrt{ghS}, \tag{1.13}$$

où l'on retrouve l'expression du coefficient de friction Eq. (1.10).

À cette formule est souvent préférée celle de Manning car elle permet un meilleur réalisme. Elle généralise la formule de Chézy en prennant $c = h^{1/6}/n$ où n le coefficient de Manning qui dépend de la taille des particules et dont une expression est donnée avec Eq. (1.12) :

$$\overline{u} = \frac{h^{2/3}S^{1/2}}{n}. \tag{1.14}$$

1.2.2 Érosion et transport de sédiments

1.2.2.1 Mise en mouvement des particules

Sous l'effet de l'écoulement, les particules du lit sont soumises à un cisaillement. Shields (1936) a établi par une analyse dimensionnelle que le problème de la mise en mouvement sur un lit horizontal soumis à un écoulement turbulent pouvait s'exprimer par une relation entre le cisaillement de Shields

$$\tau_* = \frac{\tau_b}{g(\rho_s - \rho)d} \tag{1.15}$$

et le nombre de Reynolds de grain

$$\mathrm{Re}_* = \frac{\rho u_* d}{\mu} \tag{1.16}$$

où $\tau \approx \rho g h S$ est le cisaillement à la base et ρ_s est la densité des particules. Shields (1936) a empiriquement mis en évidence la relation entre le cisaillement critique τ_{*_c} et le nombre de Reynolds de grain Re_* à partir de mesures dans un canal (Fig. 1.4). La courbe a une forme distincte pour les surfaces hydrauliquement lisses, de transitions ou rugueuses avec une valeur minimal de $\tau_{*_c} \approx 0.03$ à $\mathrm{Re}_* \approx 10$ et une valeur constante de $\tau_{*_c} \approx 0.06$ au-dessus de $\mathrm{Re}_* \approx 400$. Bien que ne prennant pas en compte la pente, la pente latérale sur les berges ou la hauteur d'eau (Shvidchenko et Pender, 2000), la courbe de Shields reste largement utilisée pour estimer le cisaillement critique de mise en mouvement.

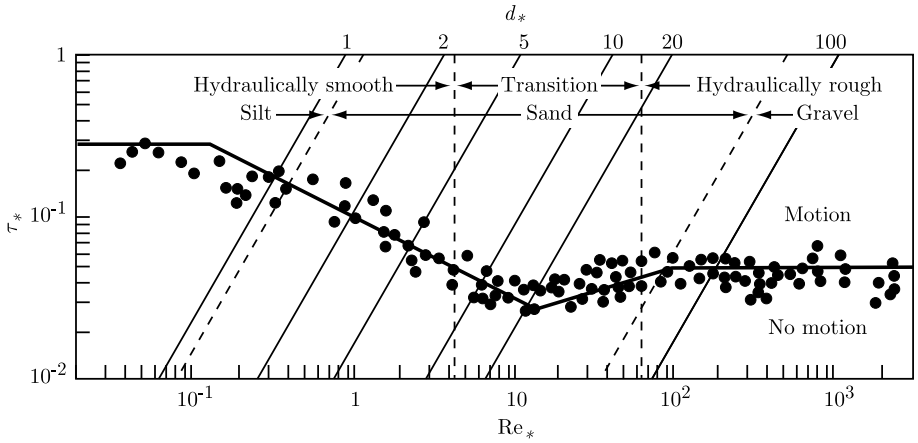

FIG. 1.4 – *Courbe de Shields (d'après Julien, 1994)*

1.2.2.2 Transport de fond

Le transport de sédiments sous forme solide peut se faire selon deux modes selon les conditions d'écoulement, de la taille et de la densité des particules : par saltation et reptation sur le fond du lit (*bedload*) ou par suspension. Le mode de transport est sélectionné essentiellement par la taille des particules, et les mesures des distributions des tailles des particules transportées dans la charge de fond et la charge en suspension dans des rivières naturelles montrent que la charge de fond transporte la plus grande partie des sédiments du lit (Fig. 1.5). De nombreuses lois de transport semi-empiriques existent pour relier le flux transporté aux cisaillement (Eq. (1.5)). Bagnold (Bagnold, 1973, 1977) a établi que le flux de sédiments par unité de largeur pouvait s'exprimer en terme de puissance de l'écoulement selon :

$$q_s = \frac{\beta u_b}{\gamma_s}(\tau_b - \tau_c), \tag{1.17}$$

où u_b est la vitesse dans la couche limite où l'initiation et le transport prennent place, τ_b et τ_c sont respectivement le cisaillement à la base et le cisaillement critique pour la mise en mouvement, $\gamma_s = (\rho_s - \rho)g/\rho$ est le poids spécifique et β est un facteur dépendant de la taille des particules. Le terme de droite n'est autre que la puissance dissipée par l'écoulement pour transporter un certain volume de particules v_s et se déplaçant à une vitesse u_s. Selon la relation de Bagnold, $u_s = \beta u_b \approx 0.5 u_b$ (Yalin et Ferreira da Silva, 2001)

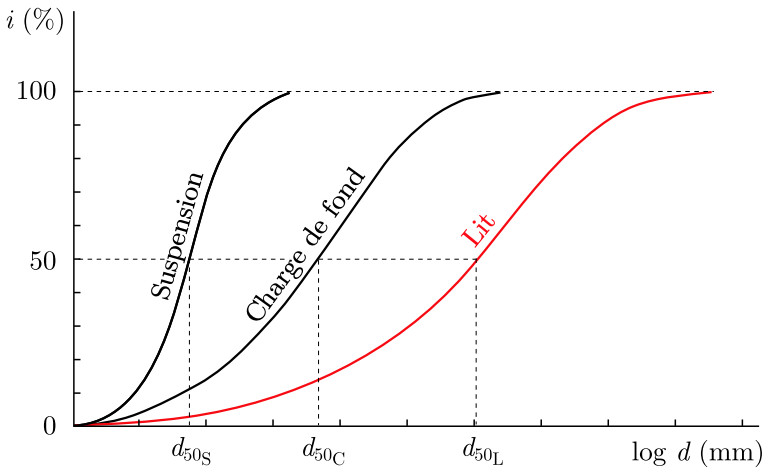

FIG. 1.5 – *Distribution schématique des différentes charges de sédiments transportée dans les rivières.*

et $v_s \sim (\tau_b - \tau_c)/\gamma_s$. Pour un écoulement uniforme, le flux de sédiment Q_s peut s'exprimer en fonction de la puissance totale de l'écoulement (Métivier et Meunier, 2003) :

$$Q_s \propto (\rho g Q S - \rho g Q S_c), \tag{1.18}$$

où $S_c = \tau_c/\rho g h$. La formule de Bagnold telle qu'elle est présentée ici, donne le transport moyen dans la direction principale de l'écoulement. Des formulations vectorielles ont été proposées et permettent de décrire le transport sur les berges (Kovacs et Parker, 1994). Toute une famille de relations de transport a ensuite été proposée en s'appuyant sur la relation de Bagnold mais elles ne sont plus basées sur des principes simples comme celui de la puissance de transport (Yalin, 1992).

Nous avons vu dans cette section les concepts les plus utilisés pour caractériser l'écoulement, les processus d'érosion et de transport contrôlant la morphologie du chenal. Par l'intermédiaire de ces mécanismes élementaires, la rivière modifie sa géométrie, et nous allons dans la section suivante aborder la question de l'existence d'un équilibre pour les rivières.

1.3 Concept d'équilibre des rivières alluviales

1.3.1 Variables indépendantes ou dépendante et échelles de temps

La capacité qu'ont les rivières alluviales de modifier dynamiquement leur chenal par les mécanismes précédemment décrits, soulève la question de l'existence d'un état d'équilibre pour de telles rivières. La notion d'équilibre au sens strict signifie que toutes les caractéristiques de la rivière n'évoluent plus dans le temps. Cependant, les rivières, en étant placées au sein d'un environnement continental, peuvent subir un forcage par exemple par le climat ou la tectonique de telle sorte qu'un tel équilibre n'est très certainement jamais atteint (Dade et Friend, 1998). Les géomorphologues et les hydrologues ont alors développé la notion d'équilibre dynamique signifiant qu'une rivière peut être considérée comme étant à l'équilibre en dessous d'une certaine échelle de temps. Au regard de la variabilité temporelle de toutes les variables susceptibles d'influencer la dynamique et donc l'équilibre des rivières, Schumm et Lichty (1965), entre autres, ont établi sur quelle échelle de temps, une variable devenait pour la rivière soit un paramètre de contrôle, soit un paramètre résultant de la dynamique (Tableau 1.1). Ils définissent ainsi qualitativement trois équilibres dynamiques respectivement pour les courtes échelles de temps typiquement de l'ordre de quelques jours, les grandes échelles de temps typiquement de l'ordre de plusieurs centaines d'années, et les très grandes échelles de temps typiquement sur plusieurs millions d'années. Ils ont ainsi suggéré par exemple que le flux de sédiment est à courte échelle de temps contrôlé par la vitesse de l'écoulement mais qu'il devient une variable de contrôle à plus grande échelle de temps (Tableau 1.1).

Si l'équilibre des rivières à très long terme peut être sujet à caution du fait de la difficulté d'observer des rivières ayant cet âge, l'on en connait déjà plus sur l'équilibre sur des échelles de temps plus courtes. Deux équilibres dynamiques ont été observé sur les rivières : (1) un équilibre dynamique à long terme dans lequel les rivières développent un profil en long à pente graduellement décroissante (*graded stream*) et (2) un équilibre à

TAB. 1.1 – *État des variables pour les rivières pendant des durées de temps décroissantes (modifié d'après Schumm et Lichty, 1965).*

	Status of variables[1]		
Variables	Steady (short term)	Graded (long term)	Geologic (very long term)
1. Geology (lithology, structure)	C	C	C
2. Paleoclimate	C	C	C
3. Paleohydrography	C	C	R
4. Valley slope, width and depth	C	C	R
5. Climate	C	C	—
6. Vegetation (type and density)	C	C	—
7. Mean water discharge	C	C	—
8. Mean sediment inflow	C	C	—
9. Channel morphology	C	R	—
10. Observed discharge and load	R	—	—
11. Hydraulics of the flow	R	—	—

[1] C : variable contrôlant la dynamique, R : variable résultant de la dynamique.

l'échelle de l'année montrant que la section de la rivière dépendant au premier ordre du débit moyen sur l'année (*regime channel*). Ces deux équilibres sont établis sur des échelles de temps différentes comme nous allons le voir.

1.3.2 Rivières à pente graduellement décroissante

Sur une échelle de temps suffisament grande, il a été observé que les rivières ont tendance à développer un profil en long de forme concave (Fig. 1.6). Devant cette constatation, Mackin (1948) en a fait l'interprétation que ces rivières devaient avoir atteint un état d'équilibre adapté au transport de sédiments de telle sorte que ni déposition, ni

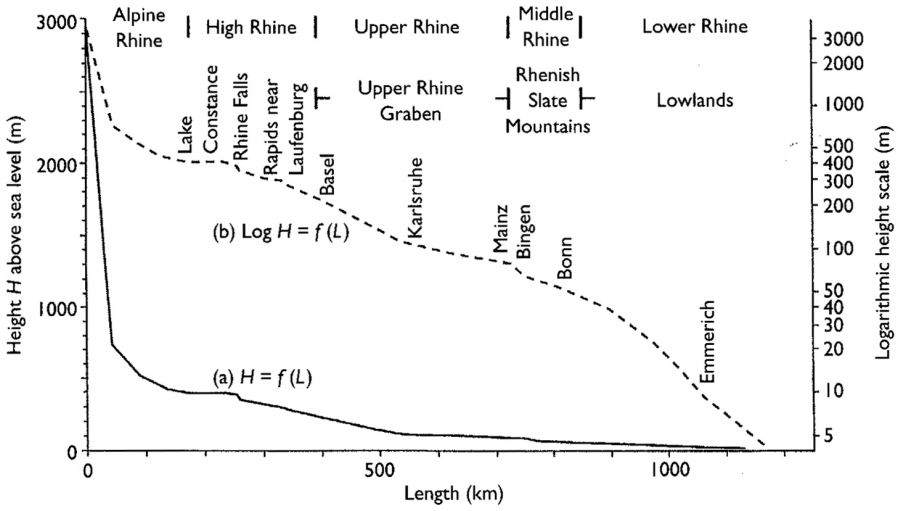

FIG. 1.6 – *Profil en long du Rhin (d'après Ahnert, 1998).*

érosion n'avaient lieu. Néanmoins, la notion de chenal à gradient décroissant de façon monotone (*graded stream*) est encore sujet à débat dans le sens où une rivière alluvial peut ne jamais atteindre exactement en tout point cet équilibre dynamique (Dade et Friend, 1998). La raison en est que les variables de contrôle sur cette échelle de temps, comme par exemple le climat, les processus tectoniques, peuvent exprimer une variabilité suffisament importante pour que la rivière n'ait pas le temps de développer ce profil d'équilibre (Tableau 1.1). En appliquant aux rivières le principe de Le Chatelier, selon lequel un système à l'équilibre subissant une perturbation réagit de telle sorte à la contrebalancer (Mackin, 1948), certains auteurs ont proposé que la formation de terrasses était un moyen pour la rivière de retourner dans un certain état d'équilibre (voir Merritts *et al.*, 1994, pour une revue). L'interprétation des terrasses alluviales afin de dater et mesurer des rejets de failles et d'en déduire des vitesses moyennes de mouvements est devenue une technique obligée de la néotectonique (*e. g.* Lasserre *et al.*, 1999; Lavé et Avouac, 2000; Avouac, 1993; Gaudemer *et al.*, 1995; Van der Woerd *et al.*, 1998).

1.3.3 Géométrie hydraulique

Sur des échelles de temps beaucoup plus courtes, typiquement à l'échelle de l'année et donc sur des durées permettant l'observation humaine, il a été observé que la morphologie du chenal montrait une certaine corrélation avec le débit liquide moyenné sur l'année. Leopold et Maddock (1953) ont mis en évidence l'existence de lois puissances reliant la géométrie de l'écoulement au débit liquide moyenné sur une année de la forme (Fig. 1.7),

$$A = aQ^b, \tag{1.19}$$

où A est la grandeur physique, *i. e.* la largeur, la hauteur et la pente, Q est le débit moyen sur une année, a et b sont des coefficients empiriques. De nombreuses mesures sur diverses rivières, ont par la suite montré que les valeurs du coefficient b montraient une remarquable constance. Ces relations de régime hydraulique signifient qu'à l'échelle d'une année, la géométrie s'équilibre avec le débit moyen sur l'année. Notons que certains auteurs utilisent la valeur du débit limite de crue (*bankfull*) et obtiennent le même type de corrélation (*e. g.* Andrews, 1984). Le débit limite de crue qui correspond à un écoulement remplissant entièrement le chenal à la limite du débordement, représente des évenements ponctuels et ne correspond pas exactement au débit moyen annuel (Fig. 1.8). Cette observation a permis de suggérer que la géométrie du chenal n'était modifiée de façon significative que durant les périodes de fort débit plutôt que de façon continue sur une année.

Deux approches ont permis d'aborder le problème de la géométrie hydraulique. La première, se basant sur l'idée de Langbein (1964) selon laquelle les relations de la géométrie hydraulique peuvent être prédites en minimisant la variance, est celle des méthodes rationnelles (*rationnal method*) dans lesqules la géométrie est résolue en minimisant un critère énergétique (Fig. 1.7).

L'autre approche détermine la géométrie en utilisant des hypothèse sur le cisaillement de fond. Ainsi Parker (1978a,b) suggère que la distribution et l'intensité du cisaillement sur une section de chenal permet, dans le cas des rivières sableuses, d'obtenir un équilibre entre l'érosion des bords et une déposition de sédiments en suspension de sorte que le chenal est à l'équilibre. Dans le cas des rivières à galets, où la suspension ne peut compenser

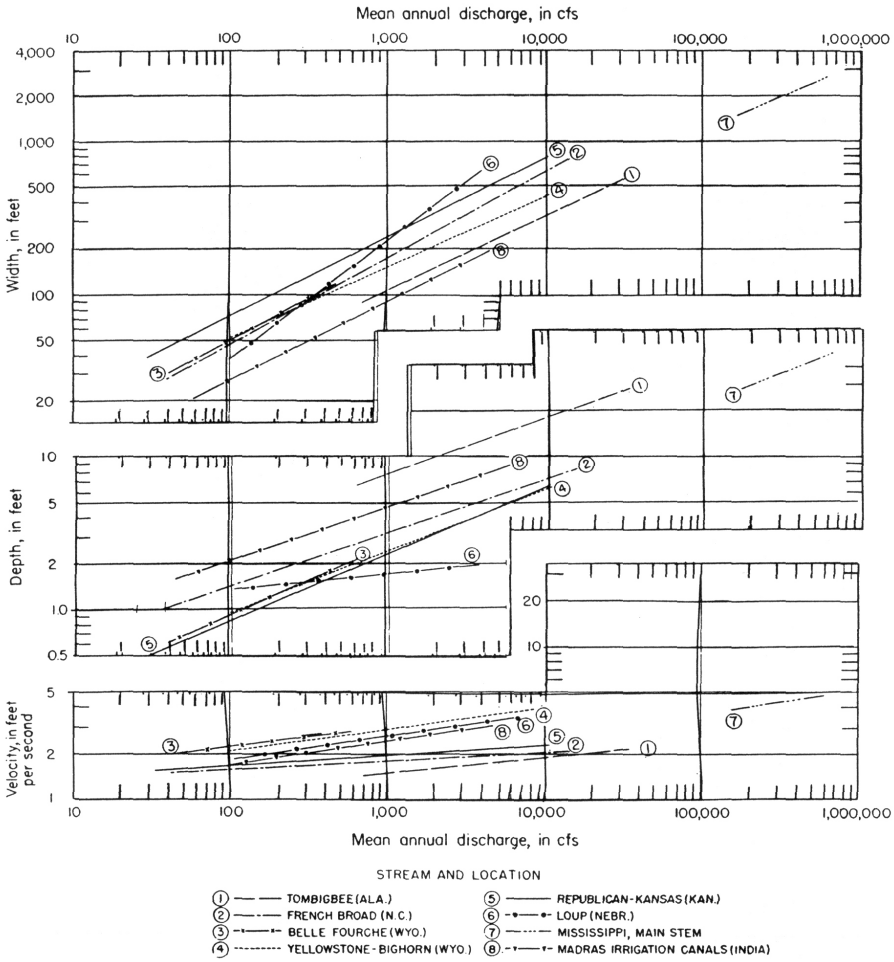

FIG. 1.7 – *Largeur, profondeur et vitesse de l'écoulement en fonction du débit liquide moyenné sur l'année et pour des débits croissants vers l'aval (d'après Leopold et Maddock, 1953).*

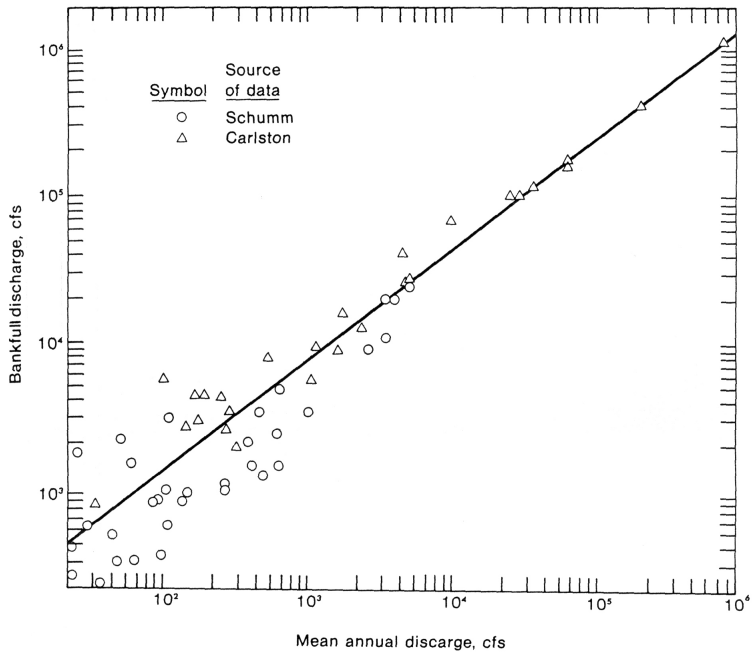

FIG. 1.8 – *Relation entre le débit maximum (bankfull) et le débit moyen annuel (d'après Chang, 1988).*

l'érosion, il postule que la géométrie d'une section à l'équilibre est telle qu'elle conduit à une redistribution du cisaillement qui peut être légerement supérieur au cisaillement critique dans la région du lit et décroitre lentement vers la région des bords jusqu'à être inférieur au cisaillement critique.

1.4 Approche expérimentale et mise à l'échelle

Il existe une relation entre la taille et les temps caractéristiques d'existence des objets géomophologiques dont il faut tenir compte dans la modélisation expérimentale. Les observations sur divers objets géomorphologiques montrent une relation croissante entre le temps T nécessaire pour modifier significativement un objet de taille L (Fig. 1.10 :

$$T = \Phi(L), \tag{1.20}$$

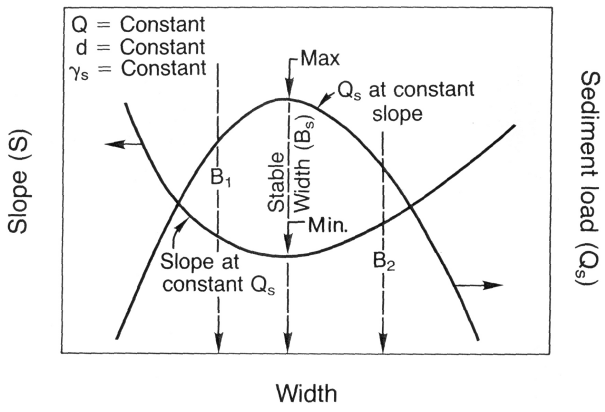

FIG. 1.9 – *Comparaison entre le critère de minimisation de la puissance hydraulique et celui de maximisation de l'efficacité de transport de sédiments permettant la determination de la largeur d'équilibre (d'après Chang, 1988).*

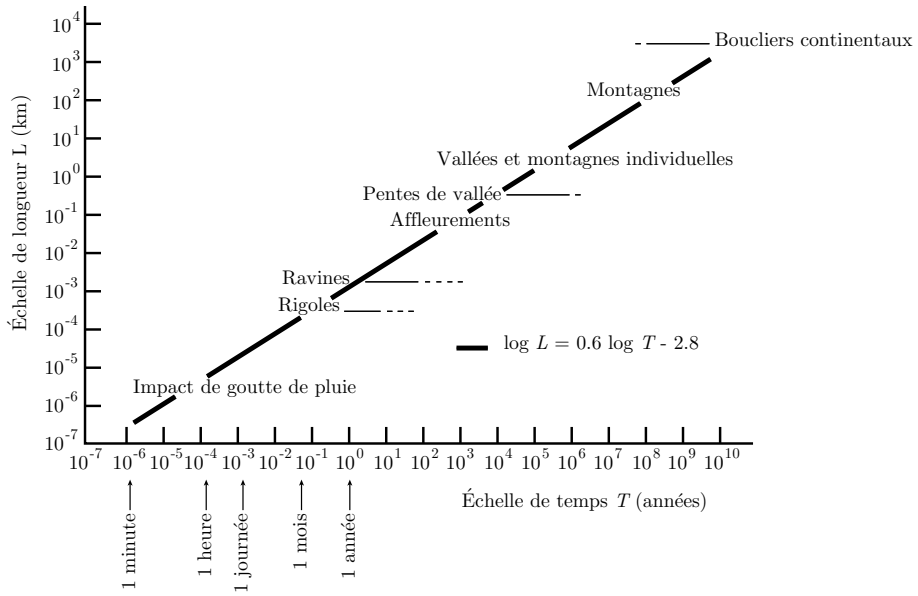

FIG. 1.10 – *Relation entre taille et durée d'existence pour différents objets géomorphologiques (d'après Ahnert, 1998).*

où Φ est une fonction croissante. Les processus unitaires d'érosion et de transport de sédiments sont à l'origine de la disparition des objets géomorphologiques. Le fait que ces mécanismes unitaires se fassent sur des échelles significativement inférieures à la taille des objets explique cette relation. Ahnert (1998) propose une relation logarithmique pour décrire quantitativement cette dépendance entre le temps de réponse et la taille. Cette relation peut se réécrire alors sous la forme :

$$T \propto L^{1/0.6} \approx L^2, \tag{1.21}$$

signifiant que le temps de réponse des objets géomophologiques augmente avec leur surface. Ce résultat très important de corrélation positive entre temps caractéristique et taille est utilisé implicitement dans les modélisations analogiques pour réduire les temps d'évolution mais sans changer l'allure générale de la réponse du système (Fig. 1.11). Mais si les modélisations expérimentales sont de tailles réduites par rapport aux cas naturels, elles sont pourtant couramment de grandes dimensions en géomorphologie expérimentale. Par exemple, l'expérience d'érosion par la pluie pour l'étude du dévelopement des réseaux de drainage à l'université du Colorado fait plus d'une centaine de mètres carrés (Fig. 1.12).

Les simulations de rivières n'échappent pas à la règle et font souvent plusieurs dizaines de metres jusqu'à la centaine de mètres de long chez certains laboratoires américains ou anglais (*e. g.*, Ackers (1964); Ikeda (1981); Diplas (1990); Macky (1999)). La raison invoquée pour cette mise à l'echelle toute relative est la nécessité d'avoir une simulation qui possède toutes les caractéristiques d'une rivière naturelle notamment celle du nombre de Froude qui est exactement mis à l'échelle. Ces expériences sont également faites dans des conditions d'équilibre global en terme de masse grâce à la recirculation à l'entrée de la rivière des sédiments transportés.

Cette mise à l'échelle présente toutefois deux inconvénients majeurs, du fait de Eq. (1.21), qui peuvent nuire à la compréhension du problème étudié. Tout d'abord, il s'en suit pour des raisons évidentes de logistiques qu'un faible nombre d'expériences peut être réalisé. La durée moyenne d'expériences de rivières est typiquement de plusieurs jours. L'acquisition de données est plus difficile sur des chenaux de grandes tailles et l'on peut

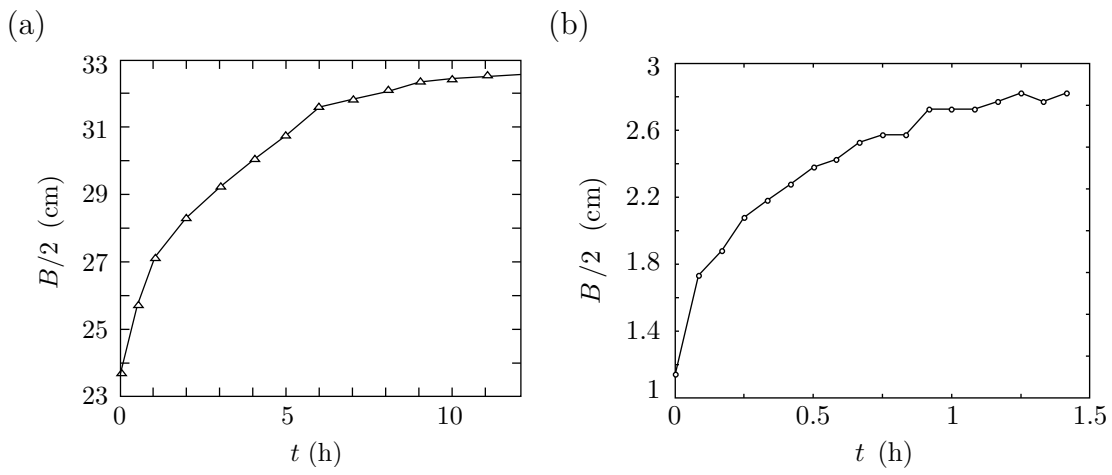

FIG. 1.11 – *Temps de réponse en fonction de la taille de l'expérience : évolution de la demi-largeur d'un chenal droit de longueur (a) $L = 15$ m (Ikeda, 1981), et (b) $L = 1.30$ m (ce travail).*

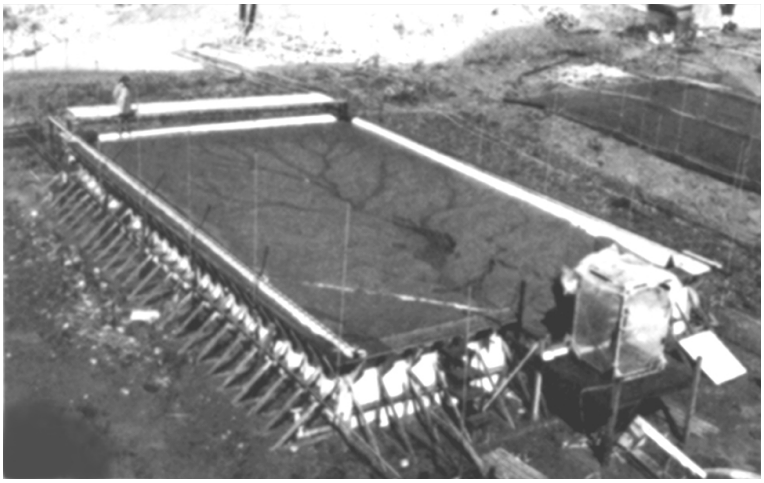

FIG. 1.12 – *Expérience d'érosion par la pluie à l'Université du Colorado. La cuve fait 9.1 m de large, 15.2 m de long et 1.8 m de profondeur (d'après Schumm et al., 1987).*

discutter de leur représentativité en espace et en temps (mesures ponctuelles de sédiments dans le temps, géométrie du bord plus difficile a mesurer le long de la rivière, ...). Ces deux raisons nous ont conduit à reconsidérer la modélisation expérimentale des rivières. L'approche adoptée fût de réduire fortement la taille du modèle expérimental afin de simuler ce que l'on peut appeler une « micro-rivière » d'une dizaine de centimètres de large et d'une longueur de l'ordre du mètre. Ce travail sert, en plus de l'aspect scientifique, à valider ce type de modélisation. Ainsi la réduction de la taille de l'expérience permet (1) une expérience simple et rapide à mettre en œuvre (réalisation d'un grand nombre d'expériences), (2) la possibilité d'observer et d'effectuer différentes mesures sur l'ensemble de la rivière expérimentale et (3) d'avoir un contrôle précis des conditions expérimentales.

1.5 Conclusion

Nous avons voulu aborder deux aspects de la dynamique des rivières alluviales au moyen d'une micro-rivière permettant de réduire au maximum les durées des expériences et des mesures en continu de diverses caractéristiques de la rivière et notament de son flux de sédiments.

Dans un premier temps, l'objectif est de caractériser l'équilibre d'une rivière alluviale à chenal droit au niveau de sa morphologie mais aussi de son transport de sédiments. Les expériences de micro-rivières ont été réalisées sans un apport de sédiments en amont afin de ne pas introduire un forçage externe du transport. Dans ce cas, la rivière est alors macroscopiquement dans un régime d'érosion, ce qui n'empêche pas, sur une durée suffisamment longue, l'existence d'un état permanent à partir d'une certaine distance de l'alimentation de la rivière (Yalin et Ferreira da Silva, 2001). La caractérisation de la dynamique de la micro-rivière est possible à partir de la réalisation d'un grand nombre d'expériences sur toute une gamme de paramètres tels que la pente, le débit liquide, la taille des grains. Ce travail permet également de valider une approche par la modélisation analogique de micro-rivières et en particulier nous nous sommes attachés à estimer les effets de tension de surface susceptibles d'apparaître dans de tels écoulements.

Nous nous sommes dans un deuxième temps, intéressés à l'étude de la réponse d'une rivière à une perturbation de son chenal par un décalage horizontal afin d'apporter des contraintes sur la dynamique de l'érosion des berges mais également sur les hypothèses faîtes en tectonique lors de l'estimation de rejets de failles. La réponse de rivières naturelles ayant subi un décalage du chenal lors du séisme de Turquie (1999) nous permet d'apporter une contrainte sur nos résultats expérimentaux.

Bibliographie

Ackers, P. (1964). Experiments on small streams in alluvium. *J. Hydrol. Div. 90*, 1–37.

Ahnert, F. (1998). *Introduction to Geomorphology.* Arnold, London.

Andrews, E. D. (1984). Bed-material entrainment and hydraulic geometry of gravel-bed rivers in Colorado. *Geol. Soc. Am. Bull. 95*, 371–378.

Avouac, J.-P. (1993). Analysis of scarp profiles: evaluation of errors in morphologic dating. *J. Geophys. Res. 98*, 6745–6754.

Bagnold, R. (1973). The nature of saltation and of bed load transport in water. *Proc. Roy. Soc. Ser. A 332*, 473–504.

Bagnold, R. A. (1977). Bed load transport by natural rivers. *Water. Resour. Res. 13*, 303–312.

Chang, H. H. (1988). *Fluvial processes in river engineering.* Kreiger Publishing Company.

Chow, V. T. (1959). *Open-channel hydraulics.* Mc Graw-Hill.

Dade, W. B. et P. F. Friend (1998). Grain-size, sediment-transport regime, and channel slope in alluvial rivers. *J. Geol. 106*, 661–675.

Dietrich, W. E. et J. D. Gallinatti (1991). Fluvial geomorphology. In O. Slaymaker (Ed.), *Fied experiments and measurement programs in geomorphology.* Balkema, Rotterdam.

Diplas, P. (1990). Characteristics of self-formed straight channels. *J. Hydr. Engrg. 116*, 707–728.

Gaudemer, Y., P. Tapponnier, B. Meyer, G. Pelzer, S. Guo, Z. Chen, H. Dai, et I. Cifuentes (1995). Partitioning of crustal slip between linked active faults in the eastern Qilian Shan, and evidence for a major seismic gap, the 'Tianzhu gap', on the wester Haiyuan fault, Gansu (China). *J. Int. 120*, 599–645.

Hinze, J. O. (1975). *Turbulence.* McGraw-Hill, New York.

Ikeda, S. (1981). Self-formed straight channels in sandy beds. *J. Hydrol. Div. 107*, 389–406.

Julien, P. Y. (1994). *Erosion and sedimentation.* Cambridge University Press.

Kovacs, A. et G. Parker (1994). A new vectorial bedload formulation and its application to the time evolution of straight river channels. *J. Fluid Mech. 267*, 153–183.

Langbein, W. B. (1964). Geometry of stable channels. *J. Hydr. Div. 90*, 301–312.

Lasserre, C., P.-H. Morel, Y. Gaudemer, P. Tapponnier, F. J. Ryerson, G. C. P. King, F. Métivier, M. Kasser, M. Kashgarian, L. Baichi, L. Taiya, et Y. Daoyang (1999). Postglacial left slip rate and past occurence of $M \geq 8$ earthquakes on the western Haiyuan fault, Gansu, China. *J. Geophys. Res. 104*, 17633–17651.

Lavé, J. et J. P. Avouac (2000). Active folding of fluival terraces across the Siwaliks Hills, Himalayas of central Nepal. *J. Geophys. Res. 105*, 5735–5770.

Leopold, L. B. et T. J. Maddock (1953). The hydrolic geometry of stream channels and some physiographic implications. *U. S. Geol. Survey. Professional Paper 252.*

Mackin, J. H. (1948). Concept of the graded river. *Geol. Soc. Am. Bull. 59*, 463–512.

Macky, G. H. (1999). Large flume experiments on the stable straight gravel bed channel. *Water. Resour. Res. 35*, 2601–2603.

Merritts, D., K. R. Vincent, et E. E. Wohl (1994). Long river profiles, tectonism, and eustasy: a guide to interpreting fluvial terraces. *J. Geophys. Res. 99*, 14031–13050.

Métivier, F. et P. Meunier (2003). Input and output mass flux correlations in an experimental braided stream. Implications on the dynamics of bed load transport. *J. Hydrol. 271*, 22–38.

Meunier, P. et F. Métivier (2000). Permanence des flux de masse d'une rivière en tresse expérimentale. *C. R. Acad. Sci., Earth and Planetary Sciences 331*, 105–110.

Parker, G. (1978a). Self-formed straight rivers with equilibrium banks and mobile bed. Part 1. The sand-silt river. *J. Fluid Mech. 89*, 109–125.

Parker, G. (1978b). Self-formed straight rivers with equilibrium banks and mobile bed. Part 2. The gravel river. *J. Fluid Mech. 89*, 127–146.

Schumm, S. A. et R. W. Lichty (1965). Time, space and causality in geomorphology. *Am. Jour. Sci. 263*, 110–119.

Schumm, S. A., M. P. Mosley, et W. E. Weaver (1987). *Experimental fluvial geomorphology.* John Wiley & Sons.

Shields, A. (1936). Anwendung der aenlichkeitsmechanik und der turbulenzforschung auf die geschiebebewegung. *Mitt. Preuss. Versuchsanst. Wasserbau Schiffbau*. translated to English by W. P. Ott and J. C. van Uchelen, CalTech, Pasadena, CA.

Shvidchenko, A. B. et G. Pender (2000). Flume study of the effect of relative depth on the incipient motion of coarse uniform sediments. *Water. Resour. Res. 36*, 619–628.

Van der Woerd, J., F. J. Ryerson, P. Tapponnier, Y. Gaudemer, R. Finkel, A. S. Mériaux, M. Caffee, G. Zhao, et Q. He (1998). Holocene left-slipe rate determined by cosmogenic surface dating on the Xidatan segment of the Kunlun fault, (Qinghai, China. *Geology 26*, 695–698.

Yalin, M. S. (1992). *River mechanics*. Pergamon Press.

Yalin, M. S. et A. M. Ferreira da Silva (2001). *Fluvial processes*. International Association of Hydraulic Engineering and Research, Delft, The Netherlands.

Chapitre 2

Protocole expérimental

2.1 Introduction

L'étude de la stabilisation des rivières alluviales et des processus (1) d'érosion des berges et (2) de transport de fond de sédiments ainsi mis en jeu est abordée au moyen d'un modèle réduit de rivière en laboratoire dîte à lit mobile. L'expérience est montée au laboratoire de Géomorphologie Expérimentale de l'IPGP à Saint Maur. Nous avons décidé d'aborder expérimentalement les phénomènes d'érosion des berges et de transport de fond de sédiments dans des rivières à chenal droit perturbées par rapport à leur état d'équilibre. Pour cela, nous nous sommes intéressés à deux cas de figure : (1) l'élargissement d'une rivière à chenal droit initialement de largeur inférieure à son état d'équilibre et (2) réponse à un décalage du chenal d'une rivière initialement droit et stable.

Dans la première configuration, l'évolution d'une rivière à chenal droit à partir d'une largeur initiale est étudiée afin de voir si un régime d'équilibre pour la rivière existe mais également pour caractériser l'évolution en temps de l'érosion des berges et du transport de fond en fonction de paramètres caractéristiques de la rivière (pente, débit liquide, taille des grains de sable et longueur de la rivière). La deuxième configuration fait l'objet de l'étude de la réponse à une perturbation d'une rivière initialement à chenal droit et stable. Dans ce cas la géométrie de l'écoulement est modifiée par un décalage latéral du chenal et

(a) (b)

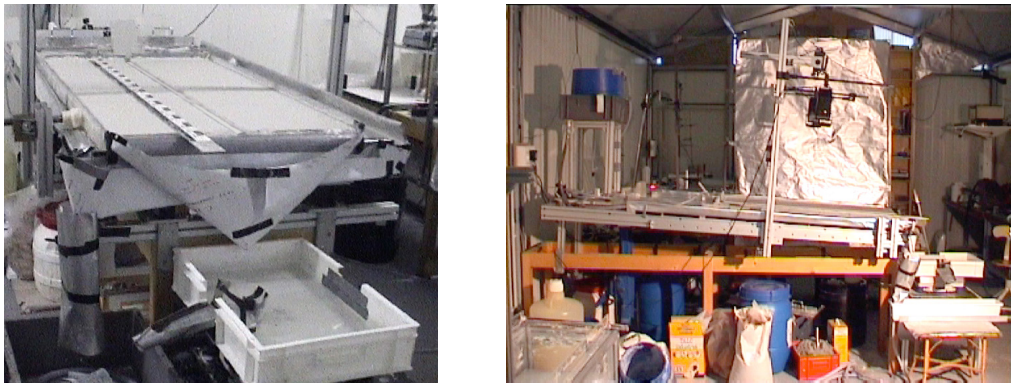

FIG. 2.1 – *Photos du dispositif expérimental. (a) Vue de face avec le système du dévidoir au premier plan et (b) vue de profil.*

l'on regarde comment la rivière réagit par l'intermédiaire de l'érosion et du transport. Il s'agit de savoir si la rivière retrouve alors un état d'équilibre ou bien si elle se déstabilise et évolue vers une nouvelle morphologie. Dans les deux cas, une série d'expérience est réalisée pour différentes valeurs de paramètres (débit liquide, taille des particules, et longueur de cuve) et conditions initiales (pente et largeur du chenal). Les variables du problème, flux sortant de sédiments, largeur ou géométrie des bords et vitesse de l'écoulement, sont alors mesurées. L'exploration du domaine des paramètres doit nous permettre de trouver des lois d'échelles entre les variables et les paramètres physiques.

Ce chapitre présente le protocole expérimental. Tout d'abord, le dispositif expérimental de micro-rivière que nous avons conçu est décrit en détail (Fig. 2.1). Puis, nous présentons les techniques d'acquisition de données et leurs précisions.

2.2 Une micro-rivière expérimentale

2.2.1 Cuve à lit mobile

Le but est de modéliser une micro-rivière, c'est-à-dire, un écoulement d'eau dans un chenal à bords érodables et qui puisse conserver un lit sableux tout au long du déroulement

TAB. 2.1 – *Dimensions des deux cuves utilisées pour les expériences de décalage de chenal et les expériences de rivière à chenal droit.*

	Cuve décalage	Cuve riv. droite
L	130 cm[1]	200 cm
W	70 cm	70 cm
H [2]	2 cm	6 cm
h [3]	1 cm	4 cm

[1]La cuve est en deux parties de 65 cm de long.

[2]Hauteur maximale de la plaine alluviale.

[3]Hauteur du niveau de base du lit de la rivière.

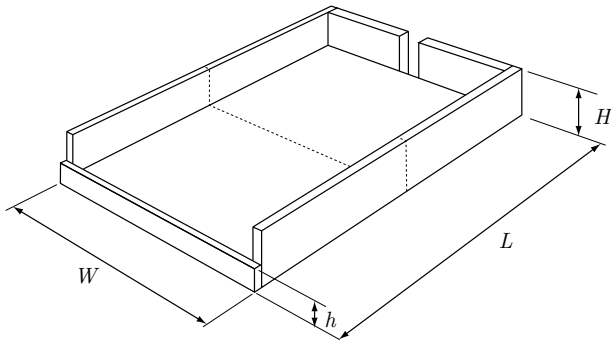

de l'expérience. Ce dernier point est fondamental car il s'agit pour la rivière de ne pas lessiver rapidement son lit afin de rester dans des conditions réalistes de fond alluvial[1]. Nous avons donc utilisé une cuve rectangulaire un peu particulière dite « à lit mobile » car elle permet de conserver un lit de billes pouvant néanmoins être mis en mouvement pendant toute la durée d'une expérience. Pour cela, un obstacle en bas de la cuve permet de limiter l'érosion du lit et impose ainsi un niveau de base à l'écoulement. La cuve possède donc l'un de ses bords (le bord aval) légèrement moins haut que les autres qui détermine ainsi l'épaisseur du lit de la rivière (Fig. 2.2). Le bord amont peut se translater de sorte à modifier la longueur de la rivière. Deux cuves en plexiglass ont été construites : la première d'une longueur de deux mètres pour les rivières à chenal droit et une deuxième de longueur de 1.30 m et coupée en deux dans sa longueur pour les expériences de décalage (Tab. 2.1). La cuve est disposée sur un cadre rigide inclinable de sorte à pouvoir faire varier la pente de la rivière. L'axe de rotation du cadre est précisément ajusté sur une position horizontale pour que le chenal de la rivière soit toujours selon la ligne de plus grande pente quelque soit l'inclinaison du cadre. Un vérin de camion permet de régler la pente. La mesure de la pente se fait grace à un niveau électronique (Tab. 2.3).

[1]Un lit de sable disposé sur un plan incliné se fait rapidement léssiver par un écoulement d'eau.

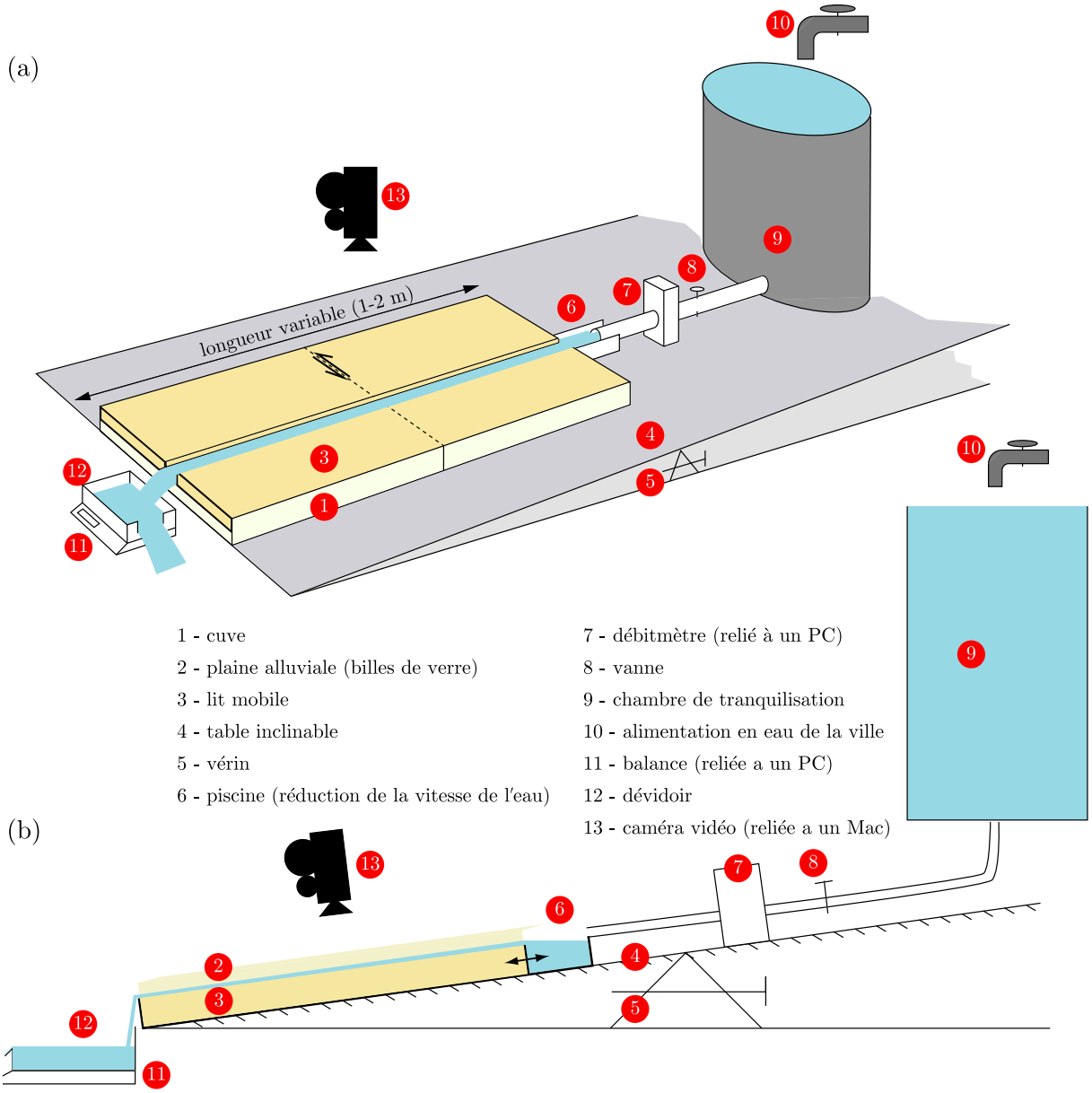

FIG. 2.2 – *Schéma du dispositif expérimental. (a) Vue générale. La cuve est de longueur variable (par translation du bord amont) et éventuellement sectionnée pour les expériences de décalage de sorte à pouvoir décaler une partie par rapport à l'autre. (b) Vue en coupe au niveau du lit. Le bord aval de la cuve permet de conserver un niveau de base : lit mobile. La chambre de tranquilisation est située en hauteur de sorte à pouvoir fournir un débit suffisament important (jusqu'à 2 l/min).*

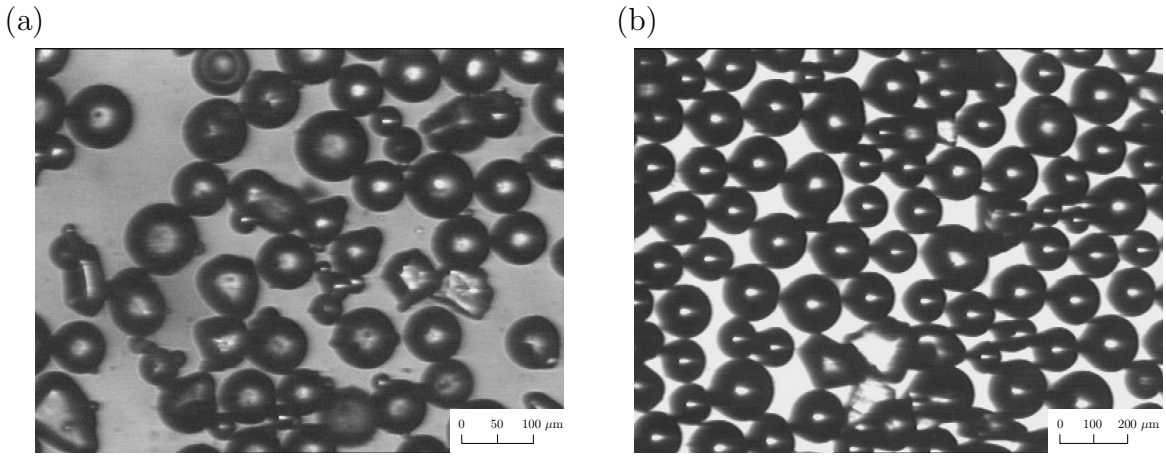

FIG. 2.3 – *Forme des particules utilisées d'après l'observation par microscope optique des deux types de sable : (a) sable A (50–100* µ*m) et (b) sable B (100–200* µ*m).*

2.2.2 Billes de verre comme materiel alluvial

Le materiel alluvial, normalement composé d'un mélange de sables, gravier et de galets plus ou moins anguleux et de différentes tailles, est ici modélisé par des billes de verre avec une distribution de taille quasi mono-disperse. Ces deux caractéristiques permettent (1) de simplifier le modèle (le milieu granulaire est ainsi homogène et représenté par un empilement de sphères) et (2) de se placer dans les hypothèses dans lesquelles les relations d'érosion ont été établies. On s'attend, dans ce cas, à une cohésion du milieu granulaire moins importante que dans le cas de particules anguleuses et pluri-disperses. Enfin, pour étudier l'effet de la taille des particules sur l'érosion et le transport, deux tailles de particules sont utilisées alternativement dans les expériences.

Les billes de verre proviennent de l'entreprise Marteau et Lemarié et sont fournies par classe de tailles. Nous avons utilisé deux sables : un sable de taille 50–100 µm (sable A) et un sable de taille 100–200 µm (sable B). Dans le but de vérifier nos contraintes pour le sable (particules sphériques de distribution mono-disperse), nous avons effectué plusieurs analyses sur ces deux sables et caractérisé dans chaque cas (1) la forme des particules, (2) la granulométrie et (3) la densité.

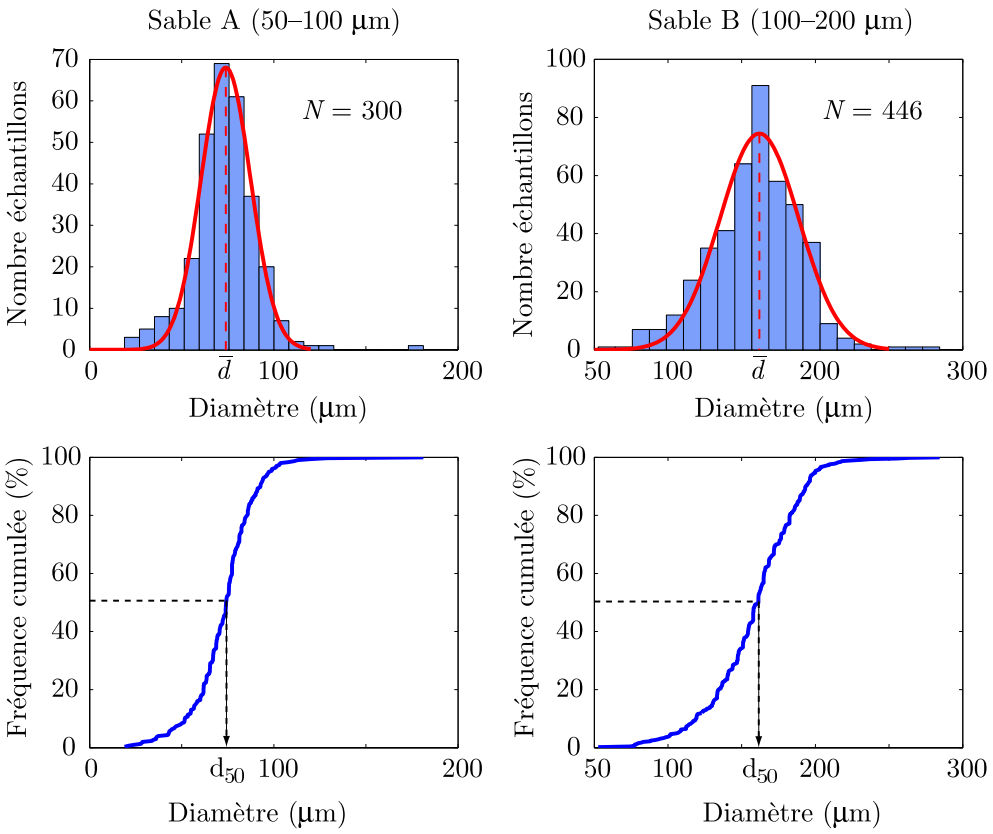

FIG. 2.4 – *Granulométrie du sable A (à gauche) et du sable B (à droite). En haut : histogramme des tailles. La distribution des tailles est gaussienne (la légère dissymétrie est certainement liée au tamisage des particules). En bas : représentation en fréquence cumulée des diamètres.*

L'observation au microscope optique permet la visualisation des sections des particules (Fig. 2.3). Pour chacun des deux sables, une dizaine d'observations de la sorte sont faites (correspondant a plusieurs centaine de particules) pour permettre un échantillonage aléatoire et représentatif. Les sections de particules sont essentiellement circulaires et quelques sections sont allongées : les particules sont donc considérées comme sphériques pour les deux sables (Fig. 2.3).

La granulométrie, ou distribution des tailles des particules, est déterminée en mesurant les diamètres des sections sur une série de 300 à 400 particules. La distribution des tailles ainsi obtenue est représentée sous la forme d'histogramme et de fréquences cumulée

TAB. 2.2 – *Caractéristiques des deux types de sable utilisés.*

	Sable A (50–100 µm)	**Sable B (100–200 µm)**
Composition	Silice	Silice
Couleur	Blanc	Blanc
Forme	Sphérique	Sphérique
Écart-type[1] (σ)	19 µm	38 µm
Diamètre moyen[1] ($\overline{d}$)	74 µm	162 µm
Diamètre médian[2] (d_{50})	74 µm	161 µm
Diamétre 90 (d_{90})	90 µm	193 µm
Coefficient de gradation[3] (σ_g)	1.25	1.20
Masse volumique (ρ_s)	2481 ± 1 kg/m^3	2482 ± 1 kg/m^3

[1]Déterminés par le fit d'une gaussienne sur les données des diamètres.

[2]Déterminé directement sur les données des diamètres.

[3] $\sigma_g = d_{90}/d_{50}$.

des tailles (Fig. 2.4). Pour les deux sables, on constate que la distribution est gaussienne d'équation

$$n(d) = N_0 \exp\left[-\left(\frac{d-\overline{d}}{\sigma}\right)^2\right], \tag{2.1}$$

où, $n(d)$ est la fréquence du diamètre d, N_0 est la fréquence du diamètre moyen $\overline{d}$ et σ est l'écart-type de la distribution. Pour les deux sables, la moyenne ainsi définie correspond au diamètre médian déterminé par la courbe de fréquences cumulées signifiant que la distribution est bien gaussienne (Tab. 2.2). On peut dire que la distribution est quasi-mono-disperse autour de la valeur du diamètre médian puisque, aux vues des valeurs des écart-types, 90 % des particules ont un diamètre égal au diamètre médian ± 50 %.

La densité de ces billes a été mesurée avec précision en laboratoire à l'aide d'un pycnomètre. Nous avons trouvé une masse volumique de 2481 ± 2 kg/m^3 pour les deux tailles de billes (Tab. 2.2).

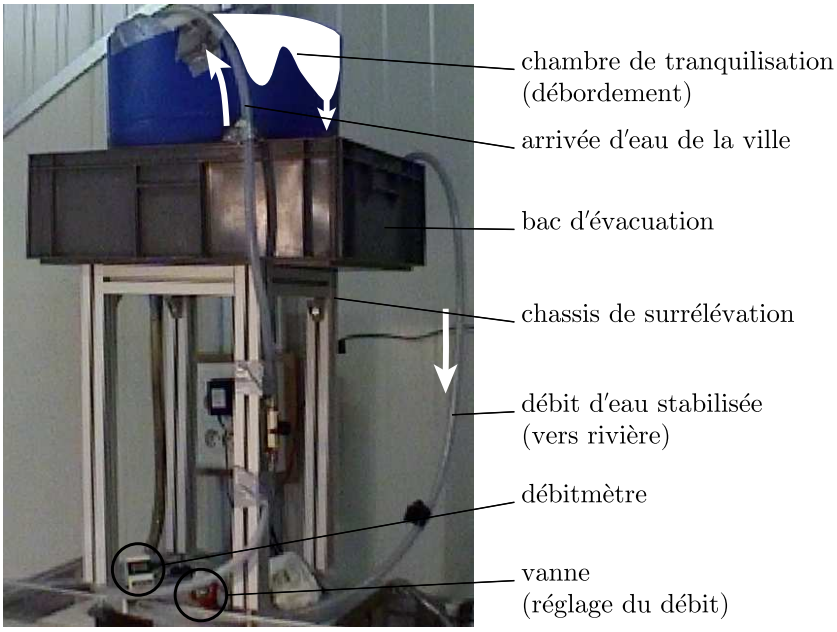

FIG. 2.5 – *Photo de la chambre de tranquilisation. L'ensemble est disposé en hauteur sur la table inclinable de sorte a obtenir une tête de pression hydraulique pour l'alimentation.*

2.2.3 Alimentation en eau

L'alimentation en eau est assurée depuis une chambre de tranquilisation afin d'avoir un débit constant. Il s'agit d'un réservoir à débordement (cylindre de 50 cm de diamètre sur 60 cm de haut) dans lequel un trop plein avec l'eau de la ville a lieu et disposé en hauteur sur la table inclinable de façon à obtenir une tête de pression hydraulique (énergie potentielle) pour assurer des débits d'eau pouvant aller jusqu'à 2 l/min (Figs. 2.2 et 2.5). Ce système permet également de tamponer les variations de débit inhérents au système d'alimentation de la ville. En bas du réservoir, une vanne permet de contrôler le débit d'eau sortant vers la cuve expérimentale. Toutefois, avant d'être distribuée dans la cuve, l'eau transite par une piscine disposée à l'entrée du chenal de la rivière (Fig. 2.2) afin de minimiser la vitesse de l'eau en début du chenal et ainsi limiter à cet endroit le creusement important d'une piscine. On évite la formation de cette piscine car celle-ci peut se propager au cours de l'expérience et modifier de façon significative la pente du chenal.

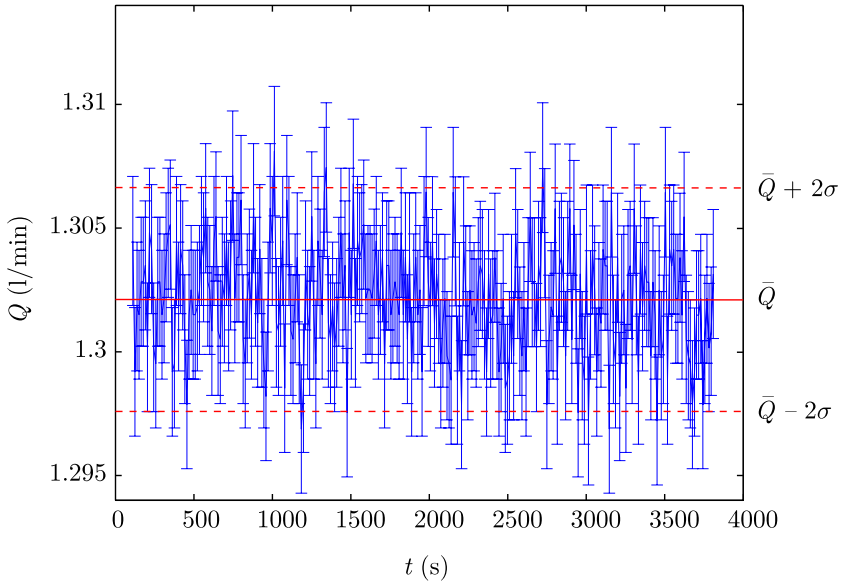

FIG. 2.6 – *Courbe typique de variation du débit liquide en fonction du temps (barres d'erreur de 3 %).* $\overline{Q}$ *est la moyenne du débit et* σ *l'écart-type. 95 % des mesures sont comprises entre* $\overline{Q} - 2\sigma$ *et* $\overline{Q} + 2\sigma$.

Le débit est mesuré par un débitmètre (Tab. 2.3). Le débitmètre est relié à un ordinateur permettant son enregistrement à un pas de temps régulier. Une courbe typique d'évolution du débit au cours d'une expérience est présentée sur la Fig. 2.6. On constate que le débit est relativement constant. Il reste des fluctuations de débit du réseau de l'eau de ville que le bac de stabilisation ne détruit pas complétement (phénomènes de tensions de surface). Puisqu'à l'échelle qui nous intéresse, le débit liquide est un paramètre constant, on considére le débit moyen $\overline{Q}$ pour caractériser l'expérience. Ce faisant, on introduit une erreur liée aux fluctuations qui ne sont pas prises en compte. On prend pour cette erreur 2σ où σ est l'écart-type, signifiant qu'au cours de l'expérience, le débit reste à 95 % entre $\overline{Q} - 2\sigma$ et $\overline{Q} + 2\sigma$. L'erreur totale sur le débit liquide est alors la somme de cette erreur lié à la moyenne avec l'erreur de mesure du débitmètre :

$$\frac{\Delta Q}{Q} = 100 \left(\frac{2\sigma}{\overline{Q}} \right) + \left(\frac{\Delta Q}{Q} \right)_d , \tag{2.2}$$

où $(\Delta Q/Q)_d$ est l'erreur de mesure du débitmètre de 3 % (Tab. 2.3). L'erreur est maximisée

(a) (b)

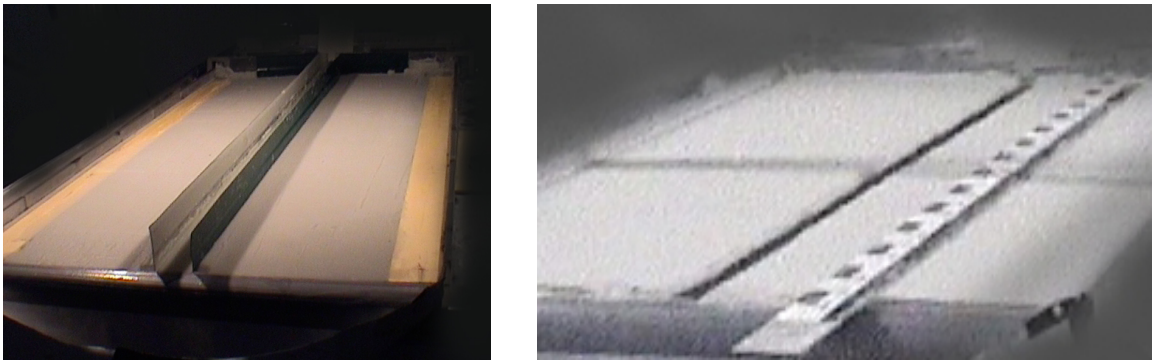

FIG. 2.7 – *Modularité du dispositif expérimental. (a) Expérience avec bords rigides et (b) expérience sans lit mobile initial (avec plaque).*

en prenant la plus grande valeur possible pour le premier terme observée sur une série de données a différents débits. Celle-ci est de 0.5 % et l'erreur sur le débit est donc

$$\frac{\Delta Q}{Q} = 0.7\ \%. \tag{2.3}$$

2.2.4 Modularité de l'expérience

La taille réduite de l'expérience permet d'adapter facilement le dispositif expérimental et effectuer d'autres types d'expériences. Ainsi, en plus des expériences de rivières à lit mobile et bord sableux, dans lesquelles la rivière à toute la liberté de modifier son chenal, deux autres types d'expériences ont été réalisées pour savoir comment l'écoulement d'eau distribue son énergie entre l'érosion du lit et l'érosion des berges.

1. Expériences de rivières à bords solides non érodables où seule l'érosion du lit est possible (Fig. 2.7a) et

2. Expérience de rivières à lit initialement solide par l'ajout d'une plaque au niveau du lit de la rivière pour empêcher l'érosion du lit (Fig. 2.7b).

TAB. 2.3 – *Références et précisions constructeurs des appareils de mesure.*

	Marque	Référence	Mesure (unité)	Précision
Niveau électronique	Bosch	DNM 60 L	angle (°)	±0.05°
Débitmètre numérique	Mc Millan	S-111 (58)	débit (l/min)	±3%
Balance de précision	Ohaus	Explorer (22 kg)	masse (g)	±0.1 g

2.2.5 Préparation et déroulement des expériences

La préparation des expériences fixe les conditions initiales de chaque manipulation. Il est important d'y attacher de l'importance car en dépend, pour une grande part, la qualité et la reproductibilité des l'expériences.

La mesure de la cohésion du milieu granulaire n'a pas été possible durant ce travail. Néanmoins, une cohésion comparable entre les expériences est obtenue de la façon suivante. Le sable est éventuellement préalablement humidifié de sorte à obtenir un milieu de texture qualitativement comparable à celle en fin d'expérience. De cette façon, même si le milieu se gorge rapidement d'eau, on garantit une cohésion du même ordre pour tous les états initiaux des expériences.

Ensuite, le chenal initial et la plaine alluviale plane sont formés. Le chenal doit être droit et également le plus rigoureusement possible selon la ligne de plus grande pente afin de minimiser et retarder la formation d'ondes d'érosion parasites sur les berges. Ces ondes s'initient au niveau de l'alimentation en eau et se propagent vers l'aval. Pour ce faire, nous avons élaboré un racloir permettant de creuser un chenal et de former dans le même temps la plaine alluviale plane. La translation du racloir calé sur les bords de la cuve assure un chenal droit centré en milieu de la cuve (Fig. 2.8a). Une pièce centrale interchangeable du racloir permet d'obtenir des chenaux de section rectangulaire et de différentes largeurs (2.5 cm, 4 cm, 6 cm et 8 cm). Pour toutes les expériences, le chenal est rectangulaire et la hauteur initiale des berges est d'un centimètre. La plaine alluviale en bas de cuve n'est retenue par aucun bord de sorte à permettre à la rivière de modifier librement la largeur du chenal (Fig. 2.8b).

(a) (b)

FIG. 2.8 – *Préparation du chenal. (a) Photo du racloir permettant de préparer le chenal initial de section rectangulaire. La pièce centrale est interchangeable pour permettre de varier la largeur initiale (ici 6 cm). (b) Photo en gros plan de l'exutoire de la rivière montrant la hauteur des berges de 1 cm et la limite de la plaine alluviale.*

Une série d'expériences est réalisée pour différentes valeurs des paramètres du système (longueur de chenal, taille des particules, débit liquide) et conditions initiales (pente et largeur du chenal). Pour quantifier les processus d'érosion et de transport mis en jeu lors de chaque expérience, des mesures sont alors effectuées sur les variables du système.

2.3 Mesures des variables de l'expérience

Nous parlons ici de la mesure des variables de l'expérience c'est à dire des quantités évoluant au cours du temps : (1) largeur moyenne du chenal (pour les expériences de rivière à chenal droit) ou position du bord actif (pour les expériences de décalage), (2) flux de sédiments transportés et (3) profil en long de vitesse de l'écoulement. La pente est normalement également une variable du système mais elle sera ici considérée comme un paramètre pourvu que ces variations soient faibles.

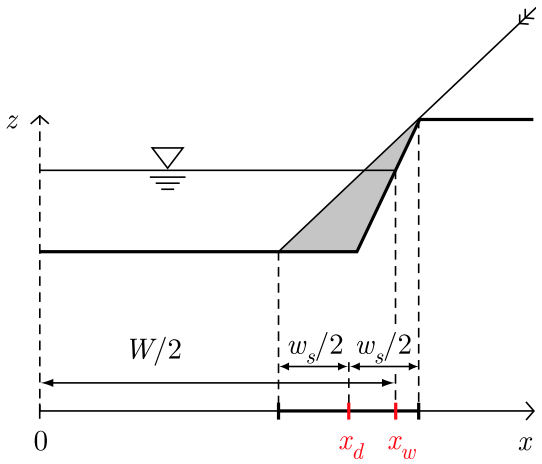

FIG. 2.9 – *Schéma en coupe du chenal avec la zone d'ombre en grisé générée par l'éclairage latéral. W est la largeur de l'écoulement que l'on cherche à détecter. La zone d'ombre est d'épaisseur w_s et encadre la position x_w du bord recherchée. x_d correspond à la position détectée automatiquement et manuellement (milieu de l'ombre).*

2.3.1 Acquisition de la géométrie des bords

L'objectif est de connaître selon l'expérience réalisée

- l'évolution de largeur en fonction du temps pour les expériences de rivière à chenal droit ou
- l'évolution de la géométrie du bord actif dans le cas des expériences de décalage de chenal.

La notion de largeur de chenal est ambiguë puisque la section est trapézoïdale. Dans notre étude, la largeur du chenal est la largeur active ou largeur de l'écoulement d'eau (Fig. 2.9). Les positions cherchées pour déterminer la largeur sont donc celles de l'interface de l'eau sur les bords (x_w). Dans ce but, des photos du chenal sont prises durant le déroulement de l'expérience afin de permette d'éstimer l'érosion par la mesure de l'évolution de la position des bords.

Une caméra vidéo numérique est utilisée pour filmer la plaine alluviale et le chenal vu de dessus. Afin de diminuer les erreurs de paralaxes, la caméra est fixée perpendiculai-

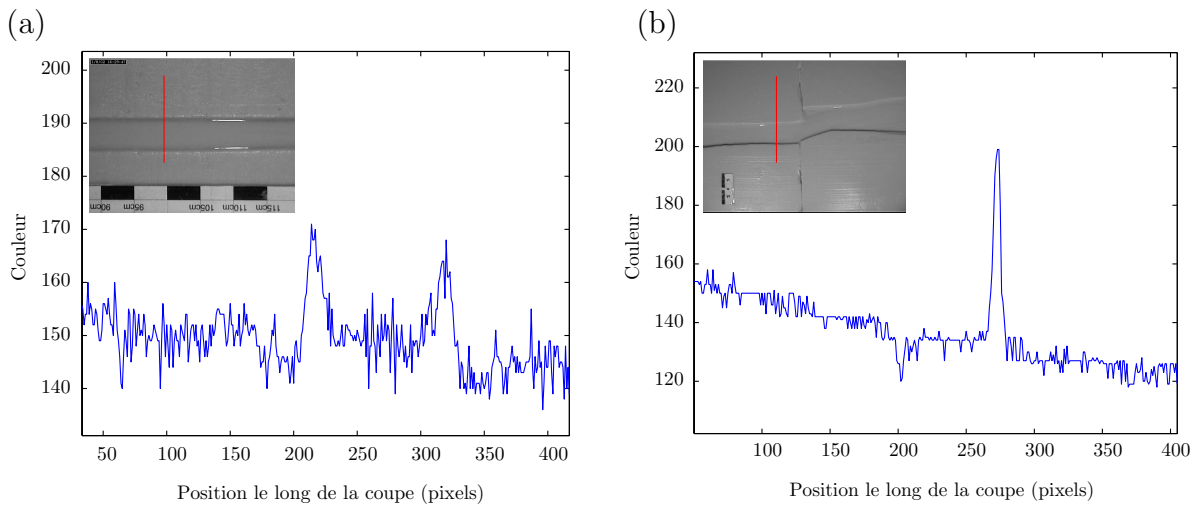

FIG. 2.10 – *Intensité lumineuse sur des coupes perpendiculaires au chenal. La position des pics correspond à l'ombre sur les bords. (a) Cas où deux spots sont utilisés et (b) cas où un spot est utilisé. Le pic est mieux défini (amplitude et largeur) lorsqu'un seul spot est utilisé.*

rement au plan de la cuve sur un cadre. Le cadre est fixé sur un rail solidaire de la table inclinée de telle sorte qu'il permet à la caméra un déplacement dans les deux directions du plan parallèle à la plaine alluviale afin d'être positionnée sur la bonne zone. Pour une meilleure visibilité, deux spots lumineux éclairent de part et d'autre la cuve de sorte à ombrager les berges. Enfin, une règle jouant le rôle d'échelle est toujours placée dans le champ de la caméra.

La caméra est reliée à un ordinateur (Macintosh) sur lequel les films des expériences sont enregistrés. Plus précisément, nous avons utilisé un logiciel permettant d'enregistrer des images à un intervalle de temps régulier soit typiquement 10 s pour trouver le bon compromis entre nombres d'images et mémoire sur le disque dur. Ceci (1) car les expériences ont une dynamique suffisament lente qui ne nécessite pas de mémoriser les images à une fréquence plus élevée et (2) pour limiter le coût en mémoire de stockage des images des expériences devant durer plusieurs heures. On a alors pour chaque expérience une série d'images de la même zone prises à un intervalle de temps régulier qu'il faut alors

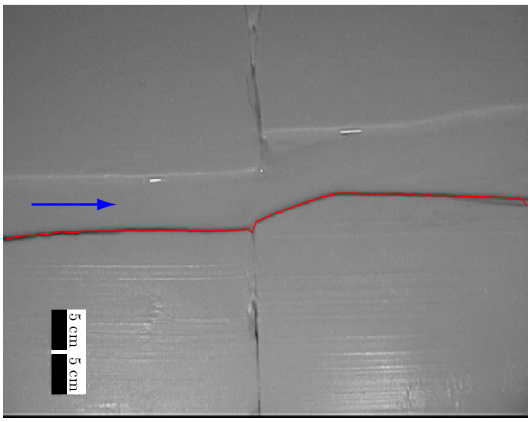

FIG. 2.11 – *Photo caractéristique d'une expérience de décalage avec en rouge, le bord actif détecté par notre code (l'écoulement va de la gauche vers la droite). Dans ce cas, un seul spot est utilisé pour avoir une ombre bien définie sur le bord actif.*

analyser pour obtenir l'évolution de la largeur (expériences à chenal droit) ou pour obtenir l'évolution de la géométrie du bord actif (expériences de décalage).

Un code de traitement des images a été écrit pour détecter les bords. Sachant qu'une image en noir et blanc est en fait une matrice dont les valeurs correspondent à l'intensité du gris (échelle entre 0 pour le blanc et 255 pour le noir), le principe du code est de repérer, sur chaque section perpendiculaire au chenal, les deux pics d'intensité laissé par l'ombre des bords (Fig. 2.10). Le code repère le milieu du pic, ce qui correspond à la position x_d sur la Fig. 2.9. L'analyse est très sensible aux conditions d'éclairage (l'utilisation de deux spots, disposés l'un en face de l'autre, diminue le contraste des ombres) et donne des résultats biens meilleurs dans le cas où seul un bord est éclairé et détecté car alors le pic d'intensité est mieux défini (Fig. 2.10b). C'est pourquoi, ce code a été essentiellement utilisé pour détecter la géométrie du bord actif lors des expériences de décalage (Fig. 2.11). Dans le cas des expériences à chenal droit, le code de détection ne donne pas de bons résultats et la position des deux bords est alors pointée à la main sur trois sections régulièrement espacées sur l'image de sorte à obtenir une largeur moyenne. Cette largeur est représentative puisque le chenal reste droit.

TAB. 2.4 – *Précision et erreur due à la vidéo*

	Grossissement	**Résolution**	**Précision du pixel**	ΔW
Chenal droit	moyen	720×540	0.005 mm	± 6 mm
Décalage	faible	640×480	0.1 mm	± 6 mm

L'erreur dans la détection est à présent analysée. Deux erreurs sont à considérer :

1. l'erreur liée à la précision de la caméra et
2. l'erreur de détection.

Le principe de la caméra vidéo est de discrétiser l'image de la réalité en une mosaïque de pixels carrés (surfaces unités). La précision dépend de la résolution de la caméra (qualité du capteur CCD) et du grossissement utilisé. Le capteur CCD fonctionne avec un certain bruit de base qui introduit une diffusion des constrastes (typiquement sur 2 pixels). Les contours sont donc moins bien définis et ceci introduit une erreur dans la mesure de distances. L'erreur sur la mesure de la position du bord provient donc du fait que la largeur de l'ombre est modifiée par la diffusion introduite par la caméra. L'erreur entre une longueur vraie l_r et sa mesure l_m est de ± 4 pixels :

$$\Delta l = l_m - l_r = \pm 4 \,\text{pixels}. \tag{2.4}$$

L'utilisation d'une échelle de longueur connue sur l'image permet de traduire l'erreur en pixels en erreur en millimètres. Pour les deux grossisement utilisés, la précision du pixel alors mesurée est inférieure au millimètre (Tab. 2.4). Connaissant cette précision, la mesure de la largeur du chenal introduit une deuxième erreur liée à l'incertitude dans la représentation de la position x_d repérée et la vraie position x_w (Fig. 2.9). Comme la vraie position recherchée est toujours contenue dans la zone d'ombre, l'erreur sur la position est toujours au maximum

$$\Delta x = \frac{w_s}{2}, \tag{2.5}$$

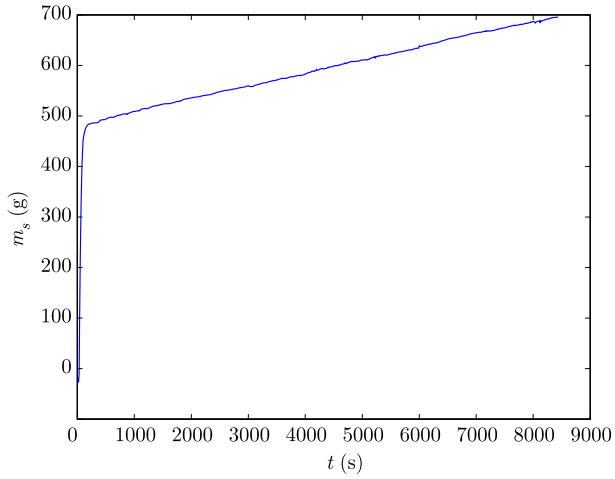

FIG. 2.12 – *Masse cumulée de sédiments en fonction du temps ($S = 3.5 \times 10^{-2}$, $Q = 0.5$ l/min et $d_{50} = 75$ µm). Typiquement plusieurs dizaines à plusieurs centaines de grammes de sédiments sont accumulés sur des durées de plusieurs heures.*

où w_s est la demi-largeur de la zone d'ombre projetée horizontalement (Fig. 2.9). Cette largeur w_s est susceptible de changer au cours de l'expérience car la hauteur des berges diminue avec l'aggradation sur le lit. Mais à la précision de la caméra, cette variation ne se voit pas. La largeur de cette ombre reste constante au cours des expériences et égale à 6 mm $\pm$ $2\Delta x$ pour les deux résolutions. L'erreur de résolution du pixel est négligeable et l'erreur sur la détection du bord est donc de $\pm$ 3mm. L'erreur sur la largeur est deux fois cette erreur donc $\pm$ 6mm.

2.3.2 Mesure continue du flux de masse de sédiments

Le transport de sédiment est mesuré à l'exutoire de la rivière grace à un dévidoir posé sur une balance et collectant l'eau chargée en sédiment en sortie de la rivière (Fig. 2.2). Ce système permet d'avoir accés à une mesure continue de la masse cumulée de sédiments en sortie de cuve représentative du transport de la rivière sur toute sa longueur.

Le dévidoir fonctionne à volume constant grace à une sortie d'eau qui maintient toujours le même niveau d'eau. Ainsi, tout apport de volume de matière dans le dévidoir

entraine la sortie du même volume d'eau. Le dévidoir est neutre vis à vis de la balance si l'apport de matière est de l'eau car les volumes échangés sont alors de même masse. Par contre, dans notre cas où de l'eau et des sédiments (plus denses) sont déversés, la masse augmente avec la sédimentation du sable. Mais cette masse représente la masse « mouillée » des sédiments et doit être corrigée de la poussée d'Archimède afin de connaître la masse à sec de sédiments effectivement transportée par la rivière. Un raisonnement sur la conservation du volume du dévidoir permet de trouver que

$$m_s(t) = \frac{\rho_s}{\rho_s - \rho} m_b(t) + m_0, \tag{2.6}$$

où m_s est la masse de sédiments à sec, m_b est la masse mouillée que mesure la balance, m_0 est la masse à $t = 0$, ρ_s et ρ respectivement la masse volumique du sable et la masse volumique de l'eau. La balance de précision placée sous le dévidoir est reliée à un ordinateur qui enregistre la masse à intervalles de temps réguliers (Tab. 2.3).

Avant chaque expérience, la balance est calibrée et tarée avec le dévidoir rempli d'eau ($m_0 = 0$ dans Eq. (2.6)). Une protection contre les ondes de surface est placée à la sortie du dévidoir pour avoir un signal le moins perturbé. Enfin, le système dévidoir et balance est protégé par un paravent de sorte à éviter les coups de vents et les chocs. La Fig. 2.12 montre une courbe typique de masse cumulée de sédiments. On constate qu'après un temps de stabilisation du dévidoir de quelques minutes, le flux de sédiments devient relativement constant sur toute la durée de l'expérience. Ainsi, dans notre étude, nous considérons le flux de sédiments moyen déterminé par ajustement d'une droite sur la partie linéaire du signal et négligons donc les variations de second ordre.

L'erreur sur le flux de sédiments Q_s est à présent analysée. Aucune erreur sur le flux ne vient de la dérive de la balance car celle-ci est très faible (+1 g sur 7000 s) et cette erreur a donc a priori quatre composantes :

$$\Delta Q_s = (\Delta Q_s)_m + (\Delta Q_s)_f + (\Delta Q_s)_d + (\Delta Q_s)_f. \tag{2.7}$$

où chaque terme représente respectivement

– l'erreur liée à la mesure de la masse par la balance,

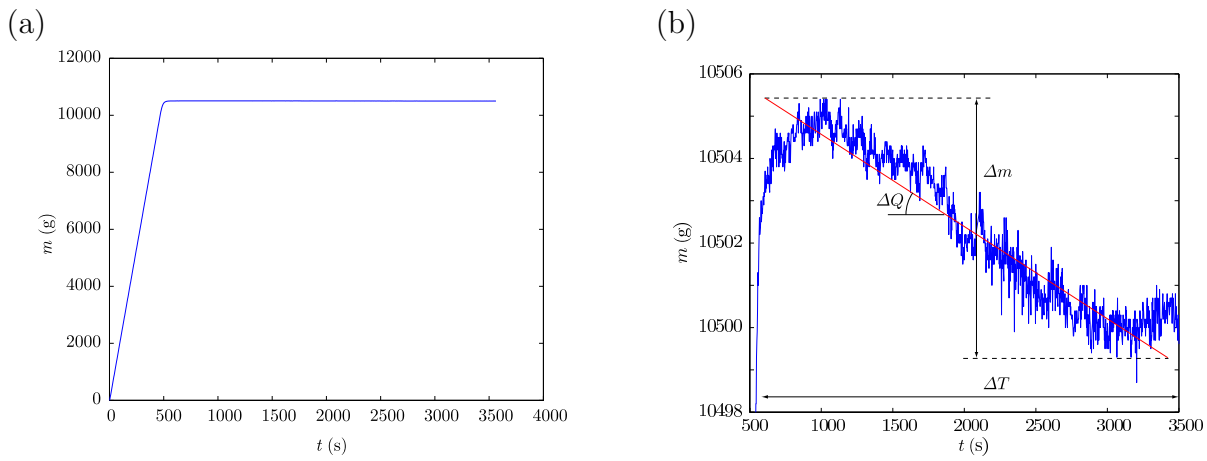

FIG. 2.13 – *Remplissage et fonctionnement du dévidoir sous un débit liquide constant (1.3 l/min). (a) Courbe typique d'évolution de la masse montrant le remplissage puis l'équilibre pendant le fonctionnement du dévidoir. (b) Zoom sur la phase d'équilibre montrant l'écart par rapport à une masse constante théorique. La variation de la masse* Δm *pendant* Δt *définit un débit moyen* ΔQ_s *qui est l'erreur par rapport au débit théorique nul.*

- l'erreur liée à la mesure d'un flux par la balance,
- l'erreur liée au fonctionnement du dévidoir et
- l'erreur faite lors de l'ajustement de la droite sur les données.

La première erreur $(\Delta Q_s)_m$ est négligable car la précision de la balance est de plusieurs ordres de grandeurs inférieures aux masses de sédiments accumulées (0.1 g pour typiquement 300 g). La deuxième erreur $(\Delta Q_s)_f$ est également négligeable car lors de la sédimentation des particules, l'impact au fond du dévidoir est faible de sorte que la balance n'enregistre aucune accélération. La troisième composante $(\Delta Q_s)_d$ est l'erreur principale sur la mesure du flux de sédiments par le dévidoir. Cette composante prend en compte l'effet du jet d'eau tombant dans le dévidoir et tient également compte du fait que le dévidoir n'est jamais parfaitement à l'équilibre car les tensions de surface du liquide entrainent un stokage d'eau plus ou moins périodique au cours du temps : le dévidoir oscille entre phase de stokage et phase de vidange. Ainsi, si ces oscillations ont des périodes

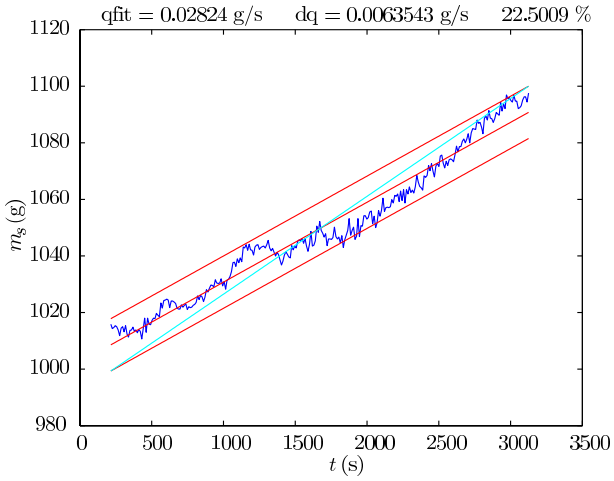

FIG. 2.14 – *Erreur sur le fit dans la partie linéaire du signal. La demi-largeur est* 2σ *(95 % des données) et l'erreur est déterminé par la diagonale du bandeau (cyan).*

de temps suffisament grandes supérieures à la durée des expériences de rivières, on peut s'attendre à ce qu'elles rajoutent une composante additive dans le flux de sédiments. Pour estimer cette erreur due au dévidoir, une série d'expériences de calibration est réalisée dans lesquelles le dévidoir est rempli puis fonctionne sous un débit d'eau constant. Ces expériences sont réalisées sur les durées caractéristiques des expériences de rivières (plusieurs heures) et pour deux jeux de paramètres correspondants aux conditions extrèmes pour les expériences de rivières, c'est à dire (1) pente de 1°et débit de 0.5 l/min et (2) pente de 3° et débit de 1.3 l/min. (Fig. 2.13a). Si au premier ordre la masse est effectivement constante, on constate néanmoins à plus petite échelle l'enregistrement du stokage d'eau (Fig. 2.13b). Sur aucune de la dizaine des expériences de calibration réalisées, on n'observe véritablement plusieurs oscillations de sorte que l'on puisse considérer un débit moyen nul. On en déduit que sur les durées des expériences de rivières, le dévidoir n'oscille pas et qu'il introduit alors une dérive moyenne de la masse (donc un flux). L'erreur par rapport à un flux théorique nul est estimée par

$$(\Delta Q_s)_d = \frac{\Delta m}{\Delta t} \tag{2.8}$$

où Δm et Δt sont définis sur la Fig. 2.13b. Pour toutes les expériences de callibration,

l'erreur est maximisée en prenant la plus grande valeur et on trouve

$$(\Delta Q_s)_d = 7.5 \times 10^{-3} \text{ g/s}. \tag{2.9}$$

Enfin, l'erreur qui est faite à la mesure de la pente sur les données s'estime en considérant le bandeau de demi-largeur 2σ où σ est l'écart-type. Ce bandeau contient 95 % des données. L'erreur sur le fit est estimée en calculant la pente de la diagonale du bandeau (Fig. 2.14). En fait cette erreur qui se mesure a posteriori (après les expériences de rivières) est dans la plupart des cas inférieure à l'erreur due au dévidoir (0.0075 g/s). Si on ne suppose rien sur la forme que doit avoir le flux de sédiments, il est difficile de dire ce que représente physiquement l'erreur sur le fit quand celle-ci est supérieure à l'erreur du dévidoir.

2.3.3 La pente comme paramètre

La pente locale est une variable dans nos expériences car elle est susceptible d'évoluer par l'action des processus de transport et d'érosion qui peuvent changer la topographie du lit. Toutefois, nous considererons la pente moyenne du chenal $< S >$ comme paramètre. Les mesures de hauteurs du chenal en fin d'experience montrent qu'au maximum une différence de hauteur de 5 mm est observée. L'erreur sur la pente moyenne est donc

$$\Delta < S >= \frac{5}{1300} = 0.0038. \tag{2.10}$$

L'acquisition de la topographie en temps réel par une méthode de Moiré effectuée pour quelques expériences a montré que le lit s'élève d'environ 5 mm à mi-longueur du chenal, ce qui confirme le résultat précédent.

2.4 Conclusion

Des expériences de rivières à chenal droit sont réalisées pour étudier l'érosion des berges et le transport de fond de sédiments lors de la stabilisation du chenal. Une série

d'expériences est réalisée pour différentes valeurs de paramètres caractéristiques (indépendants) : pente, débit liquide, tailles des billes de verre, largeur initiale et longueur de cuve (Tab. 2.5). Pour chaque expérience, plusieurs mesures sur les variables du système sont effectuées : évolution en temps de la position des berges, flux sortant de sédiments à l'exutoire de la rivière et vitesse de l'écoulement (Tab. 2.6). Plus précisement, deux grandes séries d'expériences ont été réalisées : expériences a chenal droit et expériences de décalage de chenal.

TAB. 2.5 – *Listes des paramètres.*

	Notation	**Unité**	**Gamme de variation**	**Précision**
Pente[1]	S	-	$1.72 \times 10^{-2} - 7 \times 10^{-2}$	± 10–20 %
Débit liquide	Q	m^3/s	$8.3 \times 10^{-5} - 2.2 \times 10^{-4}$	± 0.7 %
Tailles de billes	d_{50}	m	75×10^{-3} et 160×10^{-3}	-
Masse volumique des billes	ρ_s	kg/m^3	2481	± 2
Largeur initiale du chenal[2]	W_0	m	$2.5 \times 10^{-2} - 8 \times 10^{-2}$	-
Longueur du chenal	L	m	1.10 et 1.80	-

[1]La pente est considérée comme un paramètre plutôt qu'une variable car elle varie très peu.

[2]C'est plus une condition initial qu'un paramètre.

TAB. 2.6 – *Liste des variables.*

	Notation	**Unités**	**Précision**
Largeur ou position du bord	W	m	$\pm 6 \times 10^{-3}$
Flux de sédiments	Q_s	kg/s	$\pm 8 \times 10^{-6}$

Chapter 3

Equilibrium Width and Scaling of the Microscale Rivers

3.1 Introduction

Alluvial rivers possess self-formed channels resulting from the interactions between water and sediments such as erosion, transportation and deposition. Consequently, most river channels are found to display a stable or relatively stable hydraulic geometry controled on the short term by the mean annual discharge (Leopold & Maddock, 1953). Such rivers are said to be "in regime" (Lacey, 1930). On the long term, rivers can develop an adjusted longitudinal profile where neither net erosion nor net deposition takes place. Such rivers are said to be "in grade" or "graded" (Mackin, 1948; Hack, 1960) and by extension are also in regime. The notion of the graded stream has not met universal acceptance in the way that real alluvial systems may never perfectly achieve in time the dynamic equilibrium since the time response for the channel adjustments are large in front of the variabilty of climatic change (Dade & Friend, 1998).

We address herein bedload transport and bank erosion in a non stable straight river. Our interest is to quantify these mechanisms in a river far from equilibrium and look how the two are related in the transitory regime and if the river tends to an equilibrium state.

These mechanisms have been experimentally investigated through a set of controlled experiments of a a micro-scale straight gravel channel with varying slope, water discharge, grain size and channel length and for different initial slope and width. Generally, experiments would provide data for the width evolution of straight channel and eventually surface bed elevation (e.g. Ikeda, 1981; Ikeda *et al.*, 1988; Diplas, 1990; Macky, 1999) but not a precise and continuous measure of the bedload transport rate. If they do, it is an average value that is proposed (Ikeda *et al.*, 1988). This experiment will provide a precise and continuous in time measure of the sediment being transported by the river and this done upon the idea of Meunier & Métivier (2000); Métivier & Meunier (2003).

Results and interpretation are presented within two companion papers (Armstrong & Métivier, 2003a,b). In the first part (Armstrong & Métivier, 2003a, presented in the next section), we present the results on the equilibrium width and discuss about the scales of the micro-scale river. Discussion on the equilibrium of the river and especially on the transport rate of sediment takes place in the companion paper (Armstrong & Métivier, 2003b) presented in Chapter 4.

3.2 Equilibrium width and scaling of the microscale river

Independence of sediment flux and width evolution through time in a microscale straight river channel. Part 1. Scaling of microscale experiments

Lawrence Armstrong [a,*], François Métivier [a] and Gary Parker [b]

[a] *Institut de Physique du Globe de Paris, Laboratoire de Dynamique des systèmes Géologiques, Groupe de Recherche sur l'Érosion et les Eaux Continentales, 75252, Paris Cedex 05, France*

[b] *St. Anthony Falls Laboratory, Mississippi River at 3rd Ave SE, Minneapolis, MN 55414 USA*

Abstract

Study of the regime channel equilibrium and of the associated transport rate of sediment is achieved in the case of an experimental microscale straight river. The overall balance of mass is kept negative through the absence of sediment at the intlet. An erosional regime is established in which the channel can nevertheless achieve equilibrium at a certain distance from the inlet. There is in any case rapid establishment of a time independence between the mass flux of bedload and the evolution of the river width under steady uniform flow condition (see companion paper, Armstrong and Métivier, 2003). The uniform flow established is however slightly different from natural conditions. Suggestion is made about the possible influence of surface tension due to small Weber numbers and an scaling law is proposed. It is however shown that whithin measurement uncertainties the flow in microscale river channels remains close to natural conditions. From the observation that uniform flow conditions can be found in many natural rivers, to the first order, we then show how using grainsize-scaling can prove dangerous. Dimensional analysis is further performed and first order simple regime relationships are eventually derived that enable a scaling of model experiments in agreement with Shields phase diagram.

Key words: River width, Regime geometry, Scaling, Bed load transport, Microscale experiment

* Corresponding author
Email addresses: armstron@ipgp.jussieu.fr (Lawrence Armstrong), metivier@ipgp.jussieu.fr (François Métivier), parker@umn.edu (Gary Parker).

1 Introduction

Alluvial rivers are the result of water flowing on a substratum, the alluvial plain, made of sediments, from sand to gravel sizes, generally cohesionless. Due to the interactions between the flow and the sediments, alluvial rivers thus posses self-formed channels. Consequently, most alluvial river channels are found to display on short term period a stable or relatively stable hydraulic geometry where neither net erosion nor net deposition takes place. Such rivers are said to be "in grade", "graded" (Mackin, 1948; Hack, 1960), or "in regime" (Lacey, 1930). A consistency between the hydraulic geometry of the equilibrium channel and the mean annual flow discharge was provided from some empirical framework at the beginning of the last century (e.g. Blench, 1957; Inglis, 1949; Lacey, 1930; Leopold and Maddock, 1953). The hydraulic geometry parameters are found to depend at first order on a power of the mean annual flow discharge:

$$A_e = \alpha_A Q^{n_A} \tag{1}$$

where A_e represents either one of the regime characteristic of the channel (channel width W_e, flow depth h_e and slope S_e), where α_A and n_A are parameters related to A_e and where Q is the mean annual flow discharge. These empirical regime formulae lead to the following important relations that are ubiquitous for alluvial sand and gravel rivers:

$$W_e \sim Q^{1/2}, \tag{2a}$$

$$h_e \sim Q^{n_h(d_{50})}, \quad n_h \approx 1/3 \text{ for fine sand}; \quad n_h \approx 0.43 \text{ for gravel}, \tag{2b}$$

$$S_e \sim Q^{n_S(d_{50})}, \quad n_S \approx -0.1 \text{ for fine sand}; \quad n_S \approx -0.43 \text{ for gravel} \tag{2c}$$

The remarkable degree of constancy in the exponents has lead to consider these power law relations in term of water discharge as good approximations at first order for the hydraulic geometry. However, they are dimensionally inhomogeneous and the coeficients vary from locality to locality (Parker, 1979; Yalin, 1992). This denotes the possible influence of other parameters than the water discharge (such as density, grain size, fluid viscosity, gravity, cohesion for example). Based on this empirical framework and using dimensional analysis, some regime relations have been obtained that take into account the possible influence of other river parameters (see Yalin, 1992; Yalin and Ferreira da Silva, 2001, for an exhaustive derivation). Parker (1978a,b) proposed a physical explanation for the existence of stable straight river. In the case of sand bed rivers, channel is maintain stable through the shear stress distribution that allow export of material from the banks to be countered by an import of suspended sediments from lateral diffusion (Parker, 1978a). For the case gravel bed rivers with coarse material, lateral redistribution of the shear stress due to the presence of the wall decreases gradually from bed to bank region and yield

to stable and active channel (Parker, 1978b). Parker (1979) proposed, in the case of gravel beds river, scaling law for the hydraulic width and the dimensionneless water discharge scaled according to Einstein's sediment transport relation (Einstein, 1942):

$$\frac{w}{d_{50}} = 0.44 \left(\frac{Q}{\sqrt{Rgd_{50}}d_{50}^2} \right)^{0.5} . \tag{3}$$

This relation, although empirical, appears to be universal for various watershed and was found to display the same exponent of 0.5 for the discharge as in Leopold and Maddock's relation Eq. (2). Following to these progresses done to understand and explain regime channels, the question of the characteristic time scale to achieved equilibrium has not yet be addressed specificaly to our knowledge, certainly due to the difficulty of the problem. A related question is to determine when and for which discharge a river is going to erode its channel. The fact that regime relations can be obtained with the bankfull discharge suggest however a rapid response of the channel as these events are rare.

A full comprehension of the channel dynamics also requires to understand the sediment transport dynamic on the scale of the river. Sediment transport features have been widely addressed especially in the case of bedforms studies. However, the difficulties to monitor correctly bedload tranport on a large time and length scales due to the heavy procedure for the measurements, have lead to a lack of long time surveys of bedload transport for a river. Especially evolution of the bed load transport in a adjusting towards equilibrium is an interesting problem. Previous river experiments have focused on the regime equilibrium for the channel geometry and often did not address the transport problem specifically. To ensure an overall mass balance, experimental streams are often fed at the inlet with the sediments transported out the flume. This leads to a forcing in the sediment transport.

In order to bring some constraints in the regime relations of the channel morphology and on the transport rate regime, an experimental microscale straight river is used to evaluate the eventual establishment of equilibriums for both the channel and the sediment transport. A set of controled experiments of a microscaled river without grain feeding is achieved under varying slope, water discharge, grain size with measurements of the evolution in time of both channel width and sediment flux at the outlet. However, the experiments are set with absence of sediment feeding at the inlet in order to limit a possible forcing on the transport of sediment. We report here results on the channel width and the flow conditions. The effect of surface tension on the flow is discussed and a scaling law is proposed. A scaling law for the aspect ratio is proposed based on the uniform flow. Specific results on the establishment of an constant transport rate of sediments are discussed in the companion paper

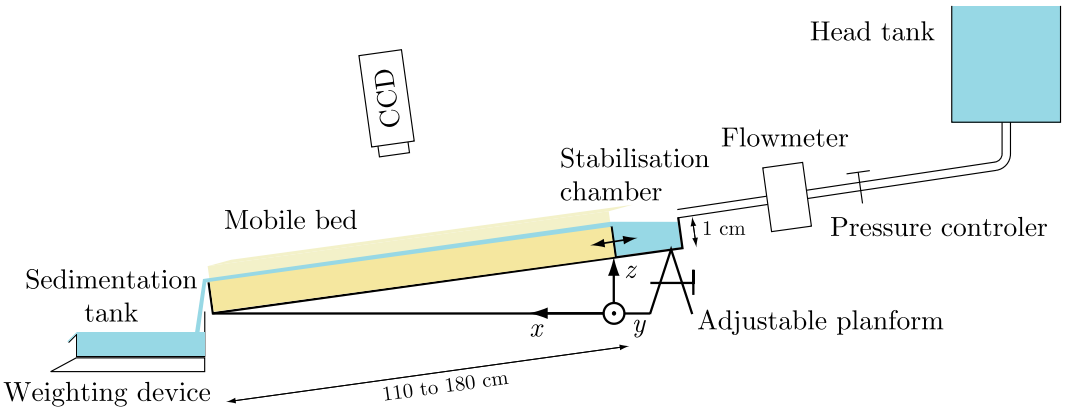

Fig. 1. Experimental setup, not to scale.

(Armstrong and Métivier, 2003).

2 Experimental apparatus and observations

2.1 Apparatus and procedure

Experiments of straight river (Ikeda, 1981; Ikeda et al., 1988; Diplas, 1990; Macky, 1999) usually model a half cross section of a straight river with the use of a central wall to suppress the tendency of meandering (Blondeaux and Seminara, 1985). We do not adopt this approach since our streams have flows that are typically a few millimeters height and can therefore be altered significantly by the presence of a wall on a distance of the same order (Blondeaux and Seminara, 1985). A full cross section is modelled in a experimental microscale river. It is reproduced using a mobile bed in a flume of variable length (1.10 m to 1.80 m) and 70 cm of width (Fig. 1). The sediments used are glass beads with a gaussian distribution of sizes so that the mean diameter of the distribution corresponds to the median diameter (d_{50}). Two sizes of sand are used separately: A sand of d_{50} =75 µm and B sand of d_{50} =160 µm. The distribution can be considered as uniform since the standard deviation in the size distribution σ = 19 µm and σ = 38 µm respectively for A sand and B sand which corresponds to a relatively small dispersion (13 % and 24 % of relative dispersion respectively for A sand and B sand). For this reason, the median diameter d_{50} is considered to be the most characteristic size to describe the size distribution of the sediment and it is used in the following physical modeling. The flume rests on a tilting planform that allows control of the bed slope. Slopes are measured using a digital level device (precision of 0.1 °). The initial cross section of the channel is rectangular of variable width (2.5 cm to 8 cm) and molded by a template. Water discharge is adjustable and measured using a flow-meter. The water discharge remains constant during the experiments

Table 1
Experimental conditions and number of runs for each set of experiments. Flume length L, grain size d_{50}, slope S, water discharge Q, initial width w_0 and number of runs #.

Series of runs	L (cm)	d_{50} (µm)	Bed	S	Q (l/min)	w_0 (cm)	#
L110_D75_mb	110	75	mobile	0.017–0.052	0.5–1.3	2.5–8	**37**
L130_D75_mb	130	75	mobile	0.017–0.052	0.5–1.3	2.5–8	**8**
L180_D75_mb	180	75	mobile	0.017–0.052	0.5–1.3	2.5–8	**17**
L130_D160_mb	130	160	mobile	0.017–0.052	0.5–1.3	2.5–8	**18**[1]
L130_D75_sb[2]	130	75	solid	0.017–0.052	0.5–1.3	2.5–8	**25**
L130_D160_mb_sw[3]	130	160	mobile	0.017–0.052	0.5–1.3	2.5–8	**29**

[1] Among this set, two experiments have been made to obtain the topography of the channel (Armstrong and Métivier, 2003).
[2] Experiments initially with a smooth solid bed.
[3] Experiments with solid walls (constant width through time).

within less than 0.7 % with the use of a head tank (Fig. 1). The sediment discharge is measured at the outlet using an overflowing sedimentation tank. The tank remains at constant water level and particles are allowed to settle. A wave protection is placed close to the exit ramp of water in the overflowing tank to absorb surface waves and therefore reduce the scattering in the measure of the mass. The tank is positioned on a high precision weighting device (0.1 g of precision) connected to a PC that collects the weight of the tank at regular time intervals (10 s). This gives access to a precise and direct measure of the cumulated mass at the outlet of the river from which the sediment discharge can be derived. There is no sediment recirculation in these experiments as it is usually done to put the river in an equilibrium state and which prevents excessive degradation at the inlet (Ikeda, 1981; Ikeda et al., 1988; Diplas, 1990; Macky, 1999). The absence of sediment input was found not to change the equilibrium regime at a given distance from the inlet but put the river is globally in an erosional regime (Yalin and Ferreira da Silva, 2001). However to prevent excessive degradation of the bed at the inlet, a stabilisation pool at the entrance of the flume reduces the velocity and degradation of the bed is reduced. A digital video camera is positioned at the vertical of the plane and a movie of each experiment is recorded on a Macintosh computer with a time lapse typically of 30 s that is enough to capture the channel adjustment and which reduces the memory cost on the hard drive. The camera covers a region of about 30 cm wide which corresponds to the best compromise to have the larger area and a good precision for the channel width detection.

The experiment starts from an initial and empty rectangular channel that is molded at a given initial width. The initial cross section is rectangular and the banks are 1cm height. The slope is set to the wanted value. The overflowing

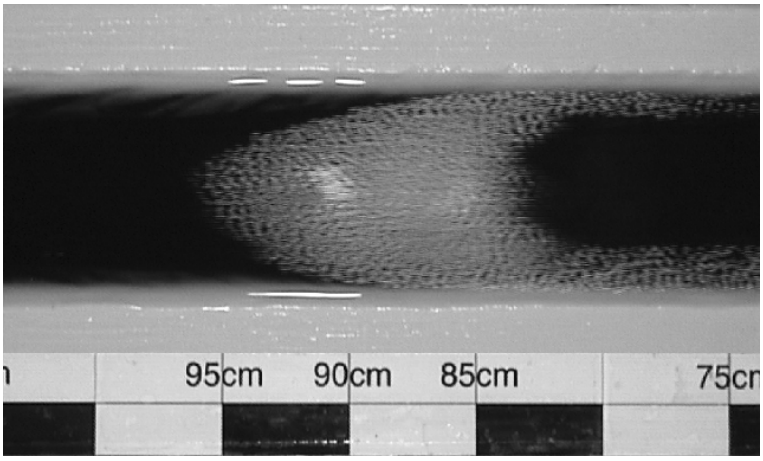

Fig. 2. Typical parabolic shape of the plastic cloud (water is flowing from right to left) in the case of a solid bed where bedload transport is not significant.

tank that collects the sediments at the outlet is filled with water so that the cumulated mass of sediments can be measured as soon as the experiment begins. When all this is set, a constant flow of water at a given discharge is turned on and the experiment starts. A series of 80 experiments (table 1) were conducted under varying water discharge (Q = 0.5–1.3 l/min), grain size (d_{50} = 75 µm or d_{50} = 160 µm), river length (L = 110–180 cm), initial slope (S = 0.017–0.052) and initial width (w_0 = 2.5–8 cm). Experiments would last for 1 to 3 hours. For this study of an adjusting straight river, any experiments would be stopped if starting to meander or having some erosional waves propagating that both put the river in a non straight configuration with variations in the width along the channel of the order of the width. Two additional series of experiments were done (1) with an initial smooth and solid bed using a cardboard as the bed so that just bank erosion could occur (the cardboard is painted in black for better visualisation of sediment transport), and (2) with solid walls to prevent bank erosion but allow for bed erosion and sediment transport (table 1). This was a way in separating arbitrarily the two processes of erosion and to analyze the river evolution of the straight channel when only one erosion process was involved.

Eventually, since precise measures of the velocity could not be achieved in the experiments of an adjusting river due to the large time lapse for the movie acquisition that does not allow to capture the water flow, separated experiments where done to measure the velocity profile of the flow along the stream for the same range of parameters of Q, w_0, S.

2.2 Flow velocities

Surface velocity of the flow is measured using some thin plastic powder that is able to float at the surface of the water (due to both the surface tension of the particles and the density close to 1). Small amount of this powder is deposited at the entrance of the flume so that the flow is disturbed a minimum and to limit inertia effect. The plastic cloud is then advected by the flow downstream and develops a parabolic shape (Fig. 2). Pictures of the powder cloud are recorded by a CCD camera positioned at the vertical of the plane at a constant time intervals (1/25 s). Velocity is deduced by measuring the distance covered by the top of the parabola between two consecutive pictures. Since the camera covers only a small region of the river, pictures are taken at different positions along the reach to provide a complete downstream velocity profile. To have a large number of data, one would follow at least 5 clouds of particles at each position of the camera. Channel widening is negligible during the time these measurements are realized. A set of experiments is done with different values of slope ($S = 0.0175$–0.0524), width ($w = 2.5 \times 10^{-2}$–8×10^{-2} m), water discharge ($Q = 8.3 \times 10^{-6}$–2.2×10^{-5} m^3/s) and length of $L = 1.30$ m. Eventually to characterize the influence of bedload transport in the fluid velocity, the velocity measurements are done in both cases of (1) a mobile bed and (2) a smooth and solid bed with alluvial banks (using a cardboard) where bedload transport did not occur significantly (Fig. 2).

2.3 Description of a representative run

Qualitative observations are presented in this section to give an overview of the main features in the experiments of adjusting straight river. These features are discussed according to the experiments with an initial solid bed for which a mobile bed is rapidly formed from the sediments from bank erosion since they provide some good observations of sediments transfers that occur in the channel (Fig. 3).

As a response to the presence of the water flow, the channel is subject to adjustments that are essentially (1) channel widening and (2) bed aggradation (Fig. 3). The flow depth measured at the outlet is of the order of 1–2 mm and means that the flow is not bankfull (bank height of 1 cm). Bank erosion strictly by the flow occurs in the submerged bank region on a height of $\sim$ 1–2 mm. This erosion induces some destabilisation of the emerged bank region so that the channel enlarges. The distribution in the widening along the stream controls the morphology of the river. First, it is observed that, within the region covered by the camera ($\sim$ 30 cm long), the channel width keeps a uniform distribution during the widening (Fig. 3). Second, over the entire length of

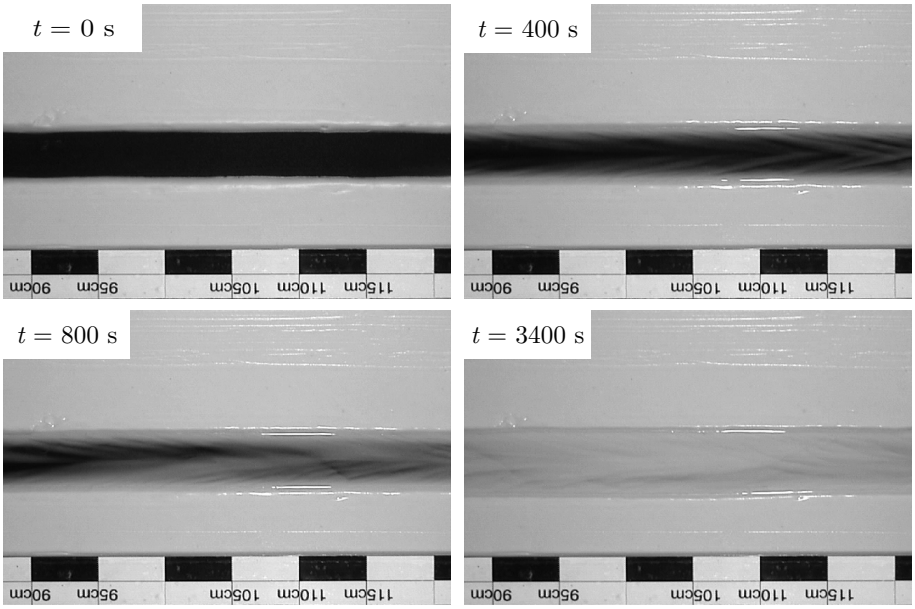

Fig. 3. Channel adjustments: channel widening and bed aggradation. Sediments eroded from the banks are transported towards the center of the channel (existence of secondary currents in the flow). Sediments finish to recover all the channel surface. Note the lateral transport of the bedload developing in the form of fingers.

the river, the channel width tends to increase downstream (this observation is done either "by eye" for a given experiment since the camera does not cover the entire stream or indirectly by comparing two experiments with the same parameters but with a camera at different positions (Fig. 9)) (see companion paper Armstrong and Métivier, 2003). This variation is nevertheless less than about 2 cm per meter (sometimes more for the experiments with B sand of 160 µm) so that the river can be considered to remain straight. This implies that the acceleration of the flow, if it exists, does not have repercussions on the distribution of the erosion:

$$\frac{\partial w}{\partial x} \neq \Phi\left(\frac{\partial v}{\partial x}\right). \tag{4}$$

The velocity profile will be discussed in the section 3.

As the channel widens, sediments are eroded from the banks and provide therefore a net input source of sediments for the river. Sediments from the bank regions are transported towards the center of the bed and tend to recover all the bed. The presence of bed aggradation denotes (1) the existence of secondary currents in the channel bed region in the direction of the center of the channel able to transport sediment in the transverse direction and (2) the fact that the sediments supply from the banks is greater than the transport capacity of the river (at least at the beginning of the experiment). This observation validates our simplification in not having a sediment recirculation apparatus since the input of sediments from the bank erosion prevents degra-

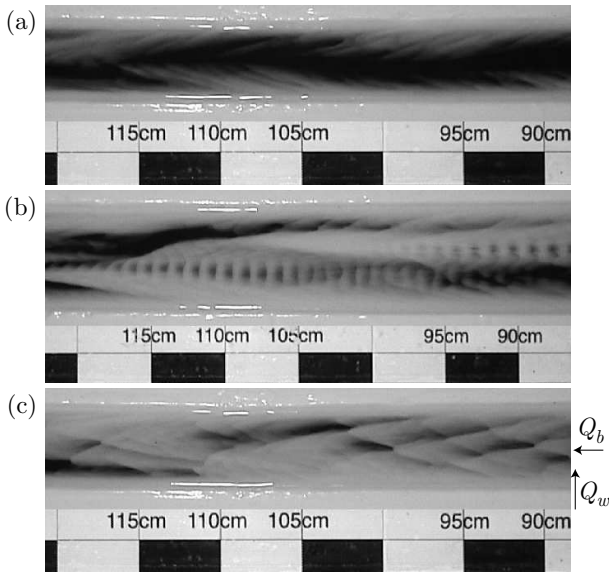

Fig. 4. Bedforms that can generate depending on the parameters (pictures are from different experiments). In chronological order of apparition: (a) analog of alternate bars formed by the lateral sediment transport eroded from the banks (secondary currents in the flow), (b) aligned succession of pools-riffles (free bars) that migrates downstream and can move laterally and (c) multiple raw bars that migrates downstream. Q_w and Q_b are respectively the net input flux from the banks and the net bedload sediment transport.

dation of the bed. Eventually, several types of bedforms develop depending on the value of the parameters (Fig. 4). Sediment transport towards the center can take the form of large alternate bars with a meandering thalweg (Fig. 4a). As another bedform, some succeeding riffles and pools organized in lines can appear (Fig. 4b). At last, multiple raw bars is a common feature when the channel is well developed (Fig. 4c).

These observations show that the channel widening provides a net input flux of sediment on the bed region Q_w. Sediment transport Q_b occurs on the channel bed and due to the presence of secondary currents on the bed region, the bedload transport must have two components: (1) one downstream (2) a second one which can transfert the sediment eroded from the banks towards the center. At last, one can say that the net input flux of sediment from the bank erosion Q_w is at the begining of the experiments larger than the capacity of transport Q_b since aggradation occurs. The relative magnitude of these flux will be discussed later.

2.4 Time evolution of the width

A detailed description of a representative run will give a general overview of the series of experiments, because the features of the experiments did not differ

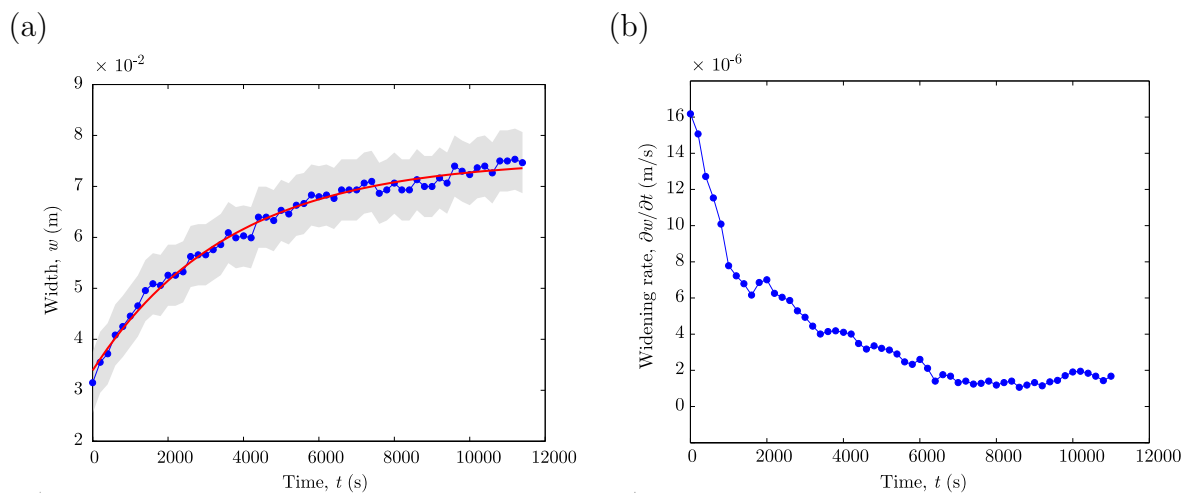

Fig. 5. (a) Variation of free surface width with time at $x = 77$ cm and (b) widening rate in function of time. The shadow region represents the measurement uncertainty and the red curve corresponds to the decreasing exponential of Eq. (5) where the parameters are found to be $w_0 = 3.4 \times 10^{-2}$ m, $W_e = 7.5 \times 10^{-2}$ m and $\tau = 3615$ s. ($S = 0.035$, $Q = 1.0$ l/min, $d_{50} = 75$ µm and $L = 130$ cm)

essentially with each other. We present here the river width evolution in time. Evolution of the mass is discussed in the companion paper (Armstrong and Métivier, 2003).

The free surface width at a given section of the channel is measured on each pictures of a movie of the experiment to obtain the width evolution in time. The width evolution in time is characterized by the existence of an equilibrium width that is reached through a decrease in the widening rate (Fig. 5). The reproducibility of the experiments is verified with several runs with the same boundary and initial conditions: the width evolutions are similar and fall in the uncertainty (Fig. 6). This gives the right to compare experiments between each other [1]. The width evolution in time can be approximated with a decreasing exponential of equation

$$w(t) = (w_0 - W_e) \exp\left(-\frac{t}{\tau}\right) + W_e, \tag{5}$$

where w_0 and W_e are respectively the initial and the equilibrium width and τ is the relaxation time of the enlargement. The exponential relation (5) appears to be a good approximation for the width evolution in time when the experiment starts from a width small enough compare to the equilibrium width (Fig. 5a). In several cases however, the exponential is not accurate and a constant widening is observed with or without reaching an equilibrium width.

[1] In particular, this allow to compare the width evolution from different runs (with the same boundary and initial conditions) measured at different section from the inlet.

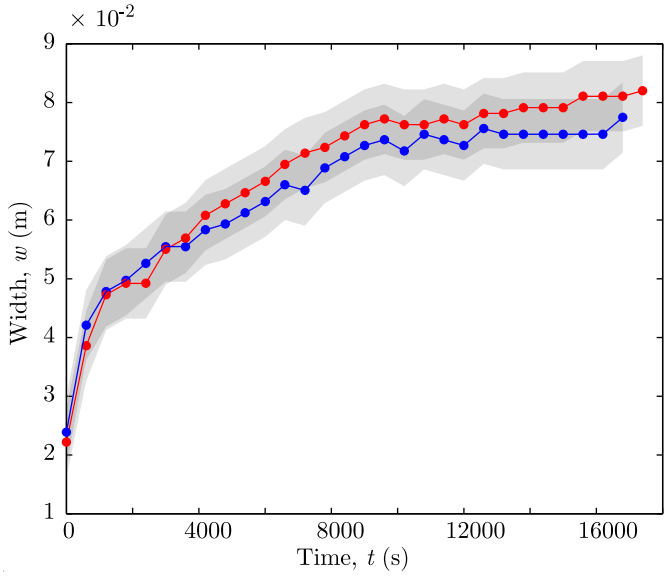

Fig. 6. Reproducibility of the experiments concerning the width time evolution. The two experiments are for the same conditions ($S = 0.035$, $Q = 1.0$ l/min, $d_{50} = 75$ µm and L=130cm at position $x = 40$ cm from inlet) and both fall in the error region (shadow).

First, for experiments starting with an initial width close to the equilibrium width, the channel enlarges at constant rate within less than 1 cm/h so that the river can be considered to have reached a stable state for the width (Fig. 7). Furthemore, as presumed by Schumm et al. (1987) or Yalin (1992), it is verified that the initial width does not change the equilibrium width but only affect the time response in the width evolution (Fig. 7). Second, in some other cases, a widening at constant rate is also observed but without achieving an equilibrium width. This occurs when an experiment gets perturbated by an erosion wave before it reaches its equilibrium width and induces the ending of the experiment (Fig. 8). In such cases, the linear evolution of the width is an artefact that raises from the duration of the experiment that is to short to allow the channel to reach its stable width. The width evolution is nevertheless compatible with an equilibrium width (Fig. 8). These instabilities that generate close to the inlet are more likely to arrive when using the B sand (160 µm) which has a smaller cohesion than with A sand (75 µm) making it easier to erode the banks and increase the sensitivity to velocity gradients in the flow [2]. Instabilities are also susceptible to happen when the flume length is long "enough" (typically for $L = 1.80$ m). These observations must also be related to the "straightness" of the river. It appears that the widening increases in the streamwise direction. As noted in the previous section 2.3, the channel

[2] On the same range of parameters, but with sand of larger diameters (250 µm and more), instabilities in the stream are such that the stream braides (Meunier, 2003).

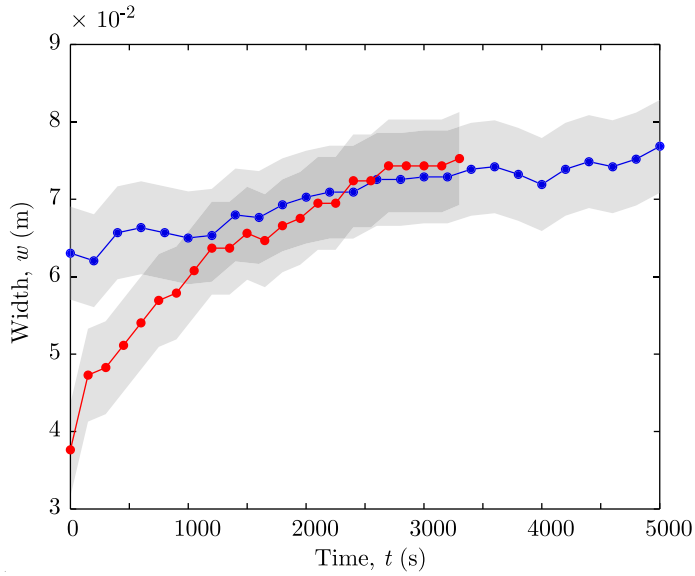

Fig. 7. Same equilibrium width for two experiments with different initial width but same other parameters ($S = 0.0524$, $Q = 1.3$ l/min, $d_{50} = 75$ µm and $L = 1.30$ m).

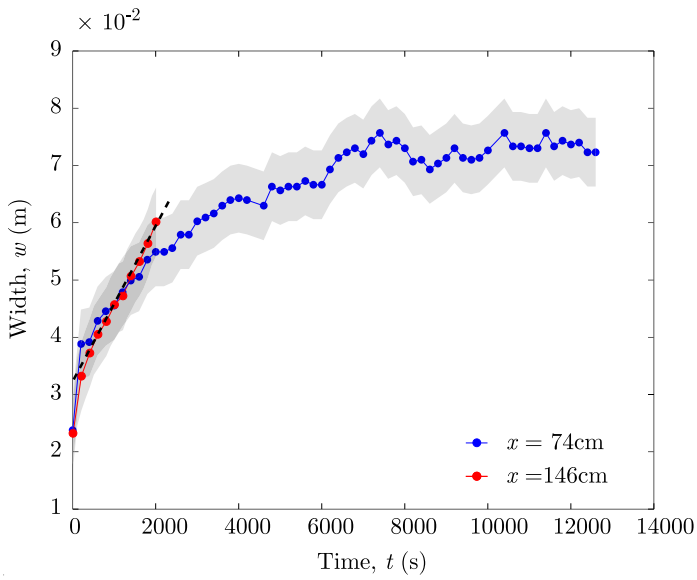

Fig. 8. Constant widening rate (dashed line) compatible with a steady state experiment ($S = 0.052$, $Q = 0.5$ l/min, $d_{50} = 75$ µm).

width increases downstream ($\partial w/\partial x > 0$). This gradient is often negligible (Fig. 9a) and is in other cases less than 1cm/m (Fig. 9b) so that the river can be considered as straight.

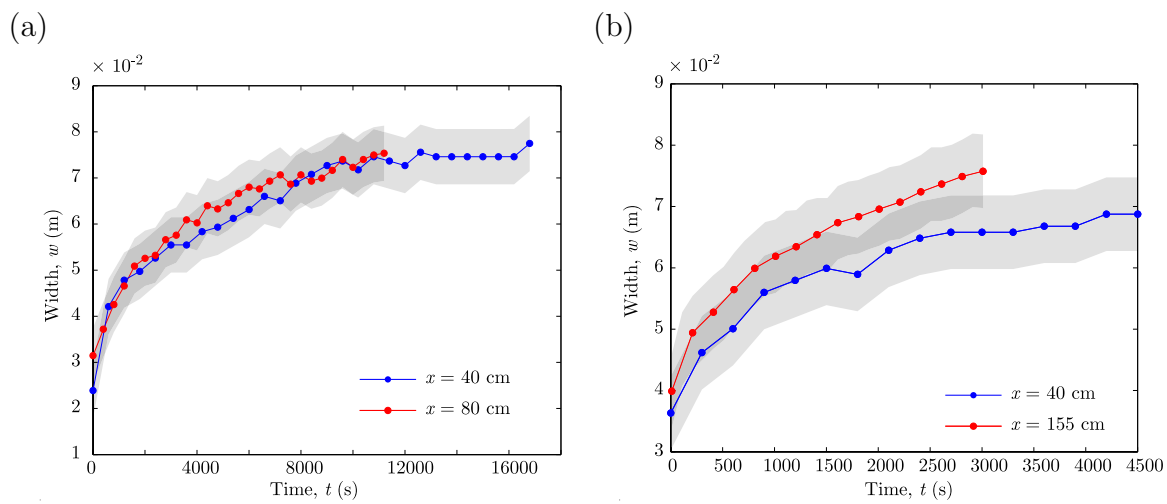

Fig. 9. Width evolution in time at two positions from the inlet in two cases: (a) $S = 0.035$, $Q = 1.0$ l/min, $d_{50} = 75$ µm and (b) $S = 0.052$, $Q = 1.0$ l/min, $d_{50} = 75$ µm.

3 Uniform flow and surface tension effects in microscale experiments

3.1 Results and comparison to uniform flow formulas

Figure 10 shows a typical velocity profile obtained from the measurements. A scattering in the data exists and is certainly due to mass variations between the different particle clouds analysed which induced magnitude variations in the inertia effect. A moving average of the velocity (width of 2 cm) is performed to smooth this scattering. The averaged velocity can be approximated as uniform along the stream (Fig. 10) since acceleration are less than 5 cm/s per meter (which correspond to a 12 % change in the velocity). To the first order, the velocity profile can be considered as constant along the reach within the precision of the measurements. We will therefore consider in the following, the reach averaged velocity $\overline{U}$ which is the mean of the moving averaged velocity along the reach ($\overline{U} = 0.36$ m/s in Fig. 10). The error on the reach averaged velocity is taken to be 2 times the standard deviation of the moving averaged velocity (2σ).

Considering the reach averaged velocity $\overline{U}$ for all the different parameters, one look for a model of uniform velocity that matches the observations. We consider the Chézy and the Manning formulas for uniform flow. Chézy's formula is

$$\overline{U} = c\sqrt{ghS}, \tag{6}$$

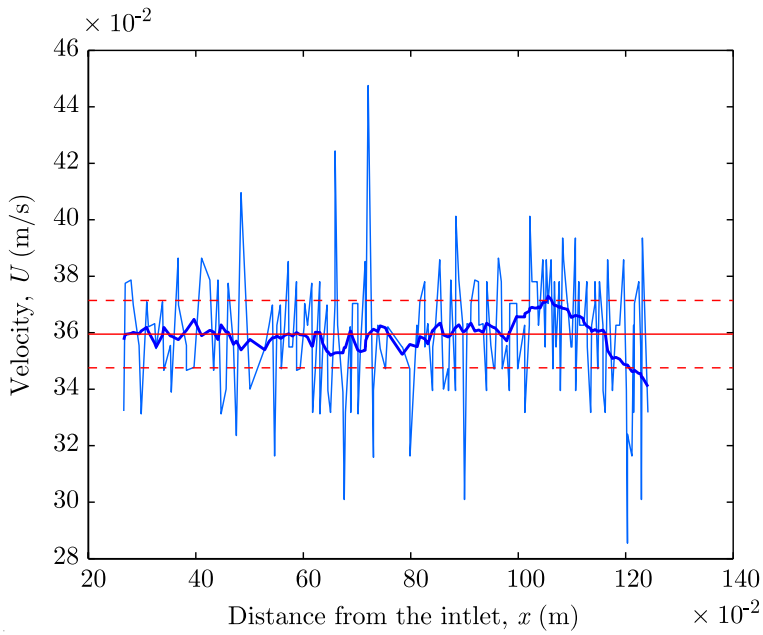

Fig. 10. Downstream velocity profile in the case of a solid bed ($S = 0.0175$, $w = 4 \times 10^{-2}$ m, $Q = 1.67 \times 10^{-5}$ m^3/s and $L = 1.30$ m). In light blue is the measured velocity and in dark blue is the moving average of the measured velocity. The mean velocity $\overline{U}$ is in red and the dashed lines represents the error at 2σ (see text for explanations).

where c is the Chézy friction coefficient that takes into account the roughness and the geometry of the bed, g is the acceleration of gravity, h is the height of the flow (assumed to be constant along the reach) and S is the energy slope also equal to the bed slope in uniform conditions (Chow, 1959). The Manning's formula for uniform flow is supposed to be more realistic and reads (Chow, 1959):

$$\overline{U} = \frac{h^{2/3} S^{1/2}}{n}, \tag{7}$$

where n is the Manning friction coefficient (m$^{-1/3}$ s) that takes into account the roughness and the geometry of the stream. In these two formulas, the flow height, which was not measured, is unknown. Considering the conservation of mass for the flow,

$$Q = \overline{U} W h, \tag{8}$$

where W is the width of the flow, the expressions of the mean velocity can be rearranged for both (6) and (7):

$$\overline{U} = c^{2/3} \left(\frac{gQS}{W} \right)^{1/3}, \tag{9}$$

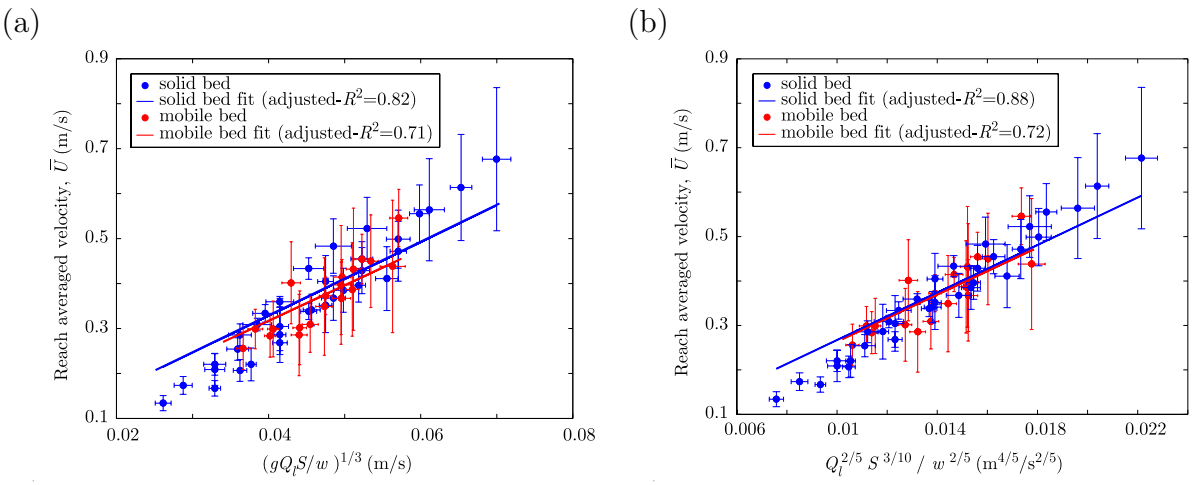

Fig. 11. (a) Chézy model. (b) Manning model. (vertical error of 2σ and horizontal error with $\Delta S = 0.1\,^{\circ}$, $\Delta Q/Q = 0.7$ % and $\Delta W = 0.001$ m).

$$\overline{U} = \frac{1}{n^{3/5}} \left(\frac{Q^{2/3} S^{1/2}}{W^{2/3}} \right)^{3/5}, \tag{10}$$

respectively for the Chezy's formula and the Manning's formula. These equations for the velocity are linear relations of the terms in parenthesis at the power 1/3 and 3/5 to which we will refer respectively as the Chézy term and the Manning term. The reach averaged velocities measured for the different parameters are reported in function of the terms in parenthesis to test these two models. It appears that both the Chézy (Fig. 11a) and the Manning (Fig. 11b) formulas correlate with the measured velocities as they fall at first order close to the linear relations. Differences in the cases of the mobile bed and of the solid bed are not significant which means that the effects on the velocity of (1) bed roughness variation and of (2) the loss of energy of the flow due to sediment transport are negligible in our experiments. The estimation of the Chezy coefficient (Fig. 11a) and of the Manning coefficient (Fig. 11b) is obtained from the slope of the adjusted lines of equations (9) and (10). Table 2 reports the Chézy and Manning coefficients estimated from the linear fit.

However, looking closely at the data, a systematic shift is observed from the Chézy and Manning model (Fig. 11). Data appears to be aligned but with

Table 2
Chezy and Manning coefficients estimated from the measurements of the velocity.

Model	Coefficient	Dimension	Solid bed	Mobile bed	Solid & Mobile bed
Chézy	c	–	23.4	22.2	23.0
Manning	n	$m^{-1/3}$ s	4.2×10^{-3}	4.3×10^{-3}	4.2×10^{-3}

a larger slope, meaning a linear correlation which does not extrapolate to a vanishing velocity at $Q = 0$ but to a negative value:

$$\overline{U} = 12.1 \left(\frac{gQS}{W} \right)^{1/3} - 0.20 \qquad \text{(Chézy)}, \tag{11}$$

$$\overline{U} = 36.7 \left(\frac{Q^{2/3} S^{1/2}}{W^{2/3}} \right) - 0.15 \quad \text{(Manning)}. \tag{12}$$

These empirical relationships can be used in our experiments to predict the velocity at given slope, water disharge and width. Surface tension effects are suspected to be responsible in modifying the flow. This problem is addressed in the following section.

3.2 Uniform flow and surface tension effects in the microscaled experiments

Surface tension is not taken into account in the uniform flow formulas of Chézy and Manning. In natural streams for which these formulas were developed, the amplitudes of surface tension forces are orders of magnitudes less than either buoyancy or inertia and gravity and shear are only considered. In the microscale experiments, however, surface tension forces are suspected to be significant in their effects on the flow velocity. Surface tension forces appear at the interface of two fluids that is at the free surface of the flow and can have only an indirect effect on the sediment transport that occurs on the bed (Rouse number less than 1). The Weber number quantifies the ratio of inertia to surface tension in a moving fluid and can apply to the case of channel flow (Peakall and Warburton, 1996; Métivier and Meunier, 2003). It is defined as

$$\mathrm{We} = \frac{\rho u^2 h}{\gamma}, \tag{13}$$

where ρ is the fluid density; u is the velocity of the flow; h is the flow depth and γ is the surface tension ($[\gamma] = \mathrm{F{\cdot}L^{-1}}$ and $\gamma = 0.07$ N/m in the case of water-air). Unfortunatly, as suggested by Peakall and Warburton (1996), there is no current consensus on the value of the critical Weber number where surface tensions begins to strongly influence sediment transport and deposition. Suggested values range from 10 to 100. However, in our experiments, the flow depth is millimetric and the Reynolds number indicates that the flow is in the transitionary regime from laminar to turbulent (Re$\sim$ 120–600). Surface tension can be significant and oppose the flow through constriction of the laminar water film on the surface of the bed.

In order to estimate the effect of surface tension on the uniform flow in the microscale experiments, one addresses the following idea that the existence of active surface tension in the flow can be indirectly highlighted if, on a

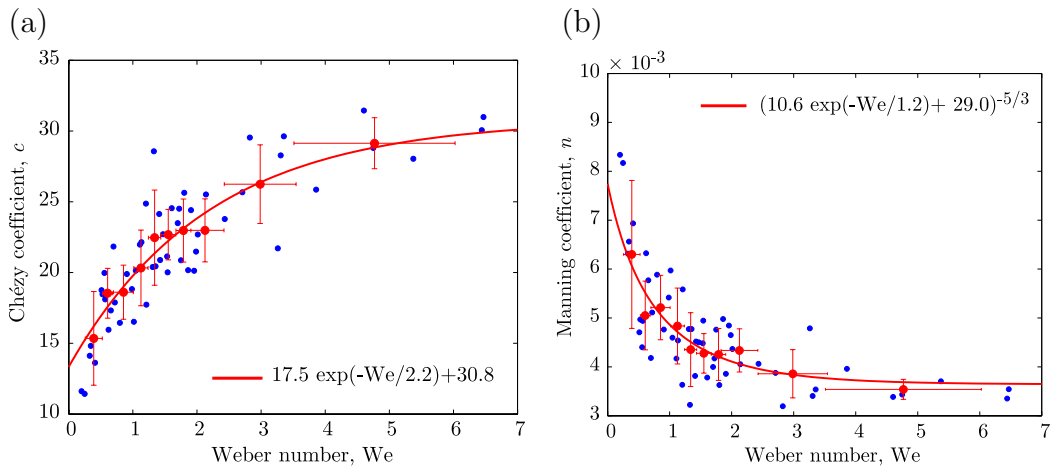

Fig. 12. (a) Chézy coefficient in function of the Weber number. (b) Manning coefficient in function of the Weber number. Blue symbols are the data and red symbols represent the running averaged of the data. Red curves represent a decreasing exponential fit of the mean data.

sufficiently large range of Weber number, non-linear variations of the ratio of the measured velocity over the Chézy formula are observed. The stream averaged velocity $\overline{U}$ (for which we will refer now as u) is therefore scaled with the Chézy term of Eq. (9). This yields

$$\upsilon = \frac{u}{\left(\dfrac{gQS}{W}\right)^{1/3}} \quad (= c^{2/3}), \tag{14}$$

which is dimensionless and equal to the coefficient of friction at the power of 2/3. This relation can be written as an expression for the Chézy friction coefficient:

$$c = \frac{u^{3/2}\, W^{1/2}}{(gQS)^{1/2}}. \tag{15}$$

The friction factor is known to depend at first order on the grain size and the roughness of the bed and can be assumed to be independent on the flow conditions. Therefore, in the case where the surface tension is negligible, the Chézy coefficient Eq. (15), should be always equal to a constant for flows on the same material but with different discharges and slopes. On this basis, variations of the Chézy coefficient, if they exist, can be interpreted as due to the effect of surface tension only. The Weber number Eq. (13) can be estimated using the conservation of fluid mass $Q \approx uWh$ for one-dimensional uniform flow. It follows

$$\mathrm{We} = \frac{\rho u Q}{W\gamma}, \tag{16}$$

Therefore, the dimensionless relation

$$c = \phi(\mathrm{We}), \tag{17}$$

where ϕ is an unknown function, should indicate possible effect of surface tension if displaying a non constant evolution. For large Weber number where surface tension is negligible, this function should be a constant. The form of the relation Eq. (17) can be estimated in our experiments plotting the Chézy coefficient Eq. (15) in function of the Weber number Eq. (16) calculated with the velocities measured in our experiments (Fig. 12a). A general trend in the data denotes that for We larger than ~ 4, the Chézy coefficient asymptotes a constant, *i. e.* surface tension are negligible and the flow is uniform. In the contrary, as the Weber number gets smaller (We< 4), the Chézy coefficient decreases. This decrease in the coefficient can be attributed to the surface tension.

The same discussion can be made with the Manning formulation for uniform flows as the Manning coefficient depends at first order on the grain size and bed roughness and may be asssumed to be independent on the flow conditions. Scaling the measured velocity with the Manning term in Eq. (10), one arrives with an expression of the Manning coefficient which is not dimensionless ($\mathrm{m}^{-1/3}$ s):

$$n = \frac{Q^{2/3} S^{1/2}}{u^{3/5} W^{2/3}}. \tag{18}$$

The dependance of this term with the Weber number Eq. (16) presents the same characteristics, but inverted since n is the inverse of the Chézy (Fig. 12b). Estimation of the Chézy friction coefficient and of the Manning coefficient from the adjustment of an exponential curve (Fig. 12) are found to be close (Table 3) to the values found in the previous section (Table 2). The empirical relationships for the Chézy and the Manning coefficients in function of the Weber number are respectively:

$$c = 17.5 \exp\left(\frac{-\mathrm{We}}{2.2}\right) + 30.8, \tag{19}$$

$$n = \left[10.6 \exp\left(\frac{-\mathrm{We}}{1.2}\right) + 29.0\right]^{-5/3}. \tag{20}$$

Although these coefficients can be corrected from the surface tension effects, the general form of the Chézy and Manning formula remain the same.

Table 3
Chezy and Manning coefficients estimated from the Weber analysis.

Model	Coefficient	Dimension	Value
Chézy	c	–	30.8
Manning	n	$\mathrm{m}^{-1/3}$ s	3.7×10^{-3}

4 Scaling of the microscale experiments

4.1 Dimensional analysis of the bed load transport problem and similarity of the experiments

The present analysis is restricted to two-dimensional, uniform flow over a plane bed composed of uniformly sized, granular, cohesionless particles of similar shape. For such a flow, the sediment discharge can be expressed as

$$q_s = f(h, d_{50}, S, \rho, \rho_s, \nu, g), \tag{21}$$

where q_s is the sediment discharge per unit width; f denotes a function; h is the depth of flow; d_{50} is the median diameter of the bed particle; S is the water surface of the uniform flow; ρ is the density of fluid; ρ_s is the material density of the bed particles; ν is the kinematic viscosity of the fluid; g is the acceleration of gravity. The gravitational acceleration can be replaced by the shear velocity u_* because $u_* = \sqrt{ghS}$, and ρ_s can be replaced by the submerged specific weight of the bed material $\gamma_s = g(\rho_s - \rho)$. Substituting these replacements into Eq. (21) results in

$$q_s = f_1(h, d_{50}, S, \rho, \gamma_s, \nu, u_*), \tag{22}$$

where f_1 denotes another function. According to the Π theorem, one obtains the dimensionless equation

$$\frac{q_s}{u_* d_{50}} = f_2(\mathrm{Re}_* \tau_*, H, S), \tag{23}$$

where f_2 denotes another function; $\mathrm{Re}_* = (u_* d_{50})/\nu$ is the grain Reynolds number; $\tau_* = (\rho u_*^2)/(\gamma_s d_{50})$ is the Shields stress; and $H = h/d_{50}$. Multiplying both side of this relation by $\sqrt{\rho u_*^2/\gamma_s d_{50}} = \sqrt{\tau_*}$, we obtain

$$q_s^* = \frac{q_s}{\sqrt{\mathscr{R} g d_{50}^3}} = \phi_{q_s}(\mathrm{Re}_*, \tau_*, H, S), \tag{24}$$

with $\phi_{q_s} = \sqrt{\tau_*} \cdot f_2$ and $\mathscr{R} = (\rho_s - \rho)/\rho$. The dimensionless combination on the left is the expression of the dimensionless Einstein's sediment discharge q_s^* (Einstein, 1942). At inception of sediment transport, q_s is just zero, and H is

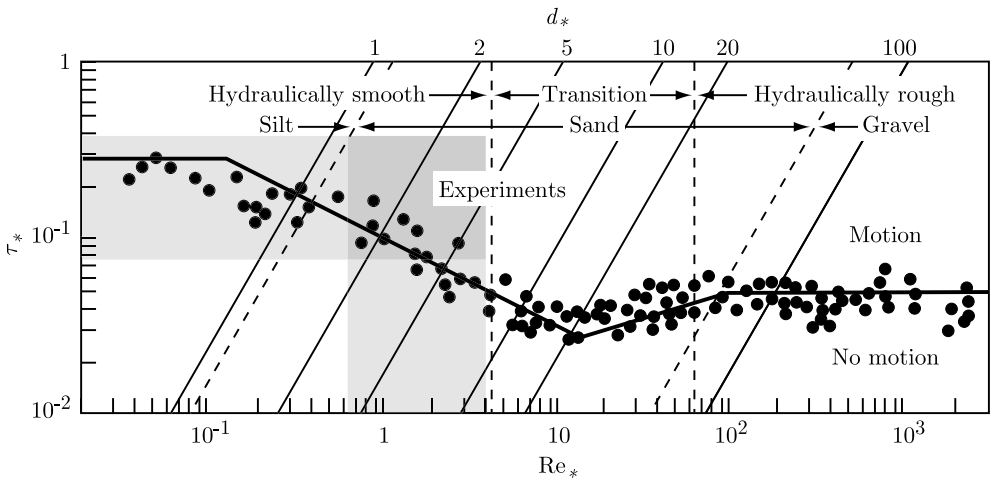

Fig. 13. Shields' curve (after Julien, 1994).

not a determining parameter as the initiation of motion is entirely due to the action of the flow in the vicinity of the bed (Bettes, 1984; Yalin and Ferreira da Silva, 2001). One obtains from Eq. (24)

$$\phi_{q_s}(Re_{*_c}, \tau_{*_c}, S) = 0 \quad \text{i.e.} \quad \tau_{*_c} = \Phi(\mathrm{Re}_{*_c}, S), \tag{25}$$

which is Shields' transport inception function with $S = 0$. In the microscale straight river, flow heights are estimated to be of the order of the millimeter ($h \sim 1$–2 mm). With the value of S and d_{50} in the experiments and with the kinematic viscosity of water $\nu = 1.1 \times 10^{-6}$ m^2·s^{-1}, the grain Reynolds number falls in the range:

$$\mathrm{Re}_* = 0.6\text{–}4.7. \tag{26}$$

The Shields stress τ_*, with $\rho_s = 2481$ kg·m^{-3}, is found to have the values

$$\tau_* = 0.08\text{–}0.44. \tag{27}$$

For the transport of sediment, the experiments of microscale river falls in the range of the natural silt and sand bed rivers (Fig. 13). Furthermore, the grain Reynolds number and the Shields number are above the Shields' curve so that sediment transport can occur.

4.2 Dimensional analysis of the equilibrium width in experimental and natural rivers

To understand the problem of the equilibrium width of alluvial rivers, it is of importance to define the parameters involved in the process and perform a dimensional analysis in order to be able to see (1) what characteristic scales can be defined in the problem, (2) the functional dependence that is to be

expected from the different fores driving the dynamics of the system and (3) if the small scale experiment can reasonably account for natural processes.

We seek the characterization of the equilibrium width W_e with physical properties of the fluid and sediment and with some river parameters. Physical properties include the density of water ρ, the density of sediments ρ_s, the fluid viscosity ν. The gravity field is the driving force and scales according to the acceleration of gravity g. Two geometric scales at least are involved, the grain size d_{50} and the height flow at equilibrium h_e. The slope of the equilibrium channel S_e is also considered. The mean flow discharge in natural stream Q (equivalent to the constant water discharge in the experiments) must be taken into account. The friction factor of the regime channel c characterizes the flow resistance through the general Chézy relation

$$u = cu_* = c\sqrt{gh_eS_e}. \tag{28}$$

One considers the specific weight of grains in water $\gamma_s = (\rho_s - \rho)g$, instead of the grain density ρ_s.

The equilibrium width is at first sight determined by nine parameters:

$$W_e = \Phi(Q, \rho, \gamma_s, \nu, g, d_{50}, c, S_e, h_e). \tag{29}$$

To reduce the number of parameters, we assume that in alluvial rivers in grade, the Shields stress is slightly above its critical value for motion inception. This is known to be the case in gravel bed rivers (Parker, 1978b; Andrews, 1984) but it is a rather crude assumption for sand bed river as is it known that the Shields stress is larger than critical values. For the microscale river, Shields stress can be above the critical values but also fall close to the curve (Fig. 13). Again, we assume that for the microscale river and for other experimental channels, this hypothesis apply. Note that Yalin and Ferreira da Silva (2001) consider the critical shear velocity as a parameter for the derivation of the regime relations which turns out to be the same hypothesis as ours by the definition of the shear velocity $u_* = \sqrt{\tau_0/\rho} = \sqrt{ghS}$. If it is true, the Shields relation Eq. (25) is verified for all gravel bed, sand bed and experimental channels when in grade:

$$\frac{\rho g h_e S_e}{\gamma_s d_{50}} = \Phi\left(\frac{\sqrt{gh_eS_e}d_{50}}{\nu}\right), \tag{30}$$

and it is clear that d_{50} (or h_e) is a function of ρ, g, S_e, ν, γ_s and h_e (or d_{50}) only:

$$d_{50} = f_d(\rho, g, h_e, S_e, \nu, \gamma_s) \quad (\text{or} \quad h_e = f_{h_e}(\rho, g, d_{50}, S_e, \nu, \gamma_s)\ ). \tag{31}$$

These two relations imply that d_{50} and h_e are not independent and one of

them can be eliminated from Eq. (29). Substituting Eq. (31) in (29), the equilibrium width can be expressed as

$$W_e = \Phi(Q, \rho, \gamma_s, \nu, g, c, S_e, \lambda), \tag{32}$$

where λ is either h_e or d_{50} and where the height parameters are now independent. According to Buckingham theorem, Eq. (32) can be put in a dimensionless form with five dimensionless numbers

$$\frac{W_e}{\lambda} = \phi_\lambda(Q_*, \mathrm{Re}, \mathscr{R}, S, c), \tag{33}$$

where

$$Q_* = \frac{Q}{\sqrt{g\lambda}\,\lambda^2}, \tag{34}$$

is the dimensionless fluid discharge,

$$\mathrm{Re} = \frac{\sqrt{g\lambda S}\,\lambda}{\nu}, \tag{35}$$

is analog to a Reynolds number and

$$\mathscr{R} = \frac{\gamma_s}{\rho g} = \frac{\rho_s - \rho}{\rho}, \tag{36}$$

is the specific density of sediments. Eq. (33) is the general form of the regime relation for the equilibrium width. The equilibrium width is supposed to be a function of the five dimensionless numbers defined above. Constraints on this function can be obtain through the confrontation with data of natural and experimental rivers for which the relationship should apply.

We will see in the next section how the use the grain size d_{50} is dangerous for a scale law for the equilibrium width as it induces non-physical relationships, and how the use of the depth flow comes out naturally in uniform flow.

4.3 Uniform flow in rivers : with or without the grainsize

For each experiment, we obtained the width evolution (Fig. 5). As can be seen, $W(t)$ tends towards a constant value which indicates that the channel as reached an equilibrium width. Value for this equilibrium is obtain by the fit of the width curve with a decreasing exponential. We consider herein experiments done with varying slope, length and water discharge at a given grain size.

Observations of experiments with constant grain size and varying discharge and slope show that the equilibrium width, W_e is coherent with Leopold's

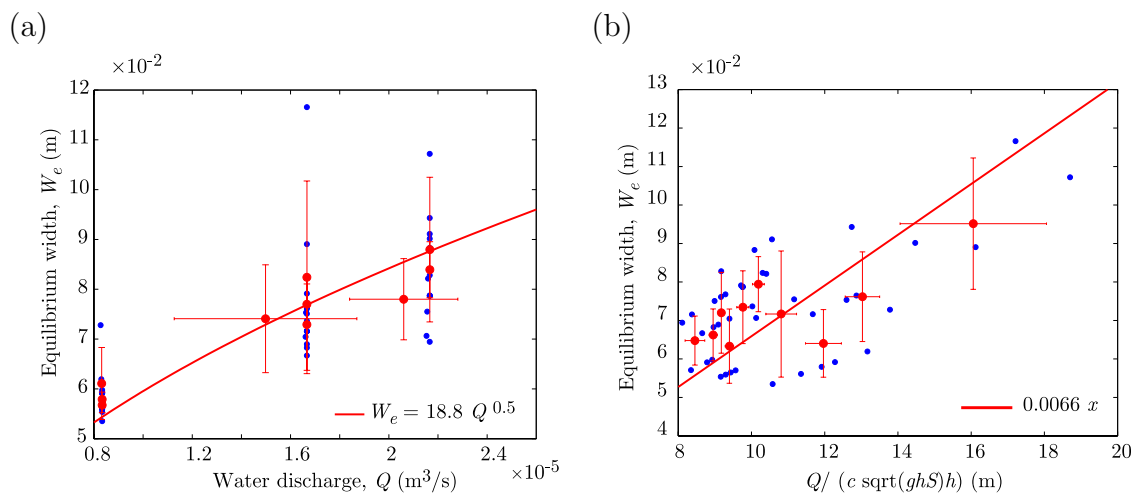

Fig. 14. (a) Equilibrium width of the microscale river in function of the water discharge for experiments of various slope and grain size of 75 µm. (b) Equilibrium width in function of the water discharge-square root ratio for the same experiments. Blue symbols represent the data and red symbol are the running averaged of the data. The fits (red curves) are estimated on the mean data.

regime relation at first order (Fig. 14a). A scattering in the data at given discharge is certainly due to the slope. Microscale rivers has uniform flow as shown in section 3 and the velocity can be estimated from the Chézy relation,

$$u = c\sqrt{gh_eS_e}. \tag{37}$$

where the friction coefficient depends on the Weber number. Considering the conservation of fluid mass, $Q = uW_eh_e$, an expression for the width is obtained from Eq. (37):

$$W_e = \frac{Q}{c\sqrt{gh_eS_e}h_e}, \tag{38}$$

which denotes the influence on the slope but also on the grain size and surface tension through the Chézy friction. Neglecting the variations on the friction coefficient due to surface tensions which are of second order, one tests for the validity of Eq. (38) for our experiments with $c = 30.8$ (Table 3) and with the flow depths estimated from the empirical relationship for the velocity Eq. (11) and from the conservation of fluid mass. The data show a general trend indicating an linear correlation in accordance with Eq. (38) and the scattering is certainly due to the effects of surface tension (Fig. 14b). This relation, however, to be significant for natural stream must be extended for a larger range of values (Yalin, 1992). We consider in the following, the case of natural and experimental streams.

Empirically, it has been established that the channel width in regime rivers can

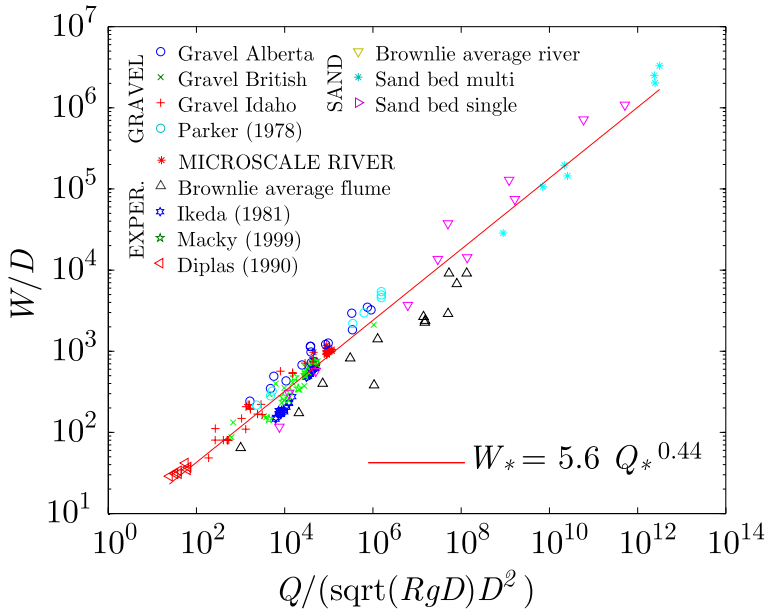

Fig. 15. Dimensionless width vs. dimensionless water discharge for natural gravel and alluvial streams and our experiments (RMSE= $6 \cdot 10^4$).

be related to the water discharge both scaled with the sediment size (Parker, 1979; Ikeda, 1981):

$$\frac{W_e}{d_{50}} \sim 4.4 \left(\frac{Q}{\sqrt{\mathscr{R} g d_{50}} d_{50}^2} \right)^{0.5} . \tag{39}$$

Confrontation of this relation to data from natural sand and gravel bed rivers and from experimental rivers shows a good consistency (Fig. 15). Noticing that the right term in brackets is equal to $Q_*/\sqrt{\mathscr{R}}$, this relation gives an expression of the unknown function in Eq. (33) in the case $\lambda = d_{50}$, and the function ϕ_d can be rewritten as a product:

$$\frac{W_e}{d_{50}} = \phi_d(Q_*, \mathrm{Re}, \mathscr{R}, S, c) = f(Q_*, \mathrm{Re}, \mathscr{R}, S, c) \cdot \left(\frac{Q_*}{\sqrt{\mathscr{R}}} \right)^{0.5} , \tag{40}$$

where f is a function of the dimensionless number equals to 4.4 that should depend on the dimensional number and In particular on the slope. It is expected that dependance of f on Q_* and $\mathscr{R}$ to be of second order. Confrontation of this relation to data from natural sand and gravel bed rivers and from experimental rivers shows a good consistency (Fig. 15). Although this scaling verifies the traditional dependency of the width to the square root of the water discharge Leopold and Maddock (1953), it is not entirely satisfying as both dimensionless width and discharge varies over a large order of magnitude. Using the sediment size, that covers the range of fraction of mm for sand bed rivers to several centimeters for gravel bed rivers, can explain that the data gets linearized. This would be an artefact. With this scaling law, natural gravel bed rivers are separated from sand bed rivers. Data from Brownlie are mixture

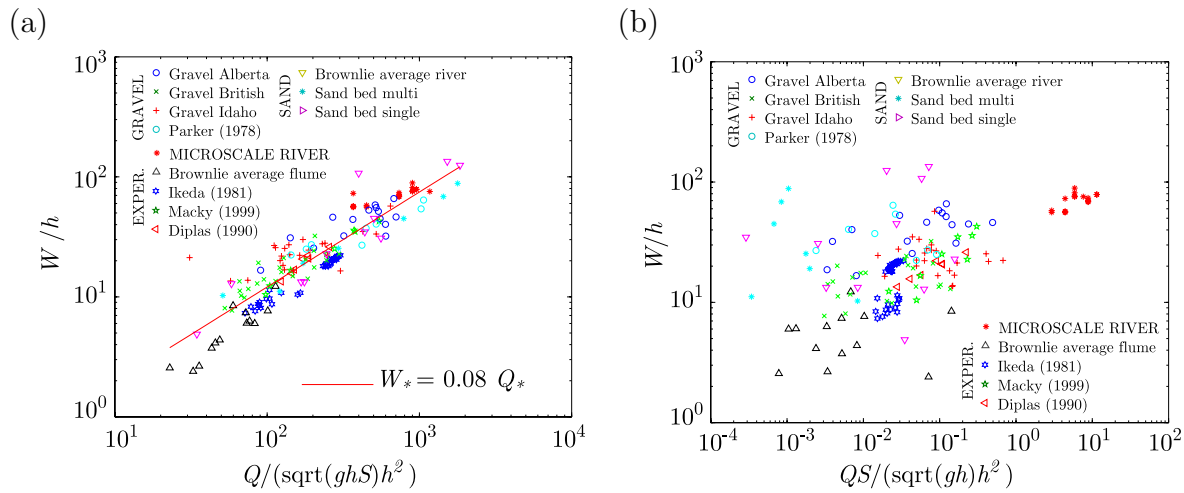

Fig. 16. (a) Dimensionless width vs. dimensionless water discharge based on the flow height (RMSE=12.0).(b) Unphysical relation with flow height.

from gravel and sand bed rivers. At last, experimental data (from ikeda: big flume, to us: microflume) falls in the range of the gravel beds (left of plot).

Eq. (38) can be rearranged into

$$\frac{W_e}{h_e} = \frac{Q}{c\sqrt{gh_eS_e}h_e^2}, \tag{41}$$

which is dimensionless. This relation is a special case of the dimensionless relation Eq. (33) in the case $\lambda = h_e$ and using the product of the dimensionless numbers $Q_*/c\sqrt{\mathscr{R}S}$ equal to the right term in Eq. (41)

$$\frac{W_e}{h_e} = \phi_{h_e}\left(\frac{Q_*}{c\sqrt{\mathscr{R}S}}\right). \tag{42}$$

This relation is similar to the previous scaling law with the flow height as a length scale instead of the grain size. The grain size dependance is included in the Chézy coefficient. It also now depends on the bed slope which was not the case before. In order to test the validity of Eq. (41), this relation is plotted for the case of several gravel bed rivers, sand bed rivers and flume experiments. Figure 16a presents this relation assuming the Chézy coefficient as a constant. It appears that it works without assuming the Chézy factor dependant on the d_{50}. Using a Manning-Strickler law does not bring any significant amelioration.

Both scale law for the width with the grain size or the depth flow show a good relation with data. The former is empirical and the latter has the advantage of being derived in the case of uniform flow. We now show that the former can bring some eroneous correlations. Based on Eq. (41), the width varies as the inverse of the square root of the slope. This dependance since its comes

from uniform is considered as the "physical" dependance of the width. One can introduce this dependance in the empirical relation for the width since it remains dimensionless:

$$\frac{W_e}{d_{50}} = f\left(\frac{Q}{\sqrt{\mathscr{R} g d_{50} S} d_{50}^2}\right), \tag{43}$$

where f is a function. The same previous data from natural and experimental streams plot coherently with this physical empirical relation (Fig. 17a). By comparison, one can also consider a non-physical empirical relation proportional to the slope:

$$\frac{W_e}{d_{50}} = h\left(\frac{QS}{\sqrt{\mathscr{R} g d_{50}} d_{50}^2}\right), \tag{44}$$

were h is a function. Data from natural and experimental streams plot coherently with this latter relation (Fig. 17b). By comparison, the relation $QS/\sqrt{gh}h^2$ does not correletate the data (Fig. 16b). This non coherent result suggests the possible existence of an artefact when using the grain size. To proove this, consider the following explanation. If one consider that the grain size is the parameter that varies the most in Eq. (39), the other parameters can be assumed as constant in front of the grain size and Eq. (39) can be written as

$$\frac{c_1}{d_{50}} = \frac{c_2}{d_{50}^{5/2}}, \tag{45}$$

where c_1 and c_2 are two constants. Letting, $\delta = 1/d_{50}^{5/2}$, Eq. (45) may be rewritten as

$$\delta^{2/5} = \frac{c_2}{c_1}\delta. \tag{46}$$

The exponent $2/5 = 0.4$ is close to the exponents found in the various correlations in Figs. 15 and 17 suggesting that those plots reflects this effect of the grain size.

5 Conclusion

An empirical relationship is proposed for the velocity in function of the Weber number which allows to assess the effect of surface tension. In this relation, the flow velocity is scaled with a characteristic velocity that comes from the Chézy formula. It shows that for a given grain size, the presence of surface tension become significant when We is less than about 4 and has the effect of slowing down the flow. The presence of sediment transport in microscale

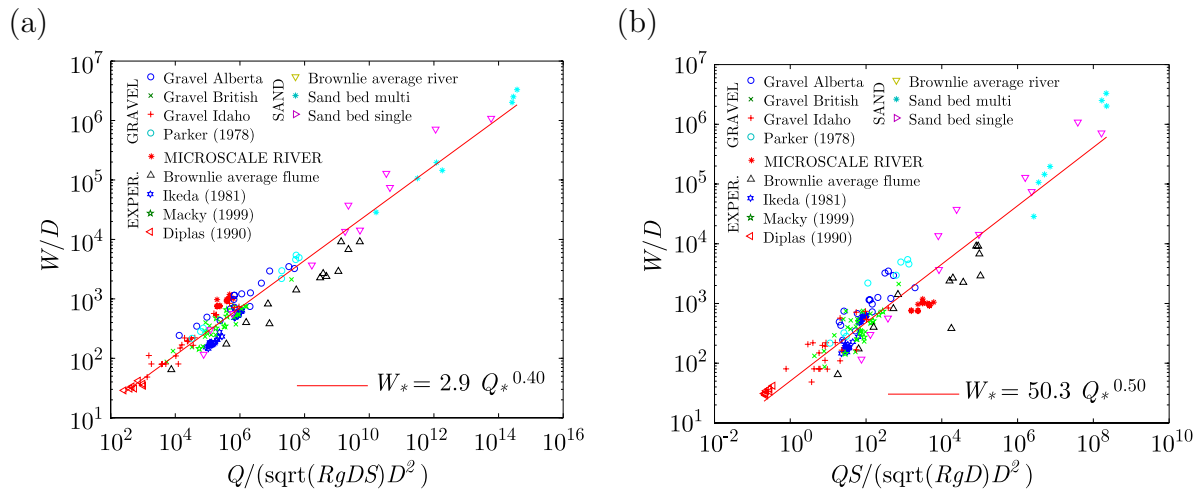

Fig. 17. (a) Physical relation with grain size (b) Unphysical relation with grain size.

experiments where We< 4, tend to proove that surface tension are present but do not affect the bedload transport as presumed by Métivier and Meunier (2003).

The flow in the microscale straight river is measured to be uniform but do not follow a strict Chézy formula. Surface tension are taken into account with the modified Chézy formula defined in the companion paper (Armstrong and Métivier, 2003).

Dimensional analysis of the regime width in alluvial rivers shows two possible characteristic length scale and is in agreement with empirical scale law with the grain size. In alluvial rivers where the flow is uniform, a hydraulic relation of the aspect ratio of the flow can be derived. This relation shows a little scatter of data from different natural rivers and experimental streams and collapse the sand bed rivers with the gravel bed rivers. It provides also a physical relation for the width with in particular a dependance that is to be expected to be function of the inverse of the square root of the slope. Introducing this factor in the empirical relation of Parker works. But having the slope on the numerator in the empirical relation works also. This prove that the scaling in this empirical relation with the use of the grain size, may not be accurate as it leeds to unphysical correlation. The large variability of the grain size can explain this artefact in the correlations.

Our microscale river, according to the Shields, diagram are comparable to silt rivers. But, with the empirical width relation, they fall in the region of the gravel beds. The uniform width relation answer partly to this incompatibilty since the microscale rivers are mixed up with the sand and gravel bed rivers.

References

Andrews, E. D. (1984). Bed-material entrainment and hydraulic geometry of gravel-bed rivers in Colorado. *Geol. Soc. Am. Bull.*, 95:371–378.

Armstrong, L. and Métivier, F. (2003). Independence of sediment flux and width evolution through time in a microscale straight river channel. Part 2. Implications on the conservation of mass and stream section evolution. *in prep.*

Bettes, R. (1984). Initiation of sediment transport in gravel streams. *Proc. Inst. of Civ. Engrs*, 77:79–88.

Blench, T. (1957). *Regime behaviour of canals and rivers.* Butterworth, London, England.

Blondeaux, P. and Seminara, G. (1985). A unified bar-bend theory of river meanders. *J. Fluid Mech.*, 157:449–470.

Chow, V. T. (1959). *Open-channel hydraulics.* Mc Graw-Hill.

Diplas, P. (1990). Characteristics of self-formed straight channels. *J. Hydr. Engrg.*, 116:707–728.

Einstein, H. A. (1942). Formulas for the transportation of bed load. *Trans. Am. Soc. Civ. Eng.*, 107:561–597.

Hack, J. T. (1960). Interpretation of erosion topography in humid temperate regions. *aam*, 258A:80–97.

Ikeda, S. (1981). Self-formed straight channels in sandy beds. *J. Hydrol. Div.*, 107:389–406.

Ikeda, S., Parker, G., and Kimura, Y. (1988). Stable width and depth of straight gravel rivers with heterogeneous bed materials. *Water. Resour. Res.*, 24:713–722.

Inglis, C. C. (1949). The behaviour and control of rivers and canals. Technical Report 13, Central Waterpower Irrigation and Naviagation Research Station, India Research Publication.

Julien, P. Y. (1994). *Erosion and sedimentation.* Cambridge University Press.

Lacey, G. (1930). Stable channels in alluvium. *Proc. ICE*, 229:259–270.

Leopold, L. B. and Maddock, T. J. (1953). The hydrolic geometry of stream channels and some physiographic implications. *U. S. Geol. Survey. Professional Paper*, 252.

Mackin, J. H. (1948). Concept of the graded river. *Geol. Soc. Am. Bull.*, 59:463–512.

Macky, G. H. (1999). Large flume experiments on the stable straight gravel bed channel. *Water. Resour. Res.*, 35:2601–2603.

Métivier, F. and Meunier, P. (2003). Input and output mass flux correlations in an experimental braided stream. Implications on the dynamics of bed load transport. *J. Hydrol.*, 271:22–38.

Meunier, P. (2003). *Transport de sédiments dans une microrivière à tresses.* PhD thesis, Université Paris VII. (in preparation).

Parker, G. (1978a). Self-formed straight rivers with equilibrium banks and mobile bed. Part 1. The sand-silt river. *J. Fluid Mech.*, 89:109–125.

Chapter 4

Time Evolution of a Straight River Channel

4.1 Time evolution of a straight river channel

Independence of sediment flux and width evolution through time in a microscale straight river channel. Part 2. Implications on the conservation of mass and stream section evolution

Lawrence Armstrong * and François Métivier

Institut de Physique du Globe de Paris, Laboratoire de Dynamique des systèmes Géologiques, Groupe de Recherche sur l'Érosion de les Eaux Continentales, 75252, Paris Cedex 05, France

Abstract

We report experiments on a microscale river channel evolution through time. The overall balance of mass is kept negative through the absence of sediment feeding at the inlet. An erosional regime is thus established. It is shown that such channels can nevertheless achieve equilibrium at a certain distance from the inlet (Armstrong and Métivier, 2003). There is in any case rapid establishment of a time independence between the mass flux of bed load (that becomes constant) and the evolution of the river width. Implications of our experiments are that (a) Bed load is globally proportional to water discharge for any given slope and grain diameter; (b) This consequence is in agreement with both uniform flow conditions and stream power dependance of the sediment flux; (c) A relationship for the bankfull river section can be derived that extends and generalises previous work by Ikeda (1981) to non equilibrium case; (d) There exist an unsaturation state in river channels that are eroding where saturation is not achieved for distance that are large with regard both to the grain size and channel width.

Key words: River width, Regime geometry, Scaling, Bed load transport, Microscale experiment

* Corresponding author
Email addresses: armstron@ipgp.jussieu.fr (Lawrence Armstrong), metivier@ipgp.jussieu.fr (François Métivier).

1 Introduction

Experiments of an adjusting microscale river with an overall negative mass balance were achieved to study the equilibrium regime of both the channel width and the sediment transport. The companion paper (Armstrong and Métivier, 2003) focuses on the equilibrium for the width as it is found that each experiments of a microscale river displays an equilibrium width at a given distance from the inlet. Uniform flow is also observed but at the scale of the microscale river, effect of surface tension leads to reduce the velocity from the prediction of uniform flows formulas. A scaling law is obtained that relate the shift in the velocity in function of the Weber number. From the observation that uniform flow can be found in many natural rivers, first order regime relationships are derived that enable a scaling of the experiments in agreement with the Shields phase diagram.

We address in this part, the problem of the sediment transport during the evolution in time of the adjusting river towards equilibrium. During the microscale experiments, sediment mass transported by the stream is measured at regular intervals using a hight precision weighting device and which gives access to the sediment output flux. The time response of the bed load transport during the widening of the channel can therefore be obtained. Experiments of topographic detection were achieved to measure the bed evolution in time and provide a constrain for the transport rate.

2 Digital elevation models of the microscale river and time evolution of the mass

The experimental setup is presented in the companion paper (Armstrong and Métivier, 2003). However to obtain some constraints for the sediment transport rate from the bed elevation evolution in time, topographic acquisition of the microscale river are achieved within specific experiments. The procedure is presented herein.

2.1 Method

Morphology of the channel is subject to adjustments in the experimental straight river through changes in the width and in the bed elevation. The evolution in time of the width is a measure relatively easy to achieve (Armstrong and Métivier, 2003). Access to the variation in time of the bed elevation is possible with the use of a method recently developed in the laboratory by Meunier & Lajeunesse (Meunier, 2003) and inspired by a Moiré method (Sansoni et al., 1999). This method allows to create Digital Elevation Models (DEM) of the topography of the microscale channel and therefore give access to

the evolution of the channel bed.

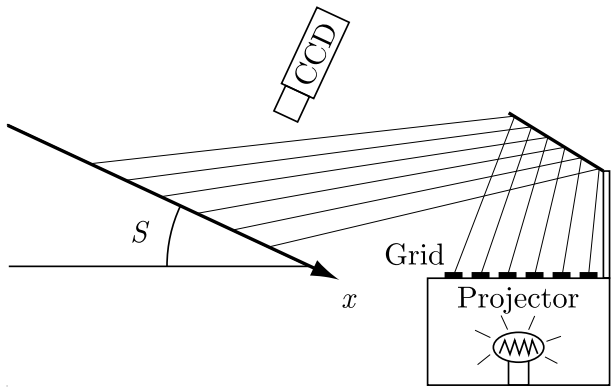

Fig. 1. Visualization method for the DEM.

A grid pattern made of horizontal sinusoidal is projected on the plane by an overhead projector, as sketched in Fig. 1. The projection angle is such that the presence of the channel induces a significant deformation of the grid (Fig. 2b). Pictures of the plane are recorded by a CCD camera positioned at the vertical of the plane. The local shift of the lines observed between the deformed pattern in the presence of the channel and the initial regular pattern when the surface is flat is proportional to the local depth of the channel. In order to quantitatively obtain the depth of the channel $z(x, y)$, we proceed as follow. The reference picture, Fig. 2a, and the picture to be analysed, Fig. 2b, are digitized which gives two real amplitudes $A_{ref}(x, y)$ and $A(x, y)$. The two-dimensional spatial Fourier transforms of both amplitudes are then computed. Both pictures being close to a regular pattern, the Fourier transforms are found to present well-defined peaks at the complex wavenumbers $(2\pi/\lambda, 0)$ and $(-2\pi/\lambda, 0)$, λ being the wavelength of the projected grid. For Fig. 2b, the information about the slight deviation from the reference pattern induced by the channel is contained in the width of the peak. In order to extract the phase of the picture, the right hand-side half of the wavenumber spectrum ($k_x > 0$) is used to reconstruct two complex amplitudes $A^c_{ref}(x, y)$ and $A^c(x, y)$. The phase $\phi_{ref}(x, y)$ and $\phi(x, y)$ of A^c_{ref} and A^c gives the phase of the pattern in Figs. 2a and 2b. The thickness is then simply proportional to the phase difference $\phi(x, y) - \phi_{ref}(x, y)$. The coefficient of proportionality is found by measuring the phase shift induced by a stair-shaped plate of 2mm increments. Figure 2c shows the height given by the analysis.

The time evolution of the channel $z(x, y, t)$ is obtained by analysing each image of a movie recorded during the river experiment. The height measurement is estimated to be precise up to ± 0.3 mm.

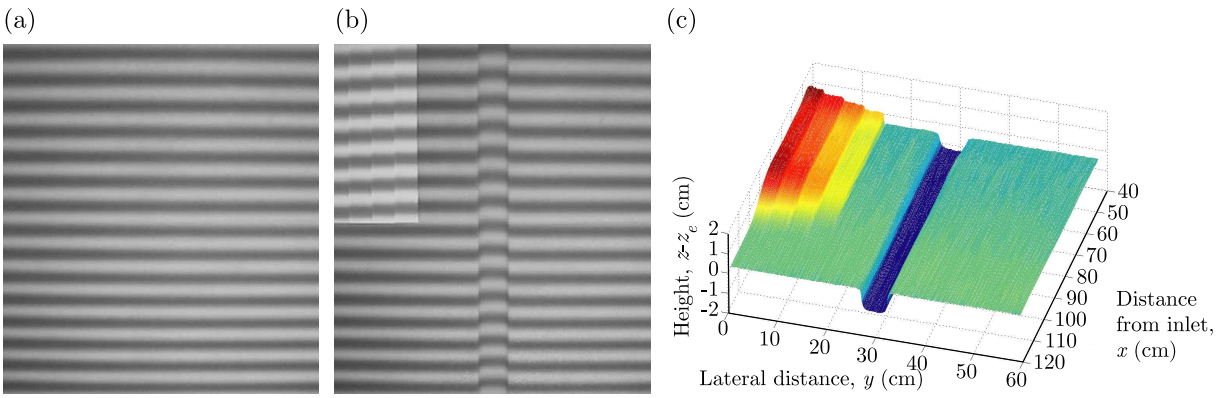

Fig. 2. (a) Reference picture. (b) Picture to be analysed. (c) Computed DEM. The rectangular shape is the stair scale.

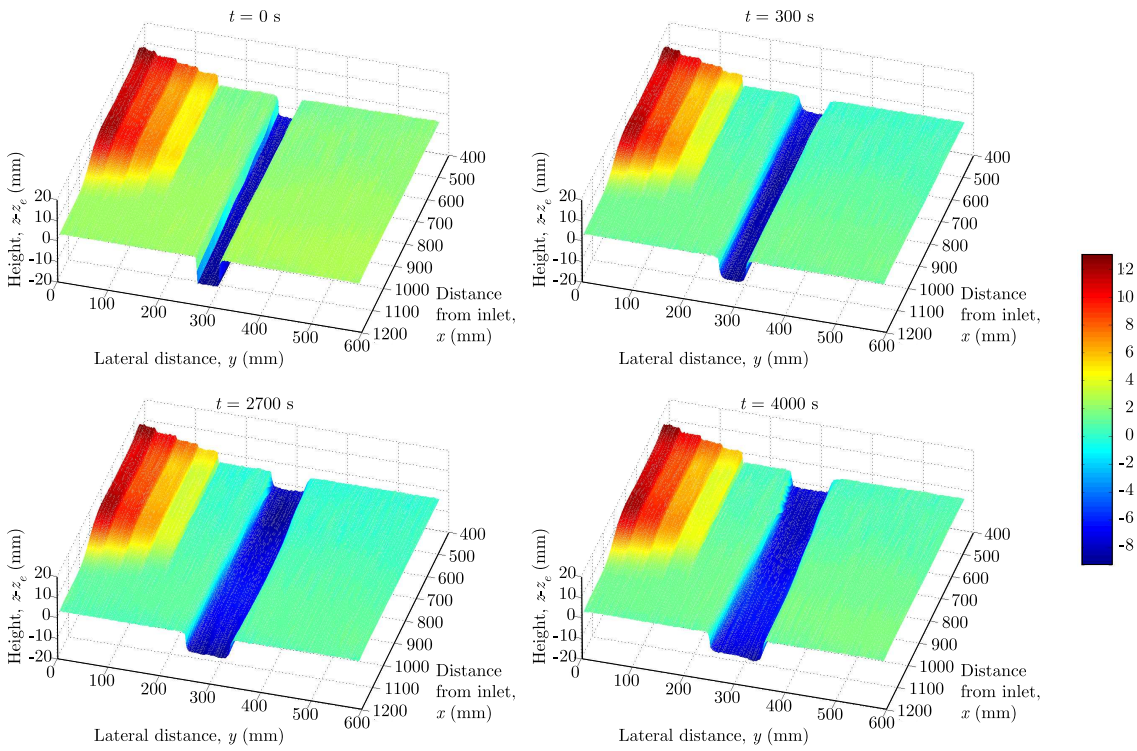

Fig. 3. Time evolution of the channel topography ($S = 0.0524$, $Q = 1.0$ l/min, $d_{50} = 160$ µm and $L = 130$ cm).

2.2 Observations from the DEM

Only two experiments were done and analyzed with this method so that the results should be qualitative more than quantitative. Figure 3 presents the evolution of the topography for one of them. The river adjusts its channel through a widening and a bed elevation as qualitatively observed in section (Armstrong and Métivier, 2003). The evolution of

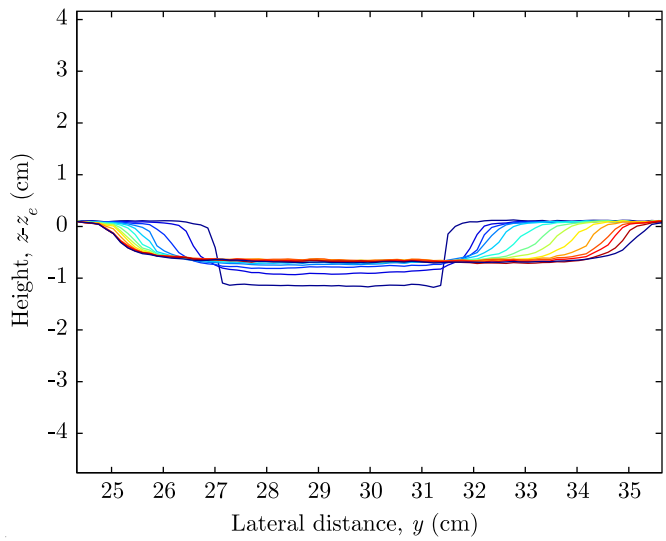

Fig. 4. Channel section at $x = 100$ cm from the inlet showing the enlargement and the bed elevation towards an equilibrium. Curves are every 300s.

a cross-section shows that the channel reaches an equilibrium morphology with constant width and bed elevation (Fig. 4). This morphologic equilibrium can be further appreciated from the time evolution of the width (Fig. 5a) and of the bed elevation (Fig. 5b) for all the sections along the reach. The width reaches an equilibrium only at upstream sections.The bed elevation remains constant within 1 or 2mm after a certain time of aggradation (Fig. 4b). This small gradient in the width $\partial w/\partial x$, can have at least two possible reasons which are (1) the presence of an acceleration in the velocity of the flow in the downstream direction and (2) the influence of the incise of the channel in the upstream region (Fig. 4b). The former may be assumed to be negliglible as the the flow is uniform (Armstrong and Métivier, 2003). The latter can be a more possible reason since the erosion of the bed upstream appears as a consequence of the drain of the flume in the absence of sediment input.

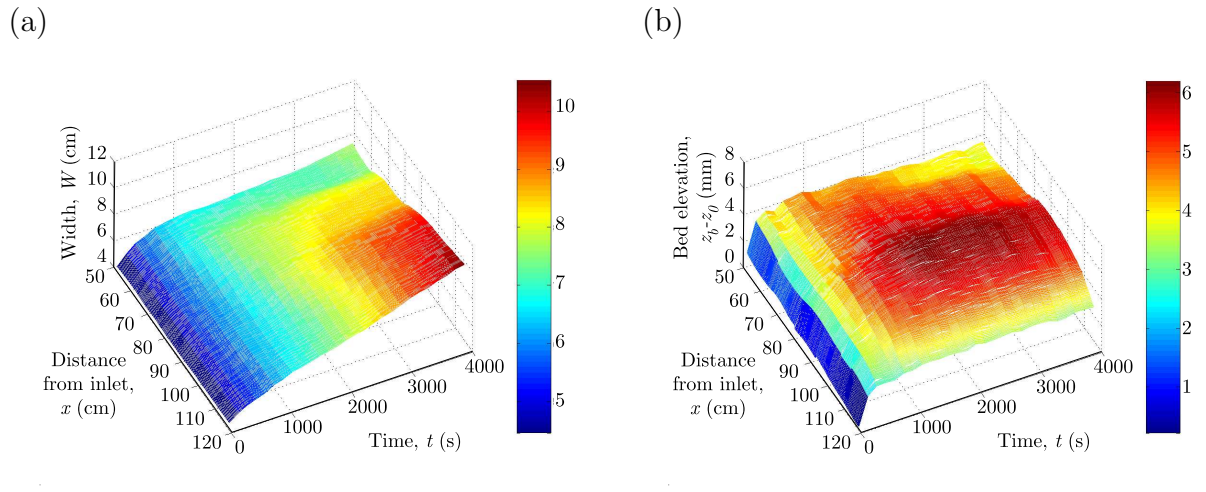

Fig. 5. (a) Time evolution of the width and (b) time evolution of the bed elevation and their distribution along the reach ($S = 0.0524$, $Q = 1.0$ l/min, $d_{50} = 160$ µm and $L = 130$ cm).

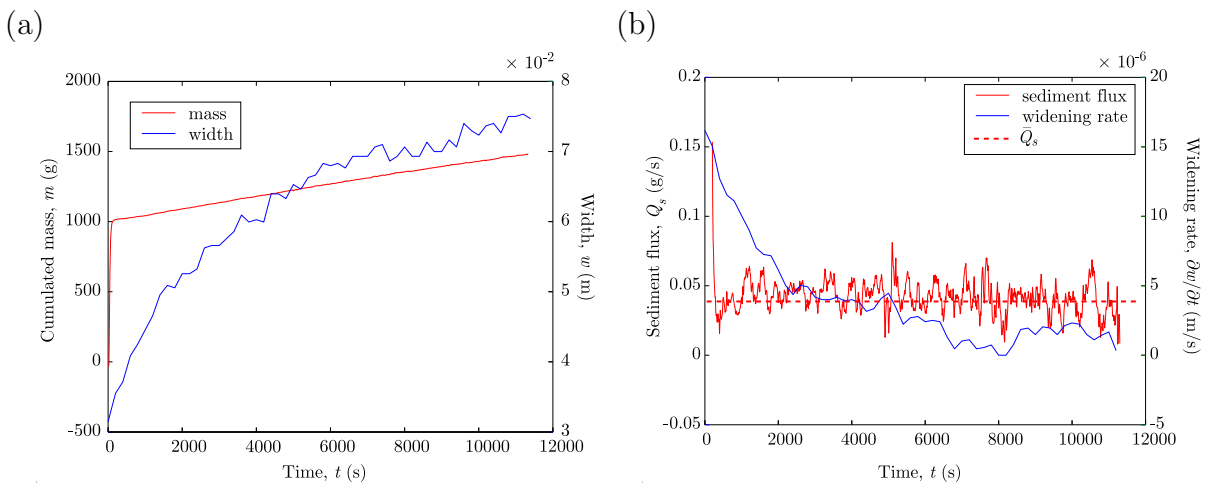

Fig. 6. (a) Typical cumulated mass of sediment at the outlet (red curve) and time evolution of the width (blue curve) for a typical experiment. (b) Corresponding sediment flux (red curve) and widening rate (blue curve). The mean flux $\overline{Q_s} = 4.3 \times 10^{-2}$g/s is noted in dashed line. The time response of the mass and the width are decorralated. ($S = 0.035$, $Q = 0.5$ l/min, $d_{50} = 75$ µm and $L = 130$ cm for this experiment)

2.3 Output sediment flux

A certain quantity of sediments of the bed is transported as denoted by the presence of moving bedforms during the experiments (Armstrong and Métivier, 2003). The mode of sediment transport is given by the Rouse number which compares the Stokes fall velocity v_s to the bed shear velocity u_*:

$$\mathrm{Ro} = \frac{v_s}{\kappa u_*}, \tag{1}$$

where κ is Von Karman constant ($\kappa = 0.4$). Measurement of the settling velocities where are of the order of 1 cm/s. With the bed shear velocity to be $u_* \approx \sqrt{ghS}$, and with flow depth of the order of 1 mm, Rouse number is approximately Ro ≈ 2 which indicates a preferential sediment transport as bed load. Figure 6 represent both the cumulated mass measured at the outlet of the experimental straight river and the corresponding sediment flux estimated from the fit of a line on the cumulated mass curve. The first several tens of seconds of the mass curve where the mass curve shows a large slope, corresponds to the adjustments of the overflowing tank at the beginning of the experiment. This slope measured during the first instants corresponds to the water discharge. The adjustment of the overflowing tank then makes it impossible to see the sediment flux due to the collapse of the banks at the outlet at the early stages since it is orders of magnitudes smaller than the water discharge. The flux curve (time derivative of the mass curve) shows that, on average, the sediment flux transported by the stream at the outlet tends rapidly towards a constant value (Fig. 6b). Oscillations around the average equilibrium flux $\overline{Q_s}$

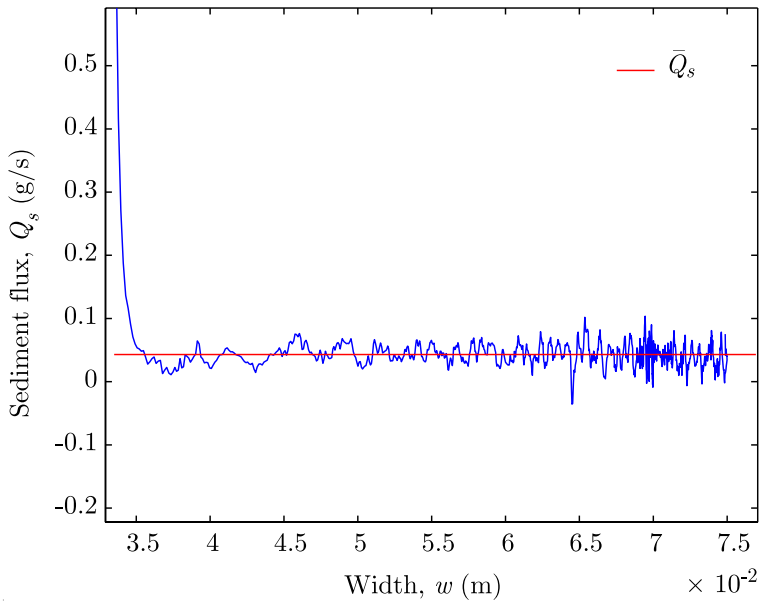

Fig. 7. Output sediment flux vs. width. The sediment flux is decoralated to the width since it remains constant at different width whereas the width continues to evolve with time.

are significant of a wave like transport of sediments inside the experimental straight river (Métivier and Meunier, 2003). The experimental straight river can be approximated with a very good precision (regression coefficient in the range of 0.98–1) to achieve a steady state regime in terms of sediment transport. Furthermore, although the average sediment flux remains constant for the duration of the experiment, the river is not in equilibrium regarding its channel width (Figs. 6). It therefore appears that the river is capable to adjusts its transport capacity as the channel is being modified. Thus a very important observation is that the two mechanisms of banks erosion and bed load transport exhibit a clear decorrelation through time. This decorrelation can better be seen when plotting the sediment flux in function of the width (Fig. 7).

We see from the evolution in time of the channel width and of the output sediment flux, that the straight river can reach two different steady states in time: first, a steady state for the sediment transport that is reached almost instantaneously and then a steady state for the width that is reached asymptotically. We will see in the next section what these observations imply.

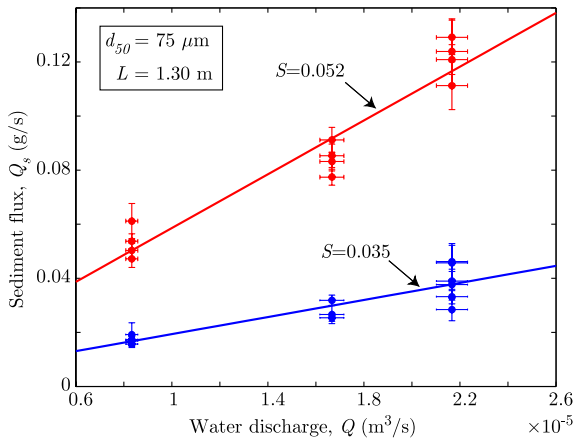

Fig. 8. Sediment flux versus water discharge for given slope and grain size.

3 Results

3.1 Direct comparison of bed load transport and total stream power

For each experiment, we obtained a cummulative mass flux at the outlet from which we derived the sediment flux $Q_s(t)$ by time derivation. Fig. 6 shows the two curves (in red). As can be seen, Q_s tends towards an constant value which indicates that the flux becomes stationary. Value for this equilibrium regime is obtained by the fit of the mass curve.

First observations indicate that the sediment transport rate is proportionnal to the flow discharge for any given slope and grain size (Fig. 8). Sediment transport can be related to the stream power on a physical basis (Bagnold, 1977). In Bagnold's formulation, the bedload transport per unit width of channel (Q_s/W) can be expressed as follow:

$$\frac{Q_s}{W} = \frac{\beta u_b}{\gamma_s}(\tau_b - \tau_c), \tag{2}$$

where u_b is the velocity in the boundary layer where sediment transport occurs, τ_b and τ_c are respectively the bed shear stress and the critical shear stress, $\gamma_s = (\rho_s - \rho)g/\rho$ is the specific gravity and β coefficient on the particle size. The right term represent the power that is lost by the stream to transport a given volume of particle v_s at the velocity u_s. According to Bagnold's formula, $u_s = \beta u_b \approx 0.5u_b$ (Yalin and Ferreira da Silva, 2001) and $v_s \sim (\tau_b - \tau_c)/\gamma_s$. However, for uniform flow, the sediment flux Q_s can be expressed as a function of the total stream power (Métivier and Meunier, 2003). With the use of the fluid mass conservation ($Q = uWh$), the Chézy formula ($u = c\sqrt{ghS}$), bed shear stress ($\tau_b = \rho ghS$), and assuming $u_b \approx u_*$, Eq. (2) becomes

$$Q_s \propto (\rho gQS - \rho gQS_c), \tag{3}$$

where S_c is the critical slope for transport inception. It should be noted that this relation is now independent of the width. Fig. 9 displays the correlation found between the sediment discharge and the total stream power. Both the cases of experiments with an initial solid bed and standard mobile bed experiments do not show any significant difference.

The stream power concept is in agreement with our observations of a decorralation between the width and the sediment flux. Since the sediment flux Q_s is constant over time, Eq. (2) implies that increase of the width in time is compensated with adjustment of the stream power that should decrease. It can be assumed that the critical shear stress remains constant during the evolution of an experiment since from the Shields phase diagram, variation of the grain Reynolds number that depends on the flow depth, may not have significant effect on the critical Shields stress. The critical variables that can change during widening are the velocity at the boundary layer and the shear stress. These two variables are proportional to the square root of the flow depth. Since it was observed that the velocity and therefore the flow depth decreases during the widening, the stream power can reasonably be expected to decrease. This results is expressed into the total stream power Eq. (3).

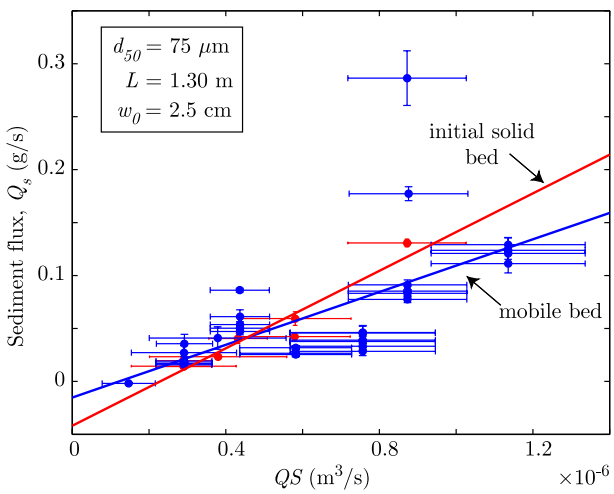

Fig. 9. Sediment flux versus the total stream discharge in the case of experiments that started initially without a mobile bed (red symbol) and in the case of mobile bed experiments (blue symbol).

3.2 Implication on the bed load transport along the stream

The sediment output flux is found to achieve rapidly a permanent regime with constant sediment discharge although the channel is still widening. We now see how the constrains of the channel morphology on the mass conservation of sediment can bring insight on the bed load transport along the stream. The results on the channel morphology of the microscale river (1) the channel remains straight at first order (Armstrong and Métivier,

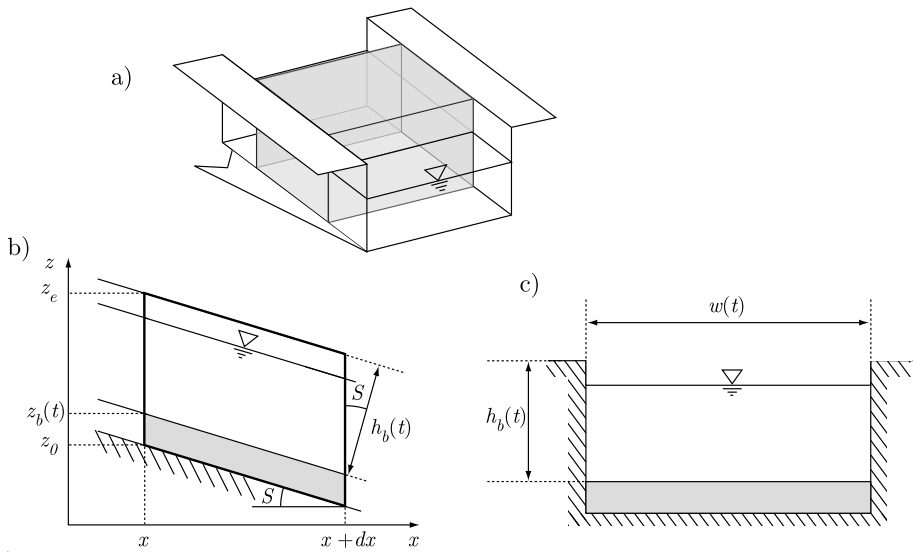

Fig. 10. Definition scheme. (a) control volume of a section of the channel for the Exner derivation. (b) Longitudinal section. (c) Cross section. z_0 is the initial bed elevation; $z_b(t)$ is the bed elevation a time t and z_e is the elevation of the alluvial plain; $h_b = z_e - z_b$ is the bank height.

2003) and (2) the bed reaches an equilibrium in which the bed height remains constant in time (see section 2.2).

3.2.1 Exner equation

We consider the case of a 1D Exner equation. Figure 10 presents the geometry used. The channel is assumed to be rectangular. In 1D, the Exner equation for mass conservation of sediment reads:

$$(1-\phi)\rho_s\left[(z_e - z_b)\frac{\partial w}{\partial t} - w\frac{\partial z_b}{\partial t}\right] = \frac{\partial Q_s}{\partial x}, \tag{4}$$

where ϕ is the porosity of the granular media. In this formulation, bed load transport Q_s (in kg/s) is taken explicitly into account whereas the sediment flux from the banks appears in the first derivative. Having the bank height $h_b = z_e - z_b$, the Exner equation Eq. (4) can be written as

$$(1-\phi)\rho_s\frac{\partial}{\partial t}(wh_b) = \frac{\partial Q_s}{\partial x}. \tag{5}$$

We now consider the following cases in the next two sections.

3.2.2 Uniform bed load transport

It is assumed that the bed load transport is uniform along the stream. This is susceptible to be the case, when in the channel, the maximum transport capacity is reached so that sediments from bank erosion must be aggraded on the bed. The Exner equation Eq. (5) reduces to

$$\frac{\partial}{\partial t}(wh_b) = 0. \tag{6}$$

With the initial conditions, $w|_{t=0} = w_0$ and $z_b|_{t=0} = z_0$, the equation has for solution

$$wh_b = w_0 h_0. \tag{7}$$

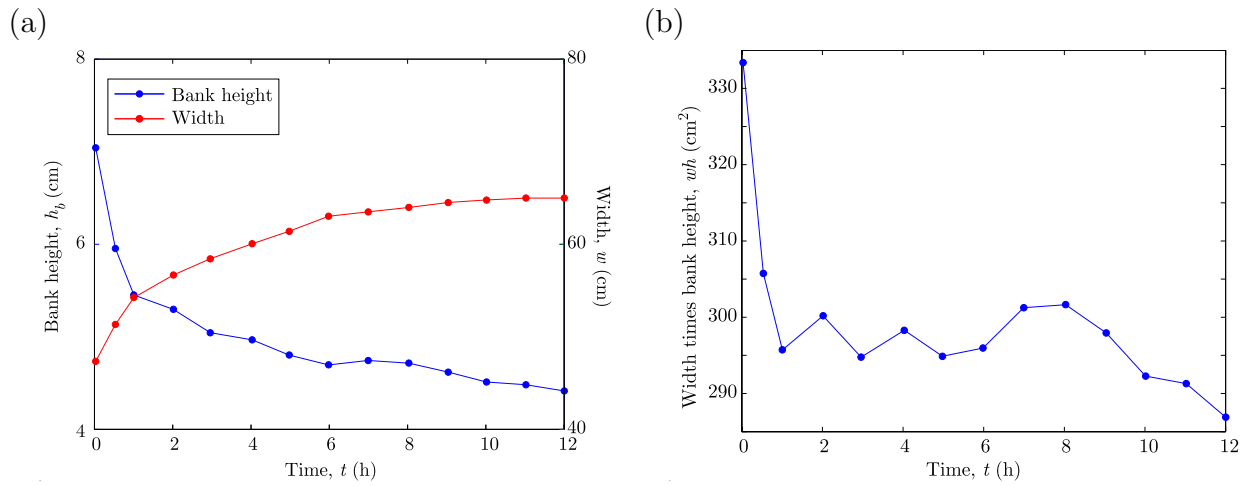

Fig. 11. (a) Variation of free surface width and the bank height with time for run 17 of Ikeda (1981). (b) Product width by bank height showing a constant value.

This hypothesis of a uniform sediment flux is tested through the validity of the relation (7) in the cases of our experiments in a overall negative mass balance and of experiments in kept in a global mass equilibrium with sediment recirculation Ikeda (1981) . In Ikeda's case, from the time evolution of the channel width and bank height (Fig. 11a), one can see that after about one hour, the product wh reaches a constant value (Fig. 11b). This suggests that in Ikeda's experiments, the input of sediments was such that the river was in its maximum transport capacity. The relation Eq. (7) is tested on our experiments with DEM which provided measurement of the width and depth of the channel (Fig. 12). For an upstream section, the product wh is never constant (Fig. 12, left). In fact, as the bed stabilizes rapidly (at a longer time scale than the output mass curve) the product increases as the channels widens. But for a section more downstream (Fig. 12, right), the product remains constant for several hundreds of seconds before increasing when the bed stabilizes. This suggest that at the beginning of the experiment, the input of sediment from bank erosion is large enough so that it exceeds the maximum transport capacity of

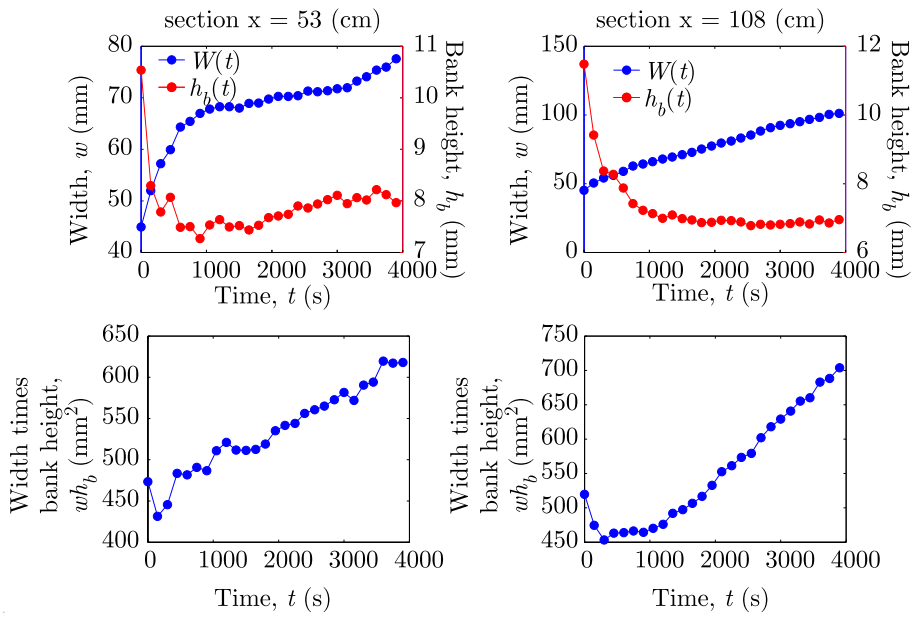

Fig. 12. Top: channel width and bank height evolution in time at two different distance from the inlet (see Fig. 3). Bottom: corresponding product width times the bank height.

the river: sediments must be aggradated on the bed and the relation Eq. (7) is verified. But as the channel widens, the input from the banks decreases and doesn't exceed anymore the transport capacity: all the sediment eroded from the banks can be now transported [1]. A linear relation is then observed:

$$wh_b = At, \tag{8}$$

where A is here a positive constant.

3.2.3 Exner solution in the case of a straight channel

Exner Eq. (5) is now considered without the assumption of a uniform transport of sediment. Exner Eq. (5) is derived in respect with x and by permuting the derivatives, one obtains:

$$(1-\phi)\rho_s \frac{\partial}{\partial t}\left(h_b \frac{\partial w}{\partial x} + w \frac{\partial h_b}{\partial x}\right) = \frac{\partial^2 Q_s}{\partial x^2}. \tag{9}$$

Since the channel remains straight at first order, the variation along the stream of the width can be neglected. The DEM shows that above a certain distance from the inlet, the bed height is uniform [2]. The derivatives $\partial_x w$ and $\partial_x h_b$ are neglected and Eq. (9) becomes

[1] This doesn't explain why upstream, we don't have wh=Cte.
[2] We don't need in this demonstration to use the observation that $\partial_t z_b = 0$.

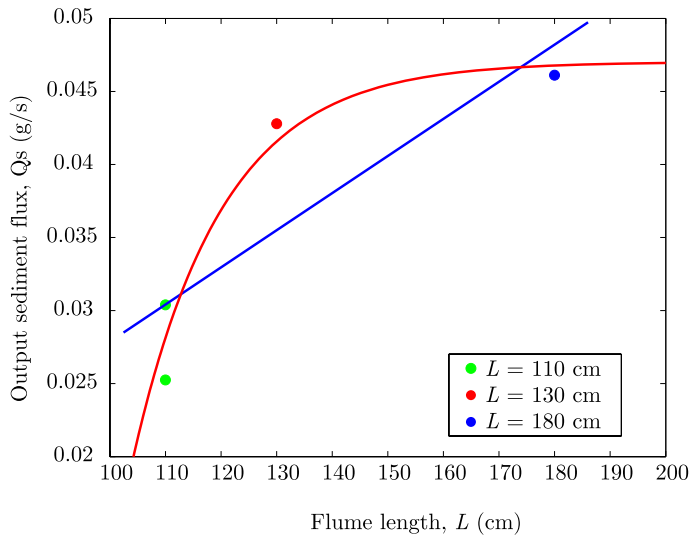

Fig. 13. Sediment flux versus in function of the flume length for experiments with $S = 0.035$, $Q = 1$ l/min and $w_0 = 2.5$ cm. The red curve correspond to the better fit (decreasing exponential) and the blue curve represents the fit of a line used for the determination of the parameter a.

$$\frac{\partial^2 Q_s}{\partial x^2} = 0. \tag{10}$$

This means a linear sediment transport along the stream

$$Q_s(x) = ax + b \tag{11}$$

where a and b are two constants that do not depend on time since we have the experimental condition $\partial_t Q_s = 0$. They should however depend on other parameters such as the slope S, the water discharge Q and the grain size d_{50}. With the boundary condition in our experiments of no sediment feeding, the parameter b, which is the sediment flux at the inlet, in Eq. (11) can be assumed to vanish. This result with Exner equation (5) yield

$$(1-\phi)\rho_s \frac{\partial}{\partial t}(wh_b) = a, \tag{12}$$

which integrates into

$$wh_b = w_0 h_{b,0} + \frac{a}{\rho_s(1-\phi)} t. \tag{13}$$

This relation is valid when the transport is unsaturated when the river does not reach its maximum transport capacity. Eq. (13) is the general form of what was postulated with Eq. (8) for the case of uniform bedload transport.

The dependance of parameter a on the river parameters can be addressed in our experiments from two independent ways giving the possibility to verify our model: (1) from

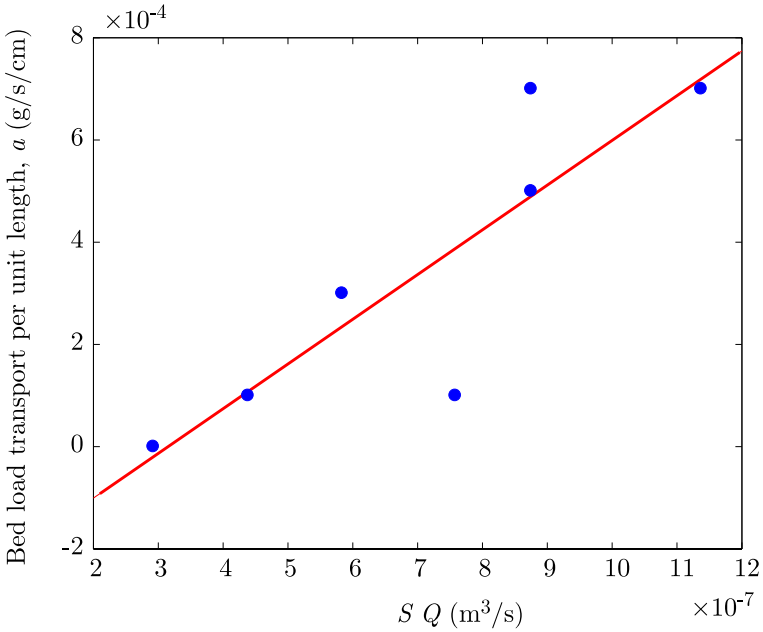

Fig. 14. Variation of coefficient a in function of stream power.

Eq. (11) for the measurements of the sediment flux at the outlet from experiments of different flume length and (2) from Eq. (13) with the measurements of the topography, provided that the bed porosity is known. In our study, a series of experiments with varying length where realized using A sand ($d_{50} = 75$ µm) and provides data for the first method. Since only two experiments were achieved with the topography and because a different grain size was used (B sand, $d_{50} = 160$ µm), they can not be used for the second method.

Evolution of the sediment flux with the flume length is observed for the experiments in overall negative mass balance (Fig. 13). Estimation of the parameter a is made with the fit of a line at given discharge and slope. The parameter a is found to show an empirical correlation with the stream power (Fig. 14). The parameter seems to be independent from the initial width. Using this correlation, the relation for the bed load transport Eq. (11) can be expressed as

$$Q_s(x) = \beta\, \rho g Q S x \tag{14}$$

where β is a constant ($[\beta]$=T^2 L^{-2}). This relation is valid when the river has not reached its maximum transport capacity. At a given length however (greater than our maximum flume length), this should be the case, and this relation becomes compatible with the total stream power relation Eq. (3). The relation Eq. (13) becomes using the correlation of a with the stream power:

$$w h_b = w_0 h_{b,0} + \beta\, \frac{\rho g Q S}{\rho_s (1-\phi)} t. \tag{15}$$

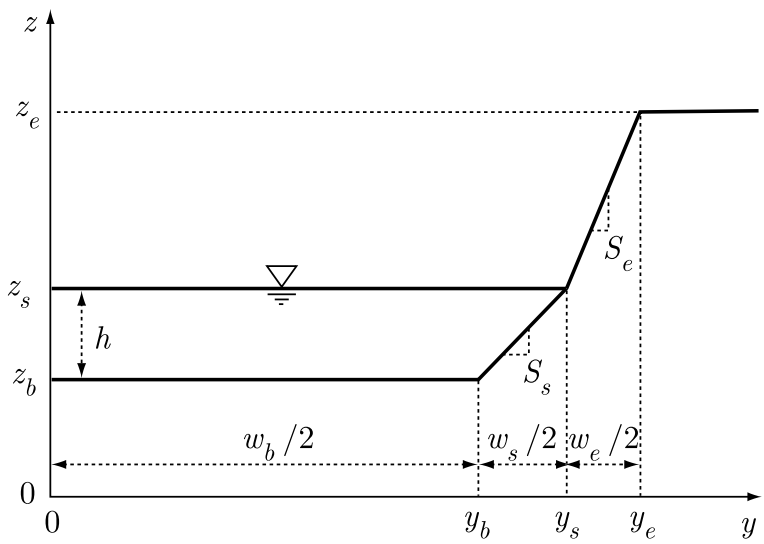

Fig. 15. Geometry of the half cross section.

4 Numerical modeling

Models of the time evolution of straight river channels have been proposed by several authors (Pizzuto, 1990; Kovacs and Parker, 1994). These models are based on parametric equations and tend to predict the channel evolution in the experiments of Ikeda (1981) and don't focus on the bed load transport. To address this point, a simplified numerical code was used to predict the channel evolution and the sediment transport associated. The model is first described and simulations are then compared with our experiments of micro-scaled river.

4.1 Model

The model used is based upon the "Sediment Digester" code written by Gary Parker to desribe river response to sediment input from lateral earthflows in Papua New Guinea (Dietrich et al., 2001). We use this to model the channel and bed load transport evolution in time in the case of a steady, uniform and one dimensional flow. For the given the geometry where the bank is composed of a submerged and emerged region (Fig. 15), the following equations are considered. The complete derivation can be found in Appendix A.

• Equations for bed and width evolution:

$$(1-\phi)\frac{\partial z_b}{\partial t} = \frac{2|q_{wy}|}{w_b}, \tag{16}$$

$$(1-\phi)\left[\frac{z_e-z_b}{2}-r(z_e-z_b-h)\left(\frac{1}{S_s}-\frac{1}{S_e}\right)\right]\frac{\partial w_b}{\partial t}= \left[1+2\frac{z_e-z_b}{w_s S_e}+\left(\frac{1}{S_s}-\frac{1}{S_e}\right)\right]|q_{wy}|. \quad (17)$$

• Equation for the flow depth

$$h=\left(\frac{k_s^{1/3}Q^2}{\alpha_r^2\, w_b^2\, gS}\right)^{3/10}\left(\frac{C_d}{C_n^3}\right)^{3/10}, \quad (18a)$$

with

$$C_d=1+2\varphi\frac{\sqrt{1+S_s^2}}{S_s}\frac{h}{w_b}, \quad (18b)$$

$$C_n=1+\frac{1}{S_s}\frac{h}{w_b}. \quad (18c)$$

• Equation for the Shields stress on the bed:

$$\tau_b^*=\tau_b/(\rho\mathscr{R}gd_{50}) \quad (19)$$

• Equation for Shields stress on the banks region:

$$\tau_w^*=\varphi\tau_b^*. \quad (20)$$

• Equation for sediment transport in the streamwise direction respectively for the bed and sidewall regions:

$$q_{bx}=\sqrt{\mathscr{R}gd_{50}}\, d_{50}\, \alpha_x(\tau_b^*)^{1.5}\left(1-\frac{\tau_c^*}{\tau_b^*}\right)^{4.5}, \quad (21a)$$

$$q_{wx}=\sqrt{\mathscr{R}gd_{50}}\, d_{50}\, \alpha_x(\varphi\tau_b^*)^{1.5}\left(1-\frac{\tau_c^*}{\varphi\tau_b^*}\right)^{4.5}, \quad (21b)$$

• Equation for sediment transport in transverse direction in the sidewall region

$$q_{wy}=-q_{wx}\,\alpha_y\sqrt{\frac{\tau_c^*}{\varphi\tau_b^*}}\,S_s. \quad (22)$$

The model is solved with the following procedure. For each time step, the flow depth is first obtained iteratively using a Newton-Raphson scheme on Eq. (18). Knowledge of the flow depth then allows for the direct calculation of the sediment load with Eqs. (19), (20), (21) and (22). With the depth and the load known, the geometry is found using an implicit scheme of Eqs. (16) and (17). With the new channel geometry, one move to the next time

Table 1
Parameters adjusted in the numerical model.

Parameter	Symbol	Value in litterature	Value in model
Shear:			
Critical shear stress	τ_c^*	–	0.06–0.08
Side-slope shear factor	φ	2/3–4/5	0.17–0.53
Flow:			
Manning-Strickler parameter	α_r	8.1	8.1–20
Roughness factor	n_k	2–4	2.5–4
Transport:			
Streamwise coefficient	α_x	11.2	11.2
Normal coefficient	α_y	2.65	2.65

step where the same procedure is performed. This allows to have access to the evolution in time of the flow depth, the sediment loads, and of the geometry of the channel.

For the numerical model, the parameters for the geometry, the sand characteristics and for the flow conditions are fixed to the corresponding values in the microscale experiment to be modelized. These parameters are

$$S,\ w_0,\ h_b,\ S_s,\ S_e,\ d_{50}, \rho_s,\ \phi,\ Q,\ \rho \text{ and } g, \tag{23}$$

and remain unchanged during the run. The bank slope of the submerged and emerged regions, S_s and S_e, are assumed to be equal to 45 ̊which is the value of the bank slope measured from the DEMs. The porosity ϕ is taken to be the one of a random close packing: $\phi = 0.35$ (*e. g.* Torquato et al., 2000). The initial bank height equals $h_b = 1$ cm as in the microscale experiments.

The parameters that appear in the different relations (*i. e.*, φ, α_r, n_k, α_x, α_y and τ_c^*) are less constrain than those for the geometry and the flow conditions. Their values determine the amplitude in the response of the system. They were adjusted "by hand" until the modelized width and sediment discharge would match the corresponding in the flume experiments. For this work, only values of the side slope shear stress factor φ and of the flow resistance, α_r and n_k, were adjusted (table 1). The transport coefficients are unchanged. Value of the critical Shields stress τ_{*_c} was estimated from the Shields curve (curve is displayed in the companion paper Armstrong and Métivier, 2003) for the corresponding grain Reynolds number

$$\mathrm{Re}_* = \frac{u_* d_{50}}{\nu} = \frac{\sqrt{ghS}\, d_{50}}{\nu}, \tag{24}$$

with a flow height h of the order of 1 mm.

4.2 Model results

We now see how the flow velocity is used as a constrain to modelized the straight river.

When adjusting the side-slope factor only, the width evolution can be well modelised at first order approximation (Figs. 16a and 17a). It appears that if the width can be

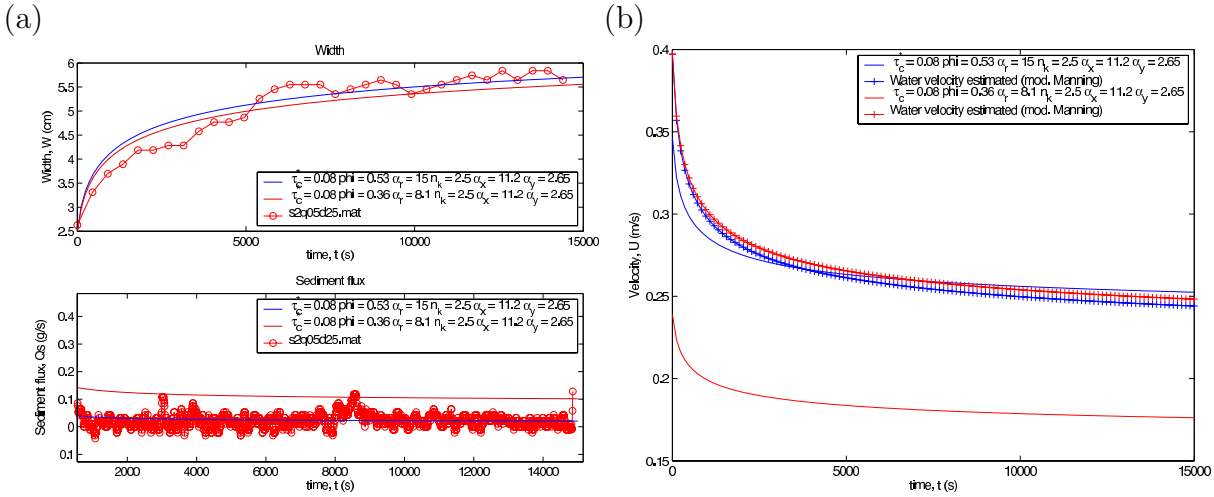

Fig. 16. (a) Width and sediment transport rate evolution in time. (b) Modelized flow velocity compared to the Manning velocity. Case of $S = 0.035$, $Q = 0.5$ l/min and $d_{50} = 75$ µm.

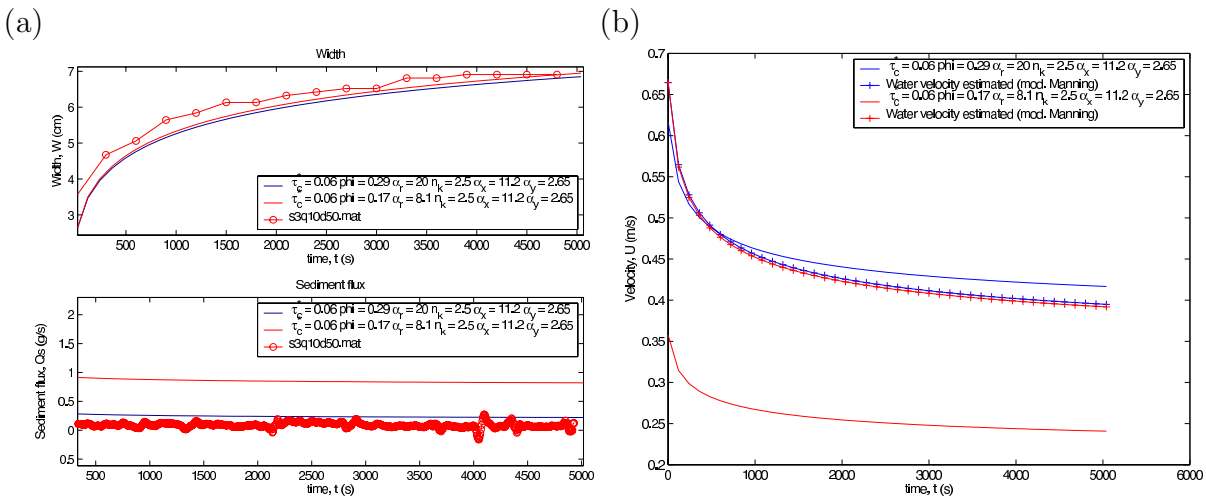

Fig. 17. (a) Width and sediment transport rate evolution in time. (b) Modelized flow velocity compared to the Manning velocity. Case of $S = 0.052$, $Q = 1.0$ l/min and $d_{50} = 75$ µm.

well estimated, the transport rate of sediment is over estimated (Figs. 16a and 17a). One reason can come from the velocity of the flow which is not well estimated. We compare the modelised velocity calculated from Eq. (19) to the velocity estimated from a uniform formula (for example, the modified Manning) which is a good approximation for the flume experiments (Armstrong and Métivier, 2003). In the case where only the side-bed shear factor is adjusted, the flow velocity appears to be underestimated (Figs. 16b and 17b). This means that the flow parameter (table 1) are not accurate for the microscale river. Adjusting them also, lead to a better approximation of the width and transport rate evolution in time (Figs. 16a and 17a). However, this adjustment is made on range that don't fall in the accepted values. Especially, the Manning coefficien α_r need to be larger than its accepted value.

5 Conclusion

Experiments of a microscale river were achieved to study and characterize the equilibrium regime of straight alluvial rivers both for the channel morphology and for the bed load transport. The river was put in an overall negative mass balance with no grain feeding so that the bed load transport at a given distance from the inlet would be only controlled by the river itself. It was verified in the companion paper (Armstrong and Métivier, 2003) that without an sediment input, an equilibrium channel can nevertheless be reached at a given distance from the inlet. Time evolution of the channel displays an independence between the width and the sediment flux: there is any case rapid establishment of a constant sediment flux at the outlet although the river is still widening. The sediment transport rate is at first order in correlation with the total stream power, which is to be expected. The stream power formulation is in agreement with a constant bed load transport during the widening of the channel. Some constrains on the sediment transport distribution along the stream are brought from experiments with channel topography measurements. Digital Elevation Map, obtained using a Moiré method, gives the access in time of the channel topography. It is observed that the channel bed reaches rapidly, and before the width, a steady and uniform heigth. This suggests that the bedload transport must increases in the streamwise direction with the input of sediments from bank erosion. Therefore an unsaturation state exists in the channel that are eroding in which saturation is not achieved for distance that are large with regard both to the grain size and more important to the channel width. With this observation, a solution to the Exner equation for the sediment mass conservation can be derived. It is found that the channel perimeter (width times the bank heigh) increases in time as a linear function. The increase factor has the dimensions of m^2 s^{-1} and is proportional to the increase rate of the sediment transport along the stream (in fact through the volume fraction of sediment). Analysis of the increase factor from experiments at different flume length shows that it can be empirically related to the total stream power.

A numerical model is used to verify if usual semi-empirical relationship for the bed load transport and for the bank shear stress can predict the decorralated time evolution of the width and the bed load in a one-dimensional adjusting river. The model, based on the assumption that the bank shear stress is proportionnal to the bed shear stress is found to predict channel evolution correctly with an over estimation of the bedload transport.

References

Armstrong, L., Métivier, F., 2003. Independence of sediment flux and width evolution through time in a microscale straight river channel. Part 1. scaling of microscale experiments and regime equations. in prep. .

Bagnold, R. A., 1977. Bed load transport by natural rivers. Water. Resour. Res. 13, 303–312.

Dietrich, W. E., Cui, Y., Parker, G., Moi, A., 2001. The damping of large sediment input signals due to attrition, channel morphologic change, and storage: the Fly River Watershed, Papua New Guinea. Eos Trans. AGU 82.

Ikeda, S., 1981. Self-formed straight channels in sandy beds. J. Hydrol. Div. 107, 389–406.

Kovacs, A., Parker, G., 1994. A new vectorial bedload formulation and its application to the time evolution of straight river channels. J. Fluid Mech. 267, 153–183.

Métivier, F., Meunier, P., 2003. Input and output mass flux correlations in an experimental braided stream. Implications on the dynamics of bed load transport. J. Hydrol. 271, 22–38.

Meunier, P., 2003. Transport de sédiments dans une microrivière à tresses. Ph.D. thesis, Université Paris VII, (in preparation).

Pizzuto, J. E., 1990. Numerical simulation of gravel bed widening. Water. Resour. Res. 26, 1971–1980.

Sansoni, G., Carocci, M., Rodella, R., 1999. 3D vision based on the combination of gray code and phase shift light projection: analysis and compensation of the systematic errors. Appl. Opt. 31, 6565–6573.

Torquato, S., Truskett, T. M., Debenedetti, P. G., 2000. Is random close packing of spheres well defined? Phys. Rev. Lett. 84, 2064–2067.

Yalin, M. S., Ferreira da Silva, A. M., 2001. Fluvial processes. International Association of Hydraulic Engineering and Research, Delft, The Netherlands.

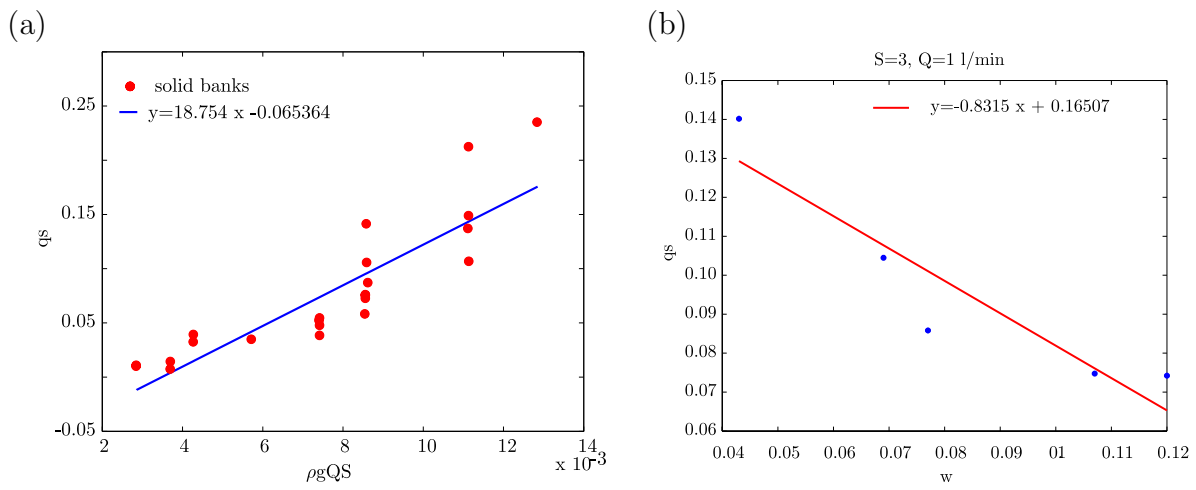

Figure 4.1 – *(a) Output sediment flux as a function of the total stream power for the experiments with solid banks. (b) Output sediment flux as a function of channel width for the experiments with solid banks.*

4.2 Discussion on the sediment budgets from the banks and the bed

It has been seen that the output sediment flux depends on the stream power and that it encreases along the reach. Some experiments with solid banks were achieved to put the river in a situation where only bed erosion could occur. We discuss here briefly on the observations and implications of these experiments with solid banks.

Experiments with solid banks also have a constant output sediment flux at the outlet. As in the case of the experiments with erodible banks, the sediment transport rate is found to correlate with the total stream power (Fig. 4.1a). A second order scattering exists in this correlation since sediment transport rate varies at constant total stream power. It is observed that the sediment transport at constant water discharge and slope, decreases as the width increases (Fig. 4.1b). This decrease in the measured output sediment flux means that the erosion capacity of sediment from the bed as well as the transport capacity as bedload must decrease with the width. Relation of the type $Q_s = \rho g S Q/w$ to include the

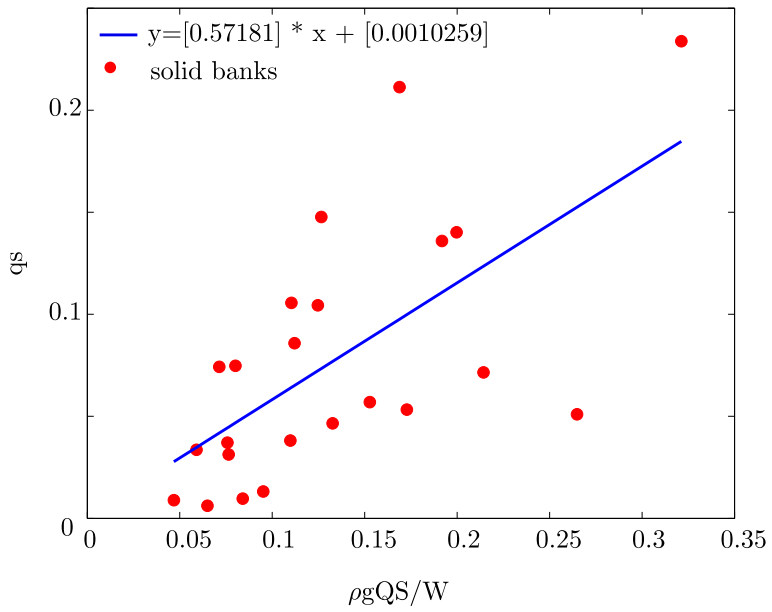

Figure 4.2 – *Sediment transport as a function of the total stream power divided by the width.*

width effet do not plot well with the experiments (Fig. 4.2). However, this dependance of the output sediment flux observed on the width in the case of the experiments with solid banks is in contradiction with the constant sediment transport observed in the experiments of with a widening channel.

To gather information about the sediment budgets in the transport, one compare experiments of solid banks with experiments with erodible bed in the same conditions. Experiments with solid banks transport sediments that must have been eroded from the bed. Experiments with erodible banks are however susceptible to transport sediment that comes from the banks and the bed. Transport rate in the later case are expected to be larger than in the first case. It is what is observed (Fig. 4.3a). Although experiments with solid banks decrease their sediment transport when the width increase, experiments with erodible banks have larger transport rate that are also constant during channel widenning (Fig. 4.3b). It can be seen that during channel widening, the transport rate of sediments remains constant and get away from the trend of the solid bed experiments.

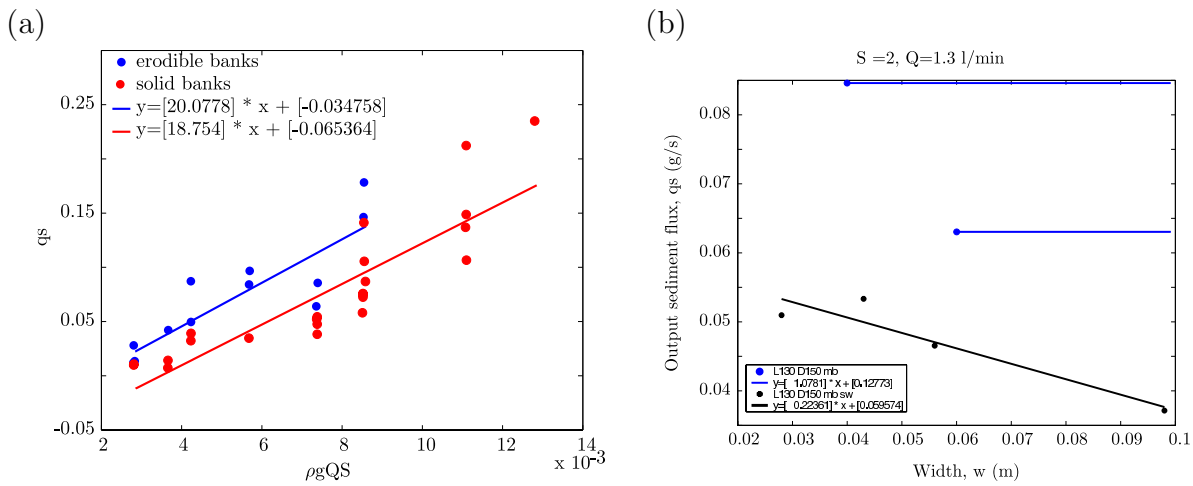

Figure 4.3 – *(a) Sediment transport as a function of the total stream power and (b) Sediment transport as a function of channel width. Transport rate in experiments with erodible banks (blue line) remains constant and balances the diminution in transport capacity (black).*

This observation suggests that the sediment input from the banks manage to balance the decrease in the transport capacity when the channel width increases. Since erosion of the bed is more difficult than of the bank due to the presence of a larger slope on the banks, experiments with solid banks gives an idea of the evolution of the erosion capacity in an enlarging channel. When the channel enlarges, the erosion capacity of sediment from the bed must decrease. The constance in transport rates that is observed suggest a balance in this decrease an input from the banks. This is consistent with higher transport rate with erodible banks than with solid bank. It is expected that in the case of river that as reached equilibrium and with no sediment feeding, the transport rate should decrease.

4.3 Conclusion

Experiments of a microscale river were conducted to study and characterize the equilibrium regime of straight alluvial rivers. The experiments are in an overall negative mass

balance due to the absence of sediment feeding at the inlet. For this purpose, a set of experiments of a widening channel in an alluvial plane were achieved under varying slope, bed load transport, grain size, length of stream and initial width. Measured parameters were the channel width and the output sediment flux at the outlet. During the microscale river experiments, bank erosion and sediment transport occurs which allow the river to change its initial geometry in respect to the flow and slope conditions. The results show that the microscale river is essentially characterized by two equilibrium regimes that appear successively during the channel evolution: there is in any case rapid establishment of a time independance between the mass flux of bedload and the evolution of the river width. First, the output sediment flux reaches a constant value very rapidly and remains constant although the river is still enlarging its channel. Second, the widening rate decreases during the channel evolution until it reaches asymptoticly a vanishing value meaning that a stable width was reached. The decrease in the widening rate is all the more large as the initial width is smaller than the equilibrium width.

The flow in the microscale straight river is measured to be uniform and is in agreement at first order with the classic Chézy and Manning formulas for uniform flow. However a shift in the correlation suggest the possible influence of the surface tension effect. For the experimental condition the flow depth is estimated to be on the order of the millimeter and surface tension can possibly modify the flow. The Chézy and Manning friction coefficients are found to depend on the Weber number. However, when the Weber number becomes larger than a critical value $\mathrm{We} \approx 4$, the friction coefficient tend to a constant value. Under this critical value, surface tension becomes non negligible and have the tendency to slow down the flow. In our microscale river experiments where the Weber number is often less than 4, the presence of sediment transport tends to proove that surface tension are present but do not affect the bedload transport as presumed by Métivier & Meunier (2003).

Dimensional analysis of the regime width in alluvial rivers show two possible characteristic length scales, the grain size or the flow depth. This analysis is in agreement with the empirical scale law with the grain size. In alluvial rivers where the flow is uniform,

an hydraulic relation of the aspect ratio of the flow can be derived. This relation shows a little scatter of data from different natural rivers and experimental streams and collapse the sand bed rivers with the gravel bed rivers. It provides also a physical relation for the width with in particular a dependance that is to be expected to be function of the inverse of the square root of the slope. Introducing this factor in the empirical relation or having the slope at the numerator of the relation are both found to correlate well with the equilibrium width. This suggests that the scaling in this empirical relation with the use of the grain size, may not be accurate as it leeds to unphysical correlations. The large variability of the grain size can explain this artefact in the correlations. Our microscale river, according to the Shields phase diagram is comparable to silt rivers. This is found to be in contradiction with the empirical width relation, which tend to indicate that the microscale fall in the region of the gravel bed rivers. The uniform width relation answers partly to this incompatibilty since the microscale rivers are mixed up with the sand and gravel bed rivers.

The sediment transport rate is at first order in correlation with the total stream power, which is to be expected. Some constraints on the sediment transport distribution along the stream are brought from experiments with channel topography measurements. Digital Elevation Map, obtained using a Moiré method, gives the access in time of the channel topography. It is observed that the channel bed reaches rapidly and before the width a steady and uniform elevation. This suggests that the bedload transport must increases in the streamwise direction with the input of sediments from bank erosion. Therefore an unsaturation state exists in the channel that are eroding in which saturation is not achieved for distance that are large with regard both to the grain size and more important to the channel width. With this observation, a solution to the Exner equation for the sediment mass conservation can be derived. It is found that the channel perimeter (width times the bank heigh) increases in time as a linear function. The increase factor has the dimensions of m^2 s^{-1} and is proportional to the increase rate of the sediment transport along the stream (in fact through the volume fraction of sediment). Analysis

of the increase factor from experiments at different flume length shows that it can be empirically related to the total stream power.

Bibliography

Armstrong, L. & Métivier, F. (2003a). Independence of sediment flux and width evolution through time in a microscale straight river channel. Part 1. scaling of microscale experiments and regime equations. *in prep.*.

Armstrong, L. & Métivier, F. (2003b). Independence of sediment flux and width evolution through time in a microscale straight river channel. Part 2. Implications on the conservation of mass and stream section evolution. *in prep.*.

Dade, W. B. & Friend, P. F. (1998). Grain-size, sediment-transport regime, and channel slope in alluvial rivers. *J. Geol.*, **106**, 661–675.

Diplas, P. (1990). Characteristics of self-formed straight channels. *J. Hydr. Engrg.*, **116**, 707–728.

Hack, J. T. (1960). Interpretation of erosion topography in humid temperate regions. *aam*, **258A**, 80–97.

Ikeda, S. (1981). Self-formed straight channels in sandy beds. *J. Hydrol. Div.*, **107**, 389–406.

Ikeda, S., Parker, G. & Kimura, Y. (1988). Stable width and depth of straight gravel rivers with heterogeneous bed materials. *Water. Resour. Res.*, **24**, 713–722.

Lacey, G. (1930). Stable channels in alluvium. *Proc. ICE*, **229**, 259–270.

Leopold, L. B. & Maddock, T. J. (1953). The hydrolic geometry of stream channels and some physiographic implications. *U. S. Geol. Survey. Professional Paper*, **252**.

Mackin, J. H. (1948). Concept of the graded river. *Geol. Soc. Am. Bull.*, **59**, 463–512.

Macky, G. H. (1999). Large flume experiments on the stable straight gravel bed channel. *Water. Resour. Res.*, **35**, 2601–2603.

Métivier, F. & Meunier, P. (2003). Input and output mass flux correlations in an experimental braided stream. Implications on the dynamics of bed load transport. *J. Hydrol.*, **271**, 22–38.

Meunier, P. & Métivier, F. (2000). Permanence des flux de masse d'une rivière en tresse expérimentale. *C. R. Acad. Sci., Earth and Planetary Sciences*, **331**, 105–110.

Chapter 5

Channel Offset of a Stable Straight River

5.1 Introduction

Alluvial rivers are dynamic systems which can respond to any perturbation by adapting their channel morphology through the elementary processes of erosion and sediment transport. For this reason, river systems have been widely used in tectonic sciences as a possible marker of faulting events. On the basis of the notion of graded rivers, for which the concave shape of the longitudinal profile is the indication of a steady state (Mackin, 1948), formation of terraces by abandonment have been interpreted to represent discreet events that testify river adjusting towards equilibrium (Merritts *et al.*, 1994). Abandonment terraces (Fig. 5.1) may be formed after some particular perturbations applied to a river: for example, decrease in the sediment supply, decrease in the water discharge but also tectonics events such as uplift which all lead to river incision and formation of terraces. Terraces have appeared useful to tectonic studies as they represent a common feature of alluvial systems. They can be used to deduce history and rates of tectonic events.

In the case of vertical offsets of terraces and when isotopic dating is not possible,

Figure 5.1 – *Lateral offset of terraces along the Haiyuan fault (China).*

morphologic dating has been developed to be an alternative method of dating scarps (Avouac, 1993). This method based on a diffusion model of scarp degradation has been used to estimate relative ages of scarps (Avouac *et al.*, 1993). In the case of purely lateral offsets, however, this method does not apply. For the particular region of Tibet in China where an important part of the deformation is accomodated by large strike-slip faults, the offset of rivers and terraces (Fig. 5.2) have long been used to estimate lateral slip rate (*e. g.* Gaudemer *et al.*, 1995; Van der Woerd *et al.*, 1998; Lasserre *et al.*, 1999). Estimation of the lateral slip rate is done by measuring an abandonment terrace riser offset and assuming the age of the event to be that of the terrace at the base of the riser (Lasserre *et al.*, 1999). A riser is assumed to be constantly rejuvenated by flow while the stream runs along its base and to start recording offset by a fault only after the stream bed at its base is completely abandoned, forming a new terrace. This assumption is valid if during two events, the first offset is completely eroded. In the case where a terrace is abandonned before eroding the offset, next event can be overestimated.

In order to assess this problem, we address the problem of a lateral offset of the channel. Bank evolution response is studied to try and obtained conditions on the bank response that will constaint tectonic slip rate estimation. To characterize bank erosion response, the reaction to an offset of an initially stable straight river has been experi-

Figure 5.2 – *Spot image showing a lateral offset on a river along the Altyn Tagh fault (North Tibet, China). Water is flowing from bottom to top of the image. Image from A.-S. Mériaux*

mentally investigated through a set of controlled experiments of a microscale river with erodible banks and bed. Microscale river models has been proven to reproduce stable straight river with stable geometry and non vanishing sediment transport (see previous chapter). In the experiments, a stable straight river undergoes a lateral offset and the channel reaction is analyzed. Eventually, order of magnitude in the channel response to lateral and vertical offsets were obtained for natural river in Turkey.

The experiments of the lateral offset of a microscale straight river are first presented. Results are then discussed and a wave like property of bank erosion is high-ligthed. Results on the bank evolution are presented. Finally, we give a first order qualitative estimation of erosion rate in natural river.

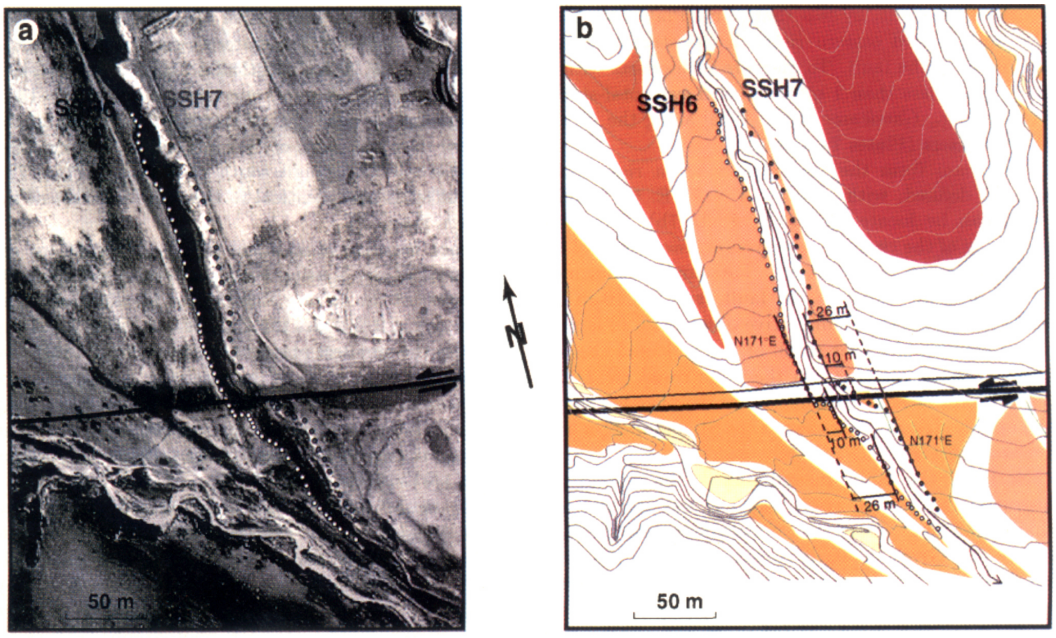

Figure 5.3 – *(a) High-resolution air photograph of small offsets along the Haiyuan fault that affect a river (North Tibet, China). (b) Map view showing the estimated slip from terrace riser (Lasserre* et al., *1999).*

5.2 Experimental setup and observations

5.2.1 Apparatus and procedure

A full cross section is modelled in an experimental micro-scale river. It is reproduced using a mobile bed in a flume of 1.10 m and 70 cm of width (Fig. 5.4). The flume is cut at half length and the downstream box can slip with respect to the upstream box so that the downstream half of the river system can be translated. The sediments used are glass beads with a gaussian distribution of sizes so that the mean diameter of the distribution corresponds to the median diameter (d_{50}). One size of sand was used, A sand of d_{50} =75 µm (standard deviation of σ = 19 µm). The flume rests on a tilting planform that allows control of the bed slope. Slopes are measured using a digital level device (precision of 0.1 °). The initial cross section of the channel is rectangular of variable width (2.5 cm to 8 cm) and 1 cm height and is molded by a template. Water discharge

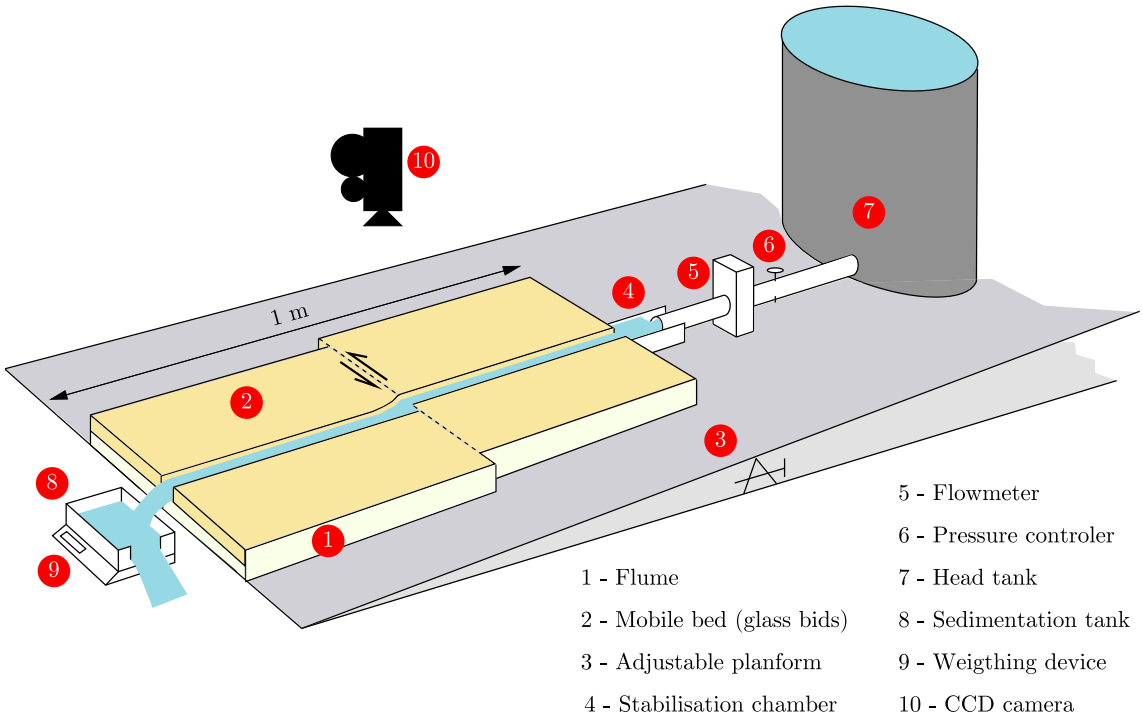

Figure 5.4 – *Experimental setup, not to scale.*

is adjustable and measured using a flow-meter. The water discharge remains constant during the experiments within less than 0.7 % with the use of a head tank (Fig. 5.4). The sediment discharge is measured at the outlet using an overflowing sedimentation tank. The tank remains at constant water level and particles are allowed to settle. A wave protection is placed close to the exit ramp of water in the overflowing tank to absorb surface waves and therefore reduce the scattering in the measure of the mass. The tank is positioned on a high precision weighting device (0.1 g of precision) connected to a PC that collects the weight of the tank at regular time intervals (10 s). This gives access to a precise and direct measure of the cumulated mass at the outlet of the river from which the sediment discharge can be derived. There is no sediment recirculation in these experiments as it is usually done to put the river in an equilibrium state and which prevents excessive degradation at the inlet (Ikeda, 1981; Ikeda *et al.*, 1988; Diplas, 1990; Macky, 1999). Instead of that, a stabilisation pool is set at the inlet of the flume so that the water velocity is reduced and degradation of the bed is delayed. The inflow of water

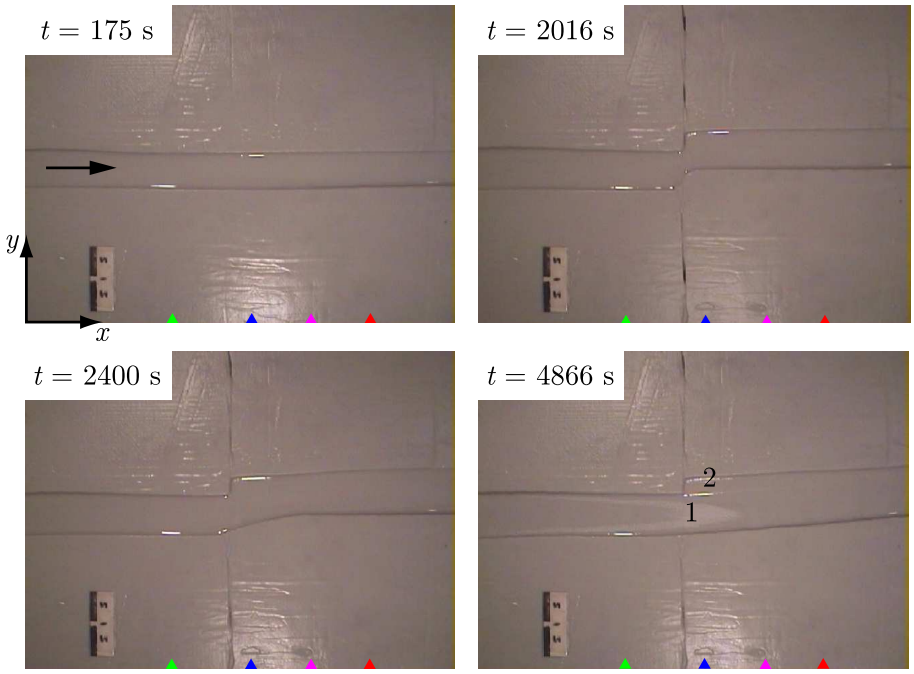

Figure 5.5 – *Views of an experimental run of an offset channel at different time steps,* $S = 0.052$, $Q = 1$ *l/min,* $d_{50} = 75$ µ*m and* $\delta/W_e = 0.54$. *Note (1) the parabolic shape of the flow and (2) the abandonment terrace.*

took place through a 2.5 cm wide aperture. A digital video camera is positioned at the vertical of the plane above the region of offset and a movie of the experiment is recorded on a Macintosh computer with a time lapse typically of 30 s that is enough to capture the channel adjustment and which reduces the memory cost on the hard drive. The camera covers a region of about 30 cm wide which corresponds to the best compromise to have the larger area and a good precision for the bank detection. Typical experiment duration was between 1 and 3 h.

5.2.2 Evolution of the experiment during a run

A series of 45 experiments were conducted under varying water discharge (Q = 0.5–1.3 l/min), initial slope (S = 0.017–0.070), and offset size over equilibrium width ratio (δ/W_e = 1/4–1/2). Fig. 5.5 presents the typical evolution the experiments. After flow

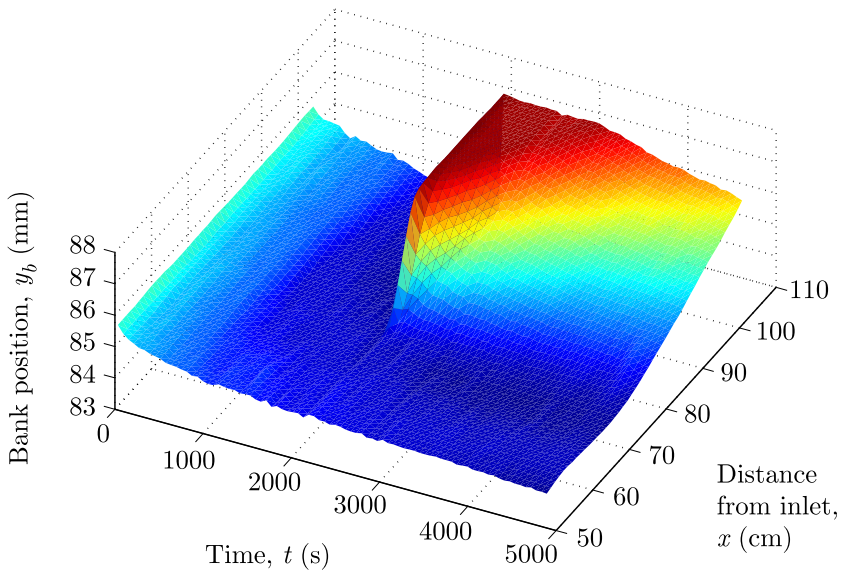

Figure 5.6 – *Evolution in time and along the stream of the position of the active bank during an experiment run of a channel offset,* $S = 0.052$, $Q = 1$ *l/min,* $d_{50} = 75$ µ*m and* $\delta/W_e = 0.54$.

of water Q, the channel starts eroding its banks and transporting sediments so that the channel finally reaches a stable configuration (see previous chapter). When this is the case, an offset is applied by displacement of the downstream part of the flume. The offset is applied rapidly in regards to the channel evolution so that it can be considered as instantaneous. The offset in all the experiments is a sinistral. Displacement of the flume is transmitted from the box boundaries to the alluvial plain and all the downstream part of the river system is translated from the upper part over a distance δ. Typical features of tectonics such as push-ups and pull-aparts are observed in the microscale alluvial plain above the flume junction. As a result of the shift of downstream channel system, a constriction of the flow is created at the region of the offset and is responsible of an active erosion in the region of the bank exposed to the flow. Modification of the streamlines do not affect however the channel upstream from the offset and all the response of the channel is localized downstream from the offset. A point of initiation of erosion is defined on the bank above which erosion on the bank does not occur. This point of initiation of erosion

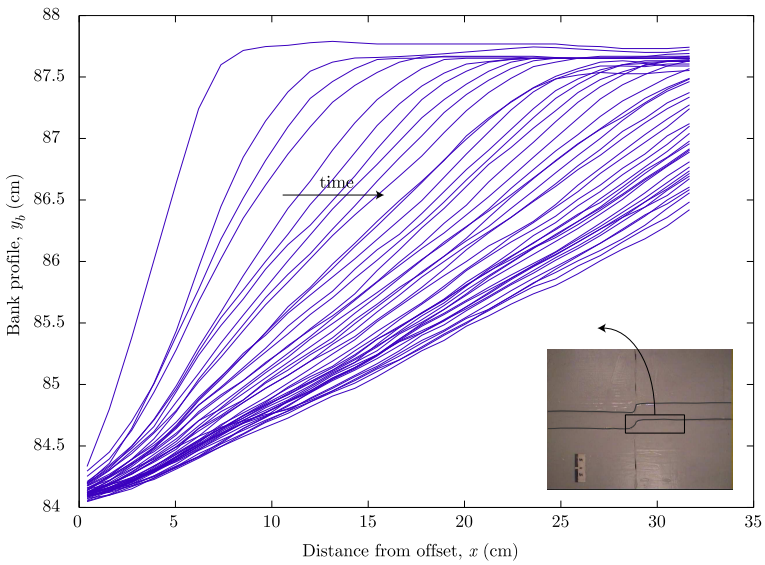

Figure 5.7 – *Profiles of the active bank in the region downstream from the offset and at different time steps,* $S = 0.052$, $Q = 1$ *l/min,* $d_{50} = 75$ µ*m and* $\delta/W_e = 0.54$.

propagates downstream through time while erosion on the bank continues upstream. This bank is refered as the "active" bank by opposition to the other bank which remains stable and do not display erosion except, depending on the flow conditions and the magnitude of the offset, locally at a downstream position where the flow arrives due to changes in the direction of the streamlines from the curvature of the active bank. Propagation of erosion on the active bank can eventually be coupled with the formation of an abandonment terrace on the opposite side of the channel in the latter stage of the run. These two features finally allow the river to reach again a straight channel which width is comparable to the one prior to the offset. The corner on the passive bank is preserved from erosion in most cases but not all.

The movie of the experiment undergoes an image processing that detects the geometry of the active bank (see Chapter 2). In the coordinate system positioned at the lower left corner of the pictures where the x is oriented downstream and y is towards the channel (Fig. 5.5), the detection of the active bank provides the knowledge of positions of the

bank y_b at any distance and any time,

$$y_b\,(x,t). \tag{5.1}$$

Fig. 5.6 represents this particular function of the bank position for the experiment displayed in Fig. 5.5. In this plot, a vertical line represents the bank profile at a given time and an horizontal line represents the time evolution of the active bank at a given distance from the inlet. The propagation of erosion that follows the offset is in the downstream direction and denotes a decrease in the velocity. Evolution in time of the active bank is however easy to visualize from the series of profiles, *i. e.* the curves $z_b\,(x,t_i)$ at each time t_i, on a same plot (Fig. 5.7). Erosion is not distributed equally along the bank in the y direction: erosion increases towards the center of the channel and vanishes at the origin of the offset ($x = 0$). Another way to observe the evolution in time of the active bank, is to represent the bank evolution in time at different positions (Fig. 5.8). It is seen that the section upstream from the offset was at equilibrium when the offset was applied. For downstream section from the offset, evolution in time of the bank position allows to see the propagation of the erosion as the time of initiation of erosion increases with the downstream distance from the offset.

Cumulated mass and mass flux at the outlet of the experimental river are reported on Fig. 5.9. The ouput sediment flux can present, depending on the flow conditions and offset magnitude, a slight increase from the average. This increase in the flux can not be attributed with certainty to the erosion on the active banks in all the experiments. The offset is placed at half flume length, *i. e.* at ~ 65 cm from the outlet. Bedload transport is known to be a diffusive mechanism and one would expect to have an attenuated signal delayed in time. The increase in the output flux could occur at the time of offset and one suspect an origin from the other bank. Incertitude exists on the origin of the signal (1) from the active bank or (2) from the local erosion that can occur on the opposite bank and therefore closer to the outlet and before the erosion front on the active bank has arrived at this distance. Since not all the experiments present this augmentation of the ouput sediment flux, we will not consider this parameter in further analysis. This will

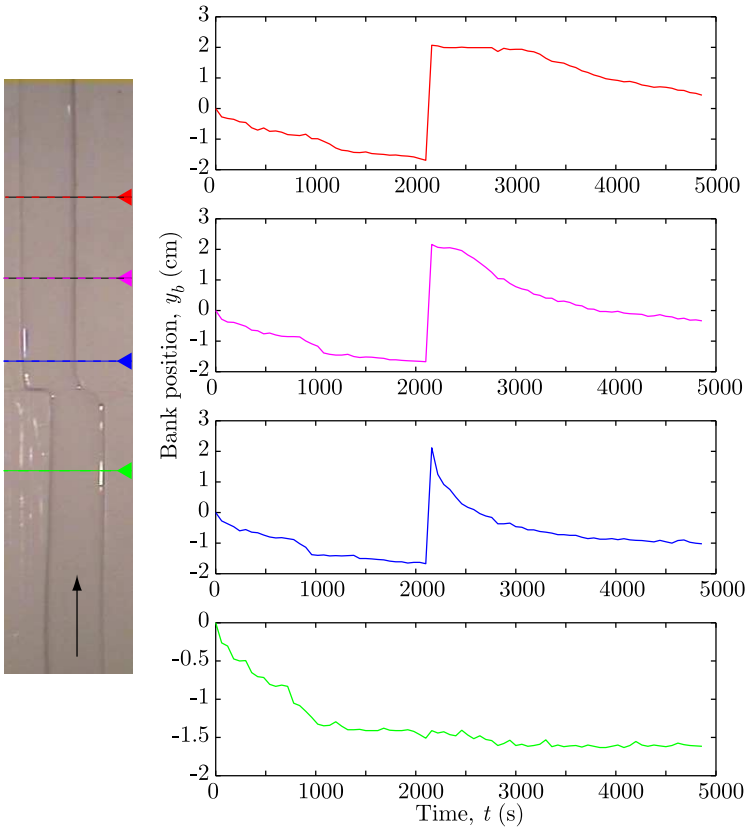

Figure 5.8 – *Evolution of the bank position at several positions along the reach,* $S = 0.052$, $Q = 1$ *l/min,* $d_{50} = 75$ µ*m and* $\delta/W_e = 0.54$. *The section upstream the offset shows that the river had reached the equilibrium width when the offset was applied.*

deserve further analysis in the future. We believe however, that origin of the signal after a channel offset in the output sediment flux would originate from the erosion on the active bank in the case where the offset is applied close enough to the outlet so that no erosion occurs on the opposite bank.

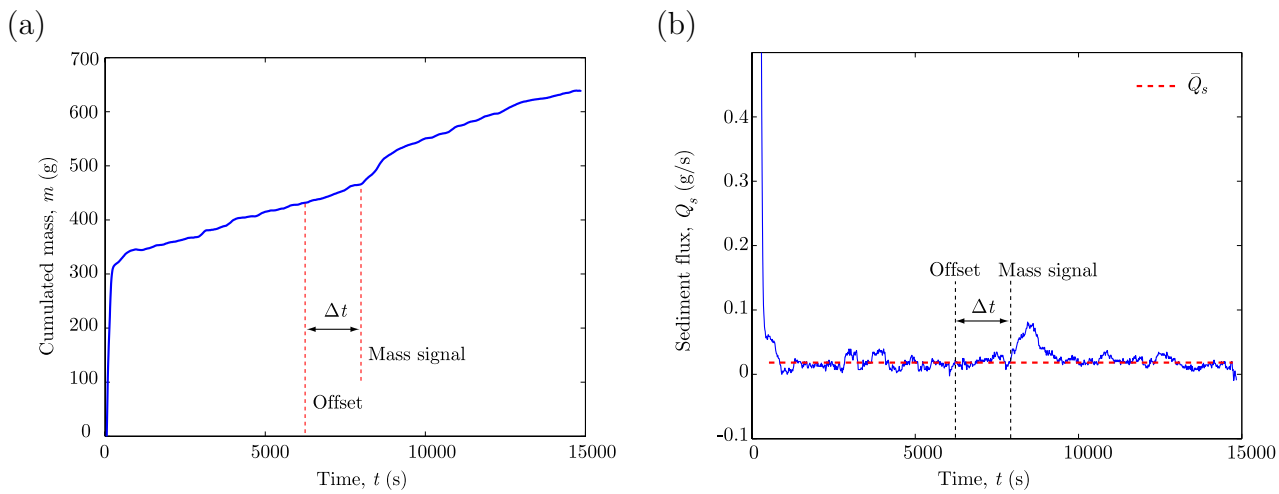

Figure 5.9 – *(a) Cumulated mass at the outlet and (b) Ouput sediment flux,* $S = 0.052$, $Q = 1$ *l/min,* $d_{50} = 75$ µ*m and* $\delta/W_e = 0.54$.

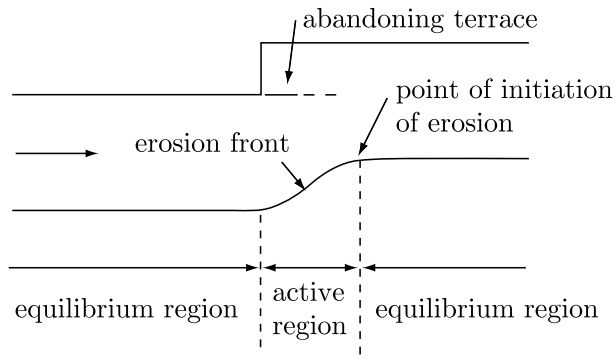

Figure 5.10 – *Scheme of the active region with front of erosion and two equilibrium region: upstream the offset and downstream the initiation of erosion.*

5.3 Results

Response of a channel to a lateral offset is localized in the downstream part of the channel above the offset and the channel is found to remain stable in the upper part (Fig. 5.10). Bank erosion occurs on the exposed bank to the flow and propagates downstream. To describe the propagation of the erosion on the active bank, three quantities (local angle of the bank with the downstream direction, local velocity of the bank in the normal direction and velocity of initiation of erosion) are first derived from the data. This allow to bring constrains on the mechanism of bank erosion. A model for the propagation of the bank is then discussed.

5.3.1 Local angle of the bank and bank velocities

To characterize the bank erosion occurring on the bank, several quantities are derived from the bank profiles. These quantities are the local bank inclination

$$\beta\left(x,t\right)=\frac{\partial y_b}{\partial x}, \tag{5.2}$$

the erosion rate or local normal velocity of the bank,

$$v_b\left(x,t\right)=\frac{\partial y_b}{\partial t}, \tag{5.3}$$

and eventually the velocity of the initiation point of erosion

$$u_b(t) = \frac{\partial x_b}{\partial t}|_{y=\delta} \tag{5.4}$$

where (x_b, y_b) are the bank coordinates. The velocity of the initiation point of erosion is estimated at the top of the front from the profiles $y_b\,(x,t)$ of the bank. These quantities are expected to vary in space along the reach and in time in the downstream region from the outlet were erosion only occurs. For clarity, the quantities are now expressed in the coordinate system placed at the offset on the inflexion point so that the point (x_b, δ) corresponds to the top of the front. At a given position along the stream, the time evolution of the bank profile, the bank inclination and the erosion rate are represented for the region downstream from the offset (Fig. 5.11). Bank profiles curves can be modeled by a decreasing exponential (Fig. 5.11a)

$$y_b = \delta \exp\left(-\frac{t - t_0}{\tau}\right), \tag{5.5}$$

where t is the time after offset, t_0 is the time of initiation of erosion and τ is a relaxation time. Evolution in time of the bank inclination (Fig. 5.11b) and of the erosion rate (Fig. 5.11c) are characteristic of a wave mechanism as their magnitude increase and then decrease with the passage of the erosion front. These quantities which were modified by the perturbation tend to return to the initial values but can show an asymptotic value close to the unchanged reference values upstream from the offset (Fig. 5.11).

Another way to describe this propagation phenomenum is to look at the previous quantities as they are advected by the front. The main front velocity is calculated at the top of the front since it is there that the erosion is initiated for a given position (Fig. 5.12a). During the propagation of the erosion front, its velocity decreases and can be modeled by a decreasing exponential (Fig. 5.12a)

$$v_b\,(t) = v_{b,0} \exp\left(\frac{-t}{\tau_b}\right), \tag{5.6}$$

where $v_{b,0}$ is the velocity of the from at $t = 0$ and τ_b is a relaxation time. Both the bank inclination (Fig. 5.12b) and the rate of erosion (Fig. 5.12c) calculated at the top of the front of erosion display a decrease as the front propagates.

These observations suggest a wave-like propagation. We look for a relashionship between the previous quantities (Fig. 5.13). It appears that, for all the experiments, the erosion rate $\partial y_b/\partial t$ is negatively correlated to the inclination $\partial y_b/\partial x$ times the front velocity $\partial x_b/\partial t|_{y=\delta}$:

$$\frac{\partial y_b}{\partial t} + \frac{\partial x_b}{\partial t}|_{y=\delta}\frac{\partial y_b}{\partial x} = 0, \tag{5.7}$$

which is the equation of a kinematic wave. Empiricaly, the erosion of the bank is found to propagate as a kinematic wave.

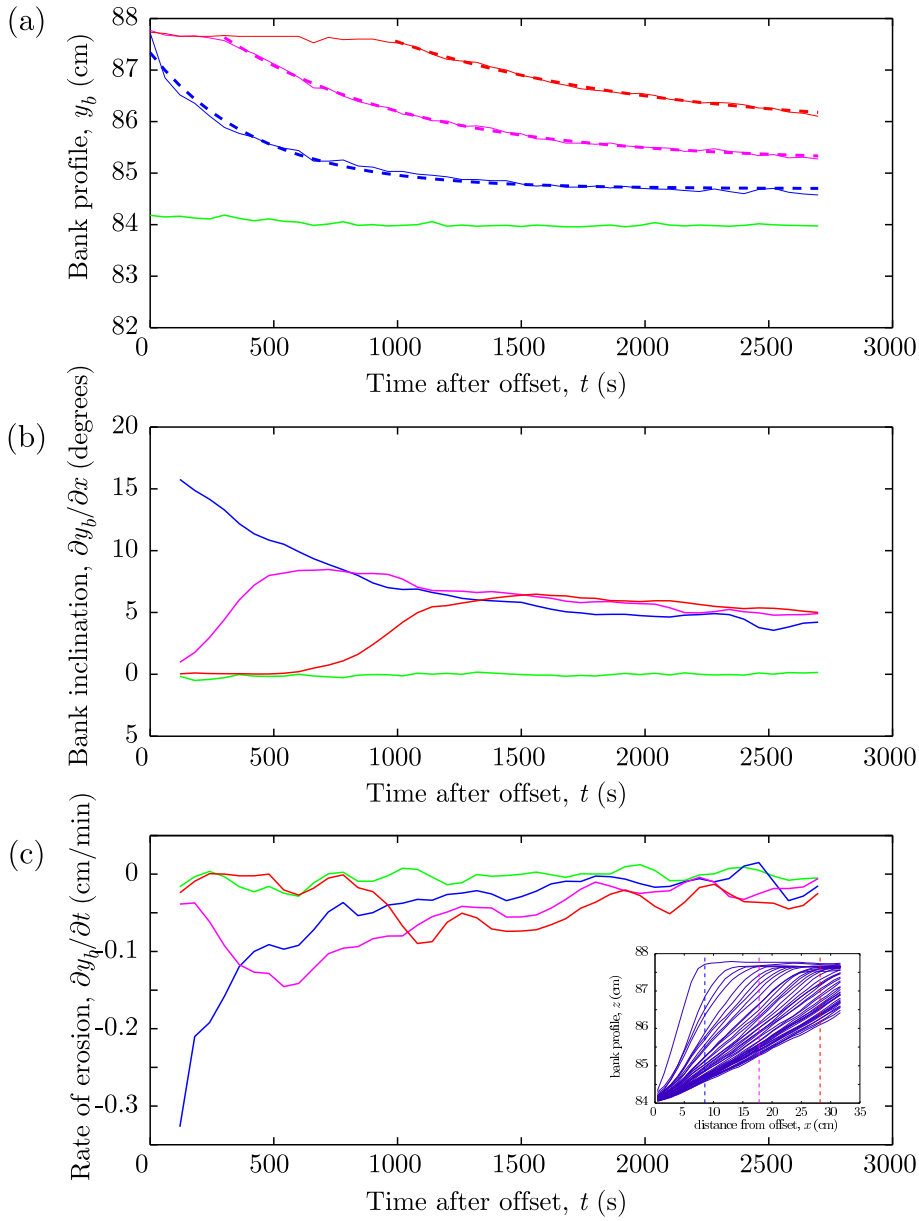

Figure 5.11 – *(a) Time evolution of the bank profile, (b) of the bank inclination and (c) of the erosion rate at 3 positions along the reach,* $S = 0.052$, $Q = 1$ *l/min,* $d_{50} = 75$ µm *and* $\delta/W_e = 0.54$. *For comparison, the respective values in an upstream section are represented in green. Dashed line in (a) represent the fit of a decreasing exponential to the bank evolution.*

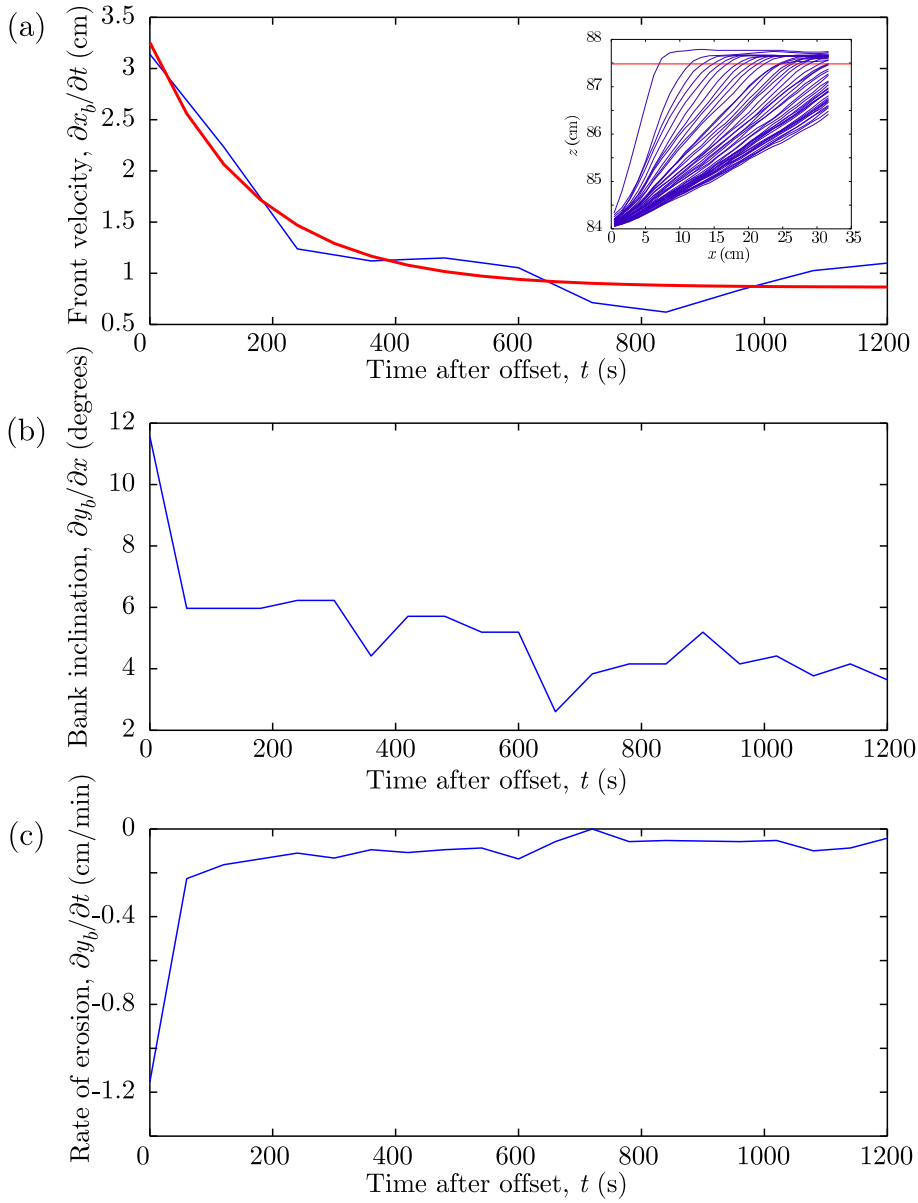

Figure 5.12 – *(a) Front velocity, (b) advected bank inclination and (c) advected erosion rate at 3 positions along the reach,* $S = 0.052$, $Q = 1$ *l/min,* $d_{50} = 75$ µ*m and* $\delta/W_e = 0.54$.

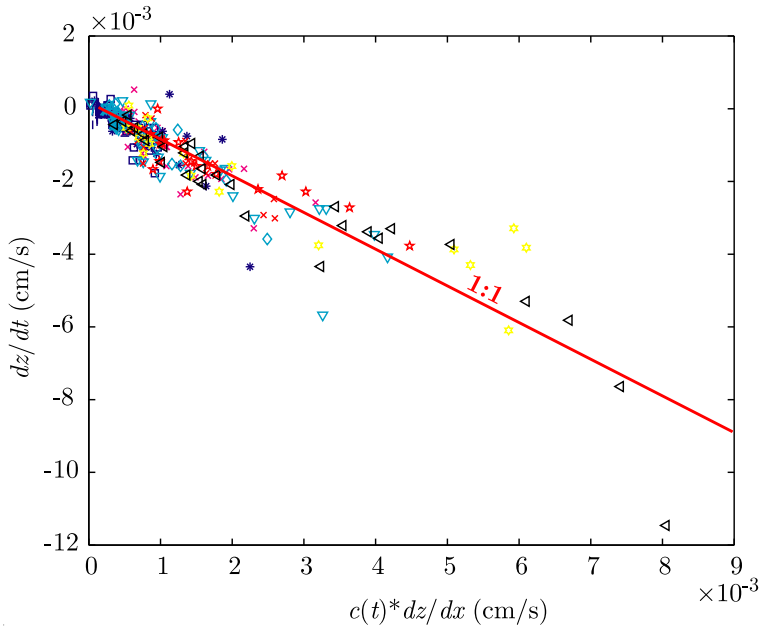

Figure 5.13 – *Correlation of $\partial z/\partial t$ vs. $c(t)\partial z/\partial x$ of slope -1 for a set of experiments with varying slope, water discharge and offset size. These data suggest a kinematic wave equation.*

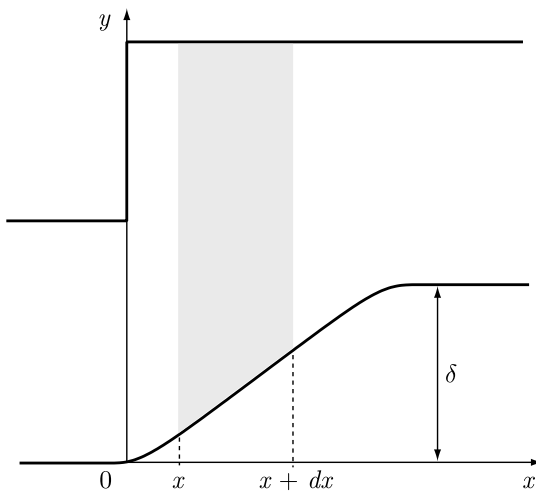

Figure 5.14 – *Definition sketch in plane view of the right bank. Bedload transport is assumed to vanish at* $x = 0$.

5.3.2 Derivation of the kinematic equation and implication on the bedload transport

Kinematic waves are, originally, features of fluid dynamic where a propriety of the fluid is advected by the flow (Wallis, 1969). The propagation of the wave is directly related to the flux of material. We apply this to the case of the channel and derive a kinematic equation from the mass equation conservation for the mass.

We assume that at the offset ($x = 0$), bedload transport from upstream is negligible in front of input sediment rate from the erosion on the active bank, $Q_s(0, t) \sim 0$ (Fig. 5.14). We assume that the maximum transport capacity is never reached during propagation of erosion so that sediment eroded from the bank are always transported. The mass conservation of sediment over the bed region with these assumptions then reads

$$(1 - \phi)\rho_s h_b \frac{\partial y_b}{\partial t} + \frac{\partial Q_s}{\partial x} = 0, \tag{5.8}$$

where ϕ is the porosity of the sediment, h_b is the bank height and Q_s is the rate of transport (kg/s). From the derivatives of the bank position y_b, the following relation can

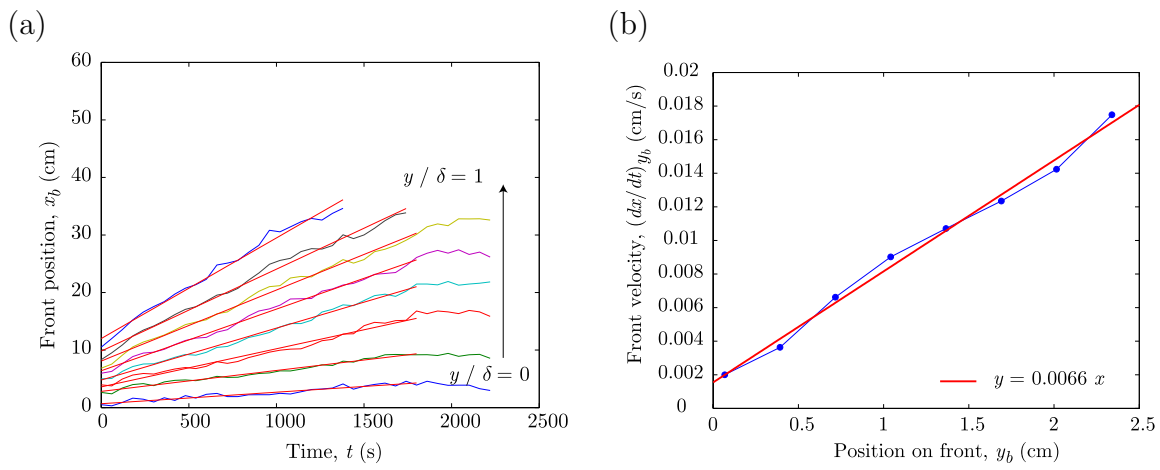

Figure 5.15 – *(a) Evolution in time of the bank position x_b at different positions on the front y_b. (b) Corresponding velocity as a function of position on the front y_b showing that the front propagates with a velocity that increases as the position on the bank is towards the center of the channel.*

be obtain

$$\left(\frac{dx}{dt}\right)_{y_b} = -\frac{\partial y_b/\partial t}{\partial y_b/\partial x}. \tag{5.9}$$

Using Eq. (5.8) and since ϕ and h_b are considered as constant, Eq. (5.9) can be rearranged as

$$\left(\frac{dx}{dt}\right)_{y_b} = \frac{1}{h_b\rho_s(1-\phi)}\frac{\partial Q_s/\partial x}{\partial y_b/\partial x} = \frac{1}{h_b\rho_s(1-\phi)}\frac{\partial Q_s}{\partial y_b}. \tag{5.10}$$

This relation relates the velocity of the front to the bedload transport. A kinematic form of the mass conservation can be obtained with Eq. (5.8) and Eq. (5.10):

$$\frac{\partial y_b}{\partial t} + \left(\frac{dx}{dt}\right)_{y_b}\frac{\partial y_b}{\partial x} = 0. \tag{5.11}$$

where the velocity of the bank is unknown and is expressed with Eq. (5.10).

An empirical form of the front velocity can be obtained from observation of the evolution of bank position at different height on the front (Fig. 5.15a). It appears that during propagation of the front, the velocity $(dx/dt)_{y_b}$ is a function of the position on the front y_b and that it can be considered as constant (Fig. 5.15a). The form of this

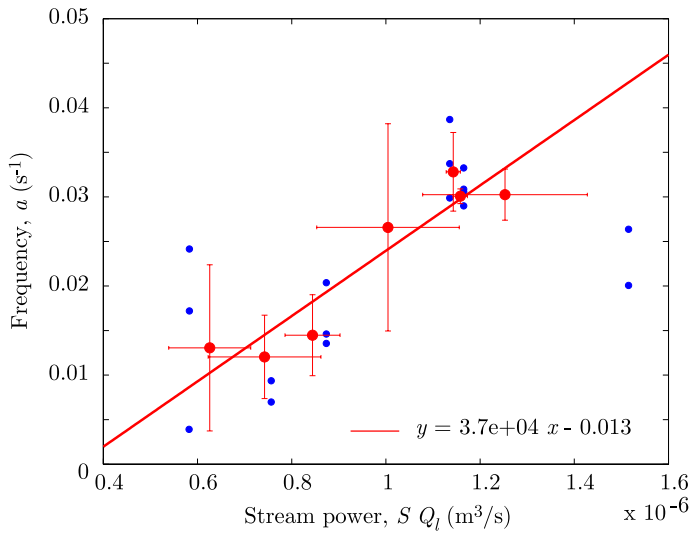

Figure 5.16 – *Variation of the frequency a for the experiments as a function of the stream power.*

function can be addressed while plotting the velocity $(dx/dt)_{y_b}$ in function of the position y_b (Fig. 5.15b). A linear correlation is observed which significate that one have at first order

$$\left(\frac{dx}{dt}\right)_{y_b} = a y_b, \tag{5.12}$$

where a has the dimension of a frequency and is expected to depend on the river and geometric parameters (S, Q). Having Eq. (5.12) into Eq. (5.11) and integrating yields

$$\frac{\partial y_b}{\partial t} + \frac{a}{2}\frac{\partial^2 y_b^2}{\partial x} = 0, \tag{5.13}$$

which is the equation for the bank evolution. The frequency a can be estimated for all the experiments of channel offset with varying slope, water discharge and size of the offset. A trend in the data appears indicating that the frequency increases with the stream power (Fig. 5.16). Using this result, Eq. (5.13) can be expressed as:

$$\frac{\partial y_b}{\partial t} + \epsilon\frac{QS}{2}\frac{\partial^2 y_b^2}{\partial x} = 0, \tag{5.14}$$

where ϵ is a constant ($[\epsilon]$ =L^{-3}) Eventually, the bed load profile can be obtained. Using

Eq. (5.10), Eq. (5.12) can be expressed as

$$\frac{\partial Q_s}{\partial y_b} = \epsilon h_b \rho_s (1-\phi) Q S \, y_b, \tag{5.15}$$

wich integrates into

$$Q_s = \epsilon h_b \rho_s (1-\phi) Q S \, y_b^2 + b, \tag{5.16}$$

where b is the bedload transport when y_b vanishes. By continuity, $b = 0$ since $Q_s(0,t) = 0$. This relation is valid in the case where all the sediment eroded from the front can be transported.

5.4 Offsets of natural rivers in Turkey

5.4.1 Tectonic setting and measurments

Two major earhtquakes occured in Turkey, the Izmit earthquake, in august 1999 of magnitude 7.6 and the Duzce earthquake, in november 1999 of magnitude 7.2. These earthquakes were located on the North anatolian Fault (NAF) which borders North of the Anatolian block (Fig. 5.17a). This fault is mainly a sinistral strike-slip fault that accommodate the westward escape of the Anatolian block. The area of the Duzce epicenter is located in the border of a mountainous region in which rivers could be affected by channel offsets (Fig. 5.17b). In order eventually monitor river response to channel offsets, two field trip where done, first about 10 days after the Duze earthquake to search for sites of channel offsets and measure the bank profile and second, 6 months later, in may 2000 to follow the river response.

During the first campaign, most of the field study consisted in founding and selecting sites of channel offsets that could be potentially interesting for monitoring the evolution in time. A total of 4 sites of channel offsets were originally selected. Two of them had to be eliminated since they had been antropomorphized by deposition on the bank of various concrete material to reduce erosion and avoid the loose of the surrounding cultivated or habited grounds. This is an indication that during the following months of

(a)

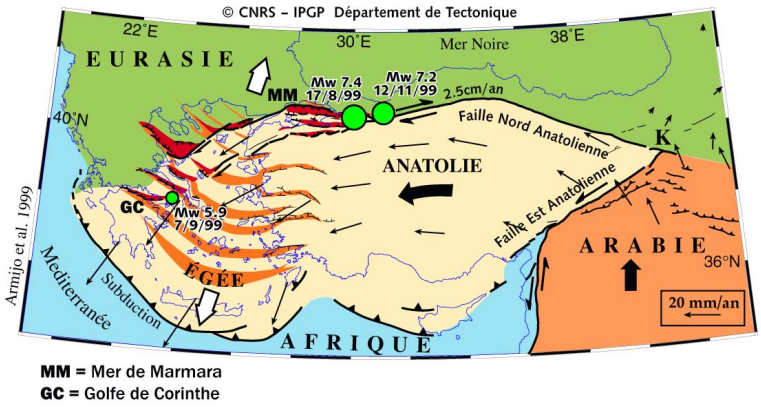

(b)

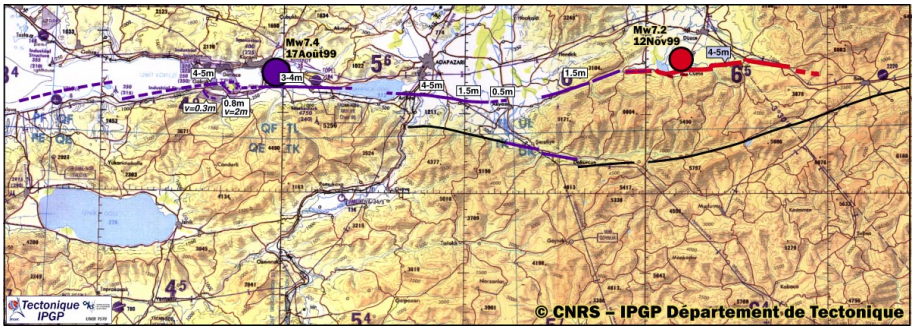

Figure 5.17 – *(a) Localisation of the Izmit and Duzce earthquakes along the North Anatolian fault that borders the Anatolian block. (b) Region of Izmit and Duzce (Turkey).*

the earthquake, bank erosion was considered important enough by local inhabitants. The two rivers left for the observations are the Urgusuyu river and the Deresuyu river. The Urgusuyu is a large gravel bed river with large boulders that can be transported during floods (Fig. 5.18a). This river underwent a large lateral offset (dextral) with geometry close to the one in the experimental study. Just after the offset, the river displayed a central bar (Fig. 5.18a). The Deresuyu river, at the reach of the offset, is a small gravel bed river which underwent an uplift (Fig. 5.19a). Topographic measurements were done using a high precision topographic maping total station (Leica Wild T2000) in order to obtain quantitative description of the channel response.

(a) (b)

Figure 5.18 – *(a) Urgusuyu river in november 1999, shortly after the Duzce earthquake. (b) Urgusuyu river, 6 months later.*

5.4.2 River response

Cartography of the banks of the Urgusuyu river shows that the initial lateral offset of 4 m on the left bank has nearly completely disappear in 6 months (Figs. 5.18b and 5.20). The disparition of the active flow on the right of the central bar is artificial and due to fluvial engineers that blocked the flow there in order to control the river. For this reason comparison to our model is hazardous since it is not known what was the repercusion of this artificial modification. The erosional wave on this period of time is not observed. However, one can give a first order estimation of the erosion rate of the offset,

$$R_u \approx 2\,\mathrm{cm/day}. \tag{5.17}$$

This average value is small but is certainly an under estimation as the erosion of the offset may have been achieved earlier. The erosion rate, on smaller time scales, is expected to be larger than the averaged value.

The Deresuyu has undergone an uplift which is no more visible after a period of 6 months (Fig. 5.19b). Topography of the channel was not measured in November 1999. Evolution of the bed can be obtained using the terraces that the river as abandoned during its response. The terrace did not exist just after the offset and correspond to the initial

(a) (b)

Figure 5.19 – *(a) Deresuyu river in november 1999, shortly after the Duzce earthquake. (b) Deresuyu river, 6 months later.*

bed level. Abandonment terraces profiles and bed profile measured in May are represented in Fig. 5.21. It is observed the incision of the bed with globaly erosion upstream the uplift and deposition downstream. A retreat of the point of inflexion is also observed denoting a mechanism of propagation of the offset with an advection component. Estimation of the rate of retreat is found to be

$$R_u \approx 10\,\mathrm{cm/day}. \tag{5.18}$$

The responses of alluvial rivers to a lateral offset and to a vertical offset show that the river in both case tend to erase the perturbation. Is is observed that on the same time of response, vertical perturbation of the channel is efficient to produce terraces whereas lateral perturbation are rapidly erased.

5.5 Conclusion

Experiments of a microscale straight river was setup to study the channel response to a perturbation of the channel. A series of controled experiments were achieved under varying slope, water discharge and size of the offset relative to the channel width. Response to

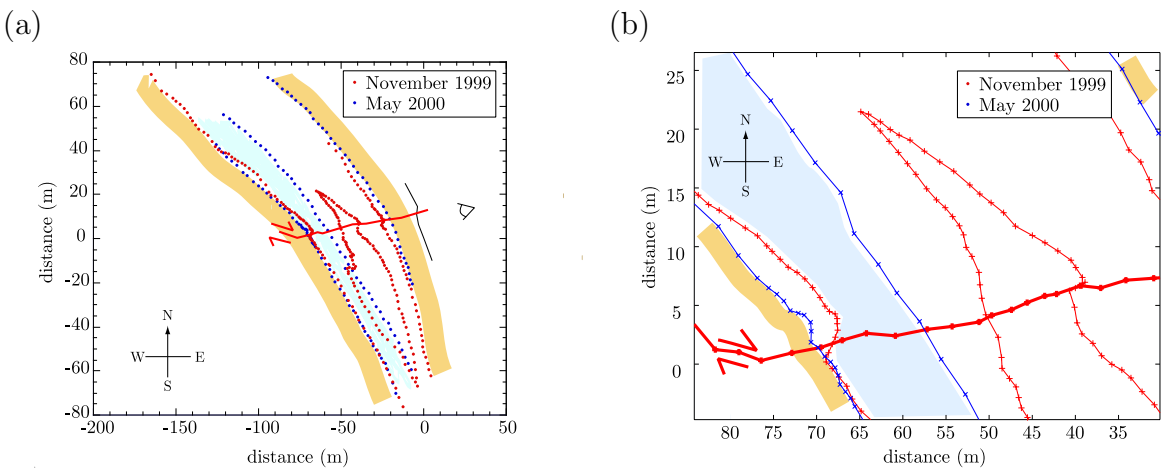

Figure 5.20 – *(a) Cartography of the bank profiles in the Urgusuyu river. Initial offset of 4 m (red dots) as disappeared 6 months later (blue dots). (b) Close up showing the residual offset (≈ 1 m). Water is flowing northward.*

a lateral offset of the channel is characterized by the apparition of a erosion front that propagates downstream on the bank exposed to the flow. Opposite bank do not display erosion and a abandonment terrace tend to appear leading to final channel which is again straight. In some cases, this terrace can be eroded partly which can lead to errors in the estimations of slip-rates.

Output sediment flux and profiles of the active bank were measured during the experimental run to constrain the response of the channel. Output sediment flux can display, depending on the flow conditions, an increased value following the offset. However, uncertainties exists on attributing its origin with the active bank and is more eventually due to parasite erosion on the opposite bank. Bank profiles are extracted from the movie of the experiment. They show a general form of a propagating wave with attenuation in the amplitude. Characterization of the wave of erosion on the active bank is done with the examination of several parameters deduces from the bank profiles. The evolution in time of the local bank inclination, the local normal velocity of the bank, the downstream velocity of the erosion front are characteristic of a wave. This quantities advected during the

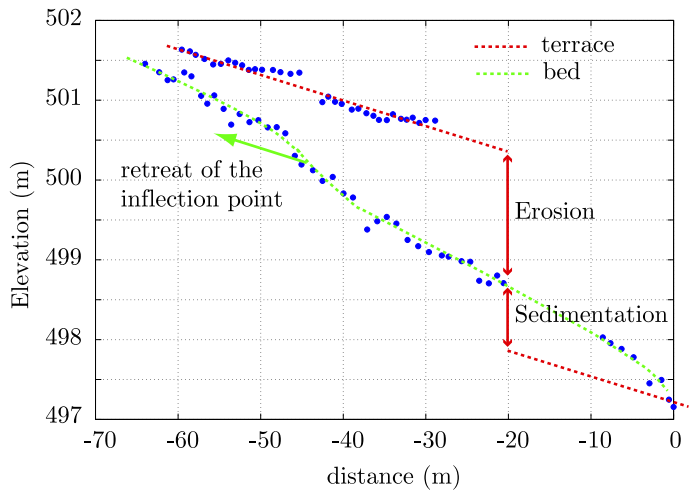

Figure 5.21 – *Longitudinal profiles of the abandonment terraces and of the bed. The bed profile denotes a retreat of the inflection point.*

propagation show a correlation in the form of a kinematic equation. Local perturbation of the bank erosion is found to propagate downstream following a kinematic wave.

A simple model is proposed to derive a kinematic wave equation for the bank. If the bedload transport coming in the offset region can be neglected in front of the input flux from the bank erosion and with the assumption that no bed aggradation occurs, a width average equation for the mass conservation can then be derived. It is shown that this equation has the general form of a kinematic equation. The front velocity can be related to the width averaged bedload transport. Comparison with the experiments show that the front velocity increases linearly at positions on the front towards the center of the channel. A general trend from the data indicate that the frequency increases with the unit stream power. During the propagation, the frequency of the front velocity can be consedered to remain constant at first order and an empirical form of the bedload transport as a function of the bank position and of the frequency can be derived.

Response of natural rivers to offsets of their channel was monitored for two rivers following the Duzce earthquake. In the case of the Urgusuyu river which underwent a lateral offset, the major part of the offset has been eroded within 6 months which gives an under estimation of the erosion rate of 2 cm/day. A small component of the offset remains

in the bank profile ($\approx$ 1 m). If for any reasons, abandonment terrace would occur, this would lead to an over estimation in the slip-rate. In the case of the Deresuyu which underwent a vertical offset, the river incises its bed with the creation of abandonment terraces. The bed profile adjusts with a advecting component of about 10 cm/day.

Bibliography

Avouac, J.-P. (1993). Analysis of scarp profiles: evaluation of errors in morphologic dating. *J. Geophys. Res.*, **98**, 6745–6754.

Avouac, J.-P., Tapponnier, P., Bai, M., You, H. & Wang, G. (1993). Active thrusting and folding along the northern Tien Shan and late Cenozoic rotation of the Tarim relative to Dzungaria and Kazakhstan. *J. Geophys. Res.*, **98**, 6755–6804.

Diplas, P. (1990). Characteristics of self-formed straight channels. *J. Hydr. Engrg.*, **116**, 707–728.

Gaudemer, Y., Tapponnier, P., Meyer, B., Pelzer, G., Guo, S., Chen, Z., Dai, H. & Cifuentes, I. (1995). Partitioning of crustal slip between linked active faults in the eastern Qilian Shan, and evidence for a major seismic gap, the 'Tianzhu gap', on the wester Haiyuan fault, Gansu (China). *J. Int.*, **120**, 599–645.

Ikeda, S. (1981). Self-formed straight channels in sandy beds. *J. Hydrol. Div.*, **107**, 389–406.

Ikeda, S., Parker, G. & Kimura, Y. (1988). Stable width and depth of straight gravel rivers with heterogeneous bed materials. *Water. Resour. Res.*, **24**, 713–722.

Lasserre, C., Morel, P.-H., Gaudemer, Y., Tapponnier, P., Ryerson, F. J., King, G. C. P., Métivier, F., Kasser, M., Kashgarian, M., Baichi, L., Taiya, L. & Daoyang, Y. (1999). Postglacial left slip rate and past occurence of $M \geq 8$ earthquakes on the western Haiyuan fault, Gansu, China. *J. Geophys. Res.*, **104**, 17633–17651.

Mackin, J. H. (1948). Concept of the graded river. *Geol. Soc. Am. Bull.*, **59**, 463–512.

Macky, G. H. (1999). Large flume experiments on the stable straight gravel bed channel. *Water. Resour. Res.*, **35**, 2601–2603.

Merritts, D., Vincent, K. R. & Wohl, E. E. (1994). Long river profiles, tectonism, and eustasy: a guide to interpreting fluvial terraces. *J. Geophys. Res.*, **99**, 14031–13050.

Van der Woerd, J., Ryerson, F. J., Tapponnier, P., Gaudemer, Y., Finkel, R., Mériaux, A. S., Caffee, M., Zhao, G. & He, Q. (1998). Holocene left-slipe rate determined by cosmogenic surface dating on the Xidatan segment of the Kunlun fault, (Qinghai, China. *Geology*, **26**, 695–698.

Wallis (1969). *One dimensional two-phase flow.* Mc Graw Hill.

Chapter 6

Conclusion and perspectives

Experiments of a microscale straight river were achieved to study the dynamic regimes of alluvial rivers. River dynamic was addressed from two different points of views.

- The equilibrium regimes in straight alluvial rivers were characterized using a microscale river. (1) There is for all the experiments rapid establishment of a time independence between the mass flux of bed load and the evolution of the river width. First the output sediment flux reaches a constant value while the channel is still widening and second, an equilibrium width is reached on a longer time scale. (2) A uniform flow is established in the microscale river and surface tension effect are susceptible to be non negligible. A relationship as been found for the friction coefficient in function of the Weber number. (3) From the observation that uniform flow conditions can be found in many natural rivers, a dimensional analysis of the equilibrium width problem is performed and a first order regime relationship for the width is derived. This relationship enable a scaling of the experiments to be representative of sand bed river in agreement with the Shields phase. (4) The constant sediment flux is found to be related to the total stream power which can explain the decorrelation with the width. Experiments are found not to be in maximum transport capacity and a bed load transport increases along the channel in the downstream direction.

- The response to a perturbation of a stable river was addressed through the case of experiments of a microscale straight channel being subject to lateral offset of its channel. This study was to give constraints for the dynamic of bank erosion and for the estimation of lateral slip-rate estimation in tectonics. (1) Experiments of a microscale river show that the erosion on the bank can develop a kinematic wave. (2) Using a mass conservation on the section of the channel, an equation for the bank profil can be derived and which can lead in futur work to modelisation of bank evolution. (3) A bed load transport relation related to the erosion front propagation is derived. (4) First order estimation of the time scale for a natural river to respond to an offset is done in the case of gravel bed river in Turkey. Observations shows that the river tend in both cases of a vertical and lateral offsets to erode the perturbation and return into a stable state.

Some interesting results were found concerning the dynamic of alluvial river and confirm that microscale rivers ($L \approx 1$ m) can be considered as good candidates to model natural streams. However several results were found that should be investigate in the futur. Within this work, sediment transport found to be highly related to the bank erosion processes. In the case of a widening straight channel, the bedload transport increases in the downstream direction from the input of sediment eroded from the banks. And in the case of a offset channel, bedload transport can be related to the geometry of the bank. An interesting problem that was partly approached in this work is the problem of characterizing the maximum bedload capacity. Experiments of the adjusting straight river show that at the begining of the run, the maximum capacity is reached in front. Experiments of offset denotes a signal in the output sediment flux. However, as it cannot be related precisely and quantitatively to bank erosion, some experiments should be done for that purpose. The offset should be applied to the channel at several position from the outlet to evaluate and catch the expected signal in the bedload transport.

Appendix A

The Sediment Digester

We present the physical model of the sediment digester of Gary Parker.

A.0.1 Hydraulics

Figure A.1 presents the geometry used in this modelisation. We consider three different regions in the channel that are the bed region of width w_b ($y \in [-y_b, y_b]$), the submerged bank region of total width w_s ($y \in [-y_s, -y_b] \cup [y_b, y_s]$) and the emerged bank region of total width w_e ($y \in [-y_e, -y_s] \cup [y_s, y_e]$). The coordinates are such that the transverse direction corresponds to the y coordinate and the altitude to the z coordinate; the x coordinate is pointing out the page such that the the coordinate system (xyz) is cartesian. The streamwise bed slope is therefore defined as

$$S = -\frac{\partial z_b}{\partial x}. \tag{A.1}$$

All other geometric parameters used in the following are shown on the Fig. A.1. Note that the free surface width w measured in our experiments corresponds here to $w = w_b + w_s$.

The flow is assumed to be steady, streamwise (1D) and uniform. If τ_b denotes the bed shear stress and τ_w the shear stress on the sidewall region, the conservation of momentum for the flow in the stream direction reads

$$\tau_b\, w_b + \tau_w \sqrt{4\, h^2 + w_s^2} = \frac{\rho g S}{2}(2\, h\, w_b + h\, w_s). \tag{A.2}$$

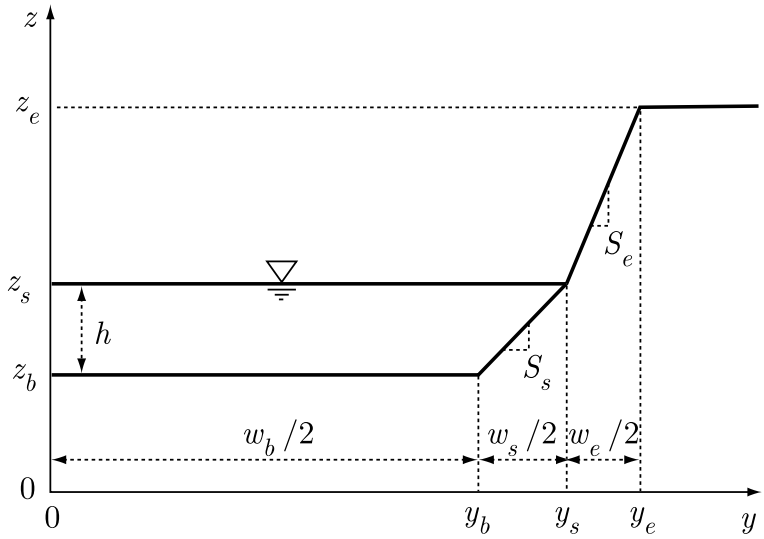

Figure A.1 – *Geometry of the half cross section.*

It is now assumed that the bank shear stress is proportional to the bed shear stress (Parker, 1978b),

$$\tau_w = \varphi \tau_b, \tag{A.3}$$

where φ is typically between 2/3 and 4/5 (Parker, 1978b). Under this relation is assumed that the critical shear stress for incipient motion on the bed and on the banks are the same (see Eq. (A.11)). This seems not to be the case in reality since the slope on the banks is higher than on the bed and thought incipient motion is easier on the banks. Nevertheless, considering a shear stress on the banks smaller than on the bed as in equation (A.3) allows for the possibility of a channel that does not erode its banks (because τ_w is below the theshold there) but that can maintain an equilibrium sediment transport rate on the bed region (because τ_b exeeds the threshold there). The mean flow velocity $\overline{U}$ is assumed to follow a Manning-Strickler relation:

$$\tau_b = \rho c \overline{U}^2, \tag{A.4}$$

where c is a friction coefficient[1] and $c^{-1/2} = \alpha_r (h/k_s)^{1/6}$ and $k_s = n_k d_{50}$. k_s is the roughness height, d_{50} is the median diameter of the sediments, α_r is a dimensionless coefficient

[1]Note that the friction coefficient c in Eq. (A.4) is an analog to the Chézy friction factor since the flow

here taken to be equal to 8.1 and n_k is a dimensionless parameter that is typically between 2 and 4 depending on the standard deviation of the grain size distribution. The water conservation is written in terms of water discharge Q and reads

$$Q = \overline{U} h \left(w_b + \frac{h}{S_s} \right). \tag{A.5}$$

Combinations of (A.2), (A.3), (A.4) and (A.5) leads to an expression for flow height h:

$$h = \left(\frac{k_s^{1/3} Q^2}{\alpha_r^2 \, w_b^2 \, g S} \right)^{3/10} \left(\frac{C_d}{C_n^3} \right)^{3/10}, \tag{A.6a}$$

with

$$C_d = 1 + 2\varphi \frac{\sqrt{1 + S_s^2}}{S_s} \frac{h}{w_b}, \tag{A.6b}$$

$$C_n = 1 + \frac{1}{S_s} \frac{h}{w_b}. \tag{A.6c}$$

The Shields number for the bed region

$$\tau_b^* = \tau_b / (\rho \mathscr{R} g d_{50}) \tag{A.7}$$

is then given as

$$\tau_b^* = \frac{hS}{\mathscr{R} d_{50}} \frac{C_n}{C_d} = \frac{S^{7/10}}{\mathscr{R} d_{50}} \left(\frac{k_s^{1/3} Q^2}{\alpha_r^2 w_b^2 g} \right)^{3/10} \frac{C_n}{C_d} \left(\frac{C_d}{C_n^3} \right)^{3/10}, \tag{A.8}$$

where $\mathscr{R} = (\rho_s - \rho)/\rho$ denotes the specific density of the sediments. The Shields number on the banks region is

$$\tau_w^* = \varphi \tau_b^*. \tag{A.9}$$

Equations (A.6), (A.8) and (A.9) indicate that as the width of the bed region increases, both the depth of the flow and the Shields stress are decreased.

is uniform.

A.0.2 Bedload transport

Some parametric laws are given for the bedload transport in function of the shear stress. Sediment transport can occur on the bed region (q_b) and on the sidewall region (q_w) and we consider for both of them, a streamwise component (in the x direction) and a transverse component (in the y direction):

$$\mathbf{q_b} = (q_{bx},\, q_{by}), \tag{A.10a}$$

$$\mathbf{q_w} = (q_{wx},\, q_{wy}), \tag{A.10b}$$

respectively for the bedload transport rate per unit width in the bed region and the sidewall region. The streamwise components for transport on the bed region q_{bx} and the banks region q_{wx} are approximations to the Einstein bedload transport and read

$$q_{bx} = \sqrt{\mathscr{R} g d_{50}}\, d_{50}\, \alpha_x (\tau_b^*)^{1.5} \left(1 - \frac{\tau_c^*}{\tau_b^*}\right)^{4.5}, \tag{A.11a}$$

$$q_{wx} = \sqrt{\mathscr{R} g d_{50}}\, d_{50}\, \alpha_x (\varphi \tau_b^*)^{1.5} \left(1 - \frac{\tau_c^*}{\varphi \tau_b^*}\right)^{4.5}, \tag{A.11b}$$

where $\alpha_x = 11.2$ and τ_c^* is the critical Shields stress (Parker, 1978b, 1979). It is assumed here that the critical stress for motion incipient on the bed region and the banks region is the same. The streamwise transport rates q_{bx} and q_{wx} are positive since they always occur downstream (in the x direction). Between Eqs. (A.8), (A.9) and (A.11), it can be seen again that an increase in the bed width is followed by a decrease in the shear stress and therefore in the bedload transport.

The transverse bedload transport per unit width in the bed region and in the bank region is approximated using the relations

$$\left(\frac{q_{by}}{q_{bx}}, \frac{q_{wy}}{q_{wx}}\right) = \left(\frac{\tau_{by}}{\tau_{bx}}, \frac{\tau_{wy}}{\tau_{wx}}\right) - \alpha_y \sqrt{\frac{\tau_c^*}{\tau_w^*}} \frac{\partial z}{\partial y}, \tag{A.12}$$

where τ_{bx}, τ_{wx} and τ_{by}, τ_{wy} are the streamwise and transverse components of the boundary shear stress in the bed region and the bank region; $\alpha_y = 2.65$ (Johannesson et Parker, 1989). This relation says that (1) in the abscence of a side slope, the bedload transport vector is parallel to that of the boundary shear stress and (2) in the presence of a side

slope, a component of bedload is directed down the slope. For the present analysis, the channel is assumed to be straight, so that τ_{by} and τ_{wy} can be approximated as vanishing. In the bed region, the transverse slope $\partial z/\partial x = 0$ and thus the transverse bedload can be assumed as vanishing

$$q_{by} = 0. \tag{A.13a}$$

In the sidewall region where $\partial z/\partial y = S_s$, the transverse bedload transport takes the form

$$q_{wy} = -q_{wx}\,\alpha_y \sqrt{\frac{\tau_c^*}{\varphi \tau_b^*}}\, S_s. \tag{A.13b}$$

Note that the transverse transport rate q_{wy} has the sign of $-S_s$ since $q_{wx} > 0$. It is therefore negative in the left bank region (since $S_s > 0$) and positive in the right bank region (where $S_s < 0$). This insures that sediments are transported from the wall region to the bed region.

A.0.3 Sediment continuity

In order to close the system, one need to consider now the sediment conservation on each part of the channel. The general 2D form of the Exner equation can be written as

$$(1-\phi)\frac{\partial z}{\partial t} = -\frac{\partial q_x}{\partial x} - \frac{\partial q_y}{\partial y}, \tag{A.14}$$

where ϕ is the bed porosity and $(q_x,\, q_y)$ are the streamwise and transverse sediment transport rates per unit width (equal to $(q_{bx},\, q_{by})$ or $(q_{wx},\, q_{wy})$ respectively in the bed region and the bank region). An integrated form of this relation is then derived for each part of the channel (bed region, submerged bank region and emerged bank region).

A.0.3.1 Sediment continuity for the bed region

Exner equation (A.14) is integrated over the bed region to yield

$$(1-\phi)\int_{-y_b}^{y_b} \frac{\partial z}{\partial t}\, dy = -\int_{-y_b}^{y_b} \frac{\partial q_x}{\partial x}\, dy - \int_{-y_b}^{y_b} \frac{\partial q_y}{\partial y}\, dy. \tag{A.15}$$

The first term in the above equation with the use of the Leibnitz rule and knowing that $z|_{y_b} = z|_{-y_b} = z_b$ and $2y_b = w_b$ (Fig. A.1) can be reduced to

$$(1-\phi)\int_{-y_b}^{y_b} \frac{\partial z}{\partial t}\, dy = (1-\phi) w_b \frac{\partial z_b}{\partial t}. \tag{A.16}$$

According to the Leibnitz rule and with $q_x|_{y_b} = q_x|_{-y_b} = q_{bx}$, the second term in Eq. (A.15) becomes

$$\int_{-y_b}^{y_b} \frac{\partial q_x}{\partial x}\, dy = w_b \frac{\partial q_{bx}}{\partial x}. \tag{A.17}$$

Integration of the last term in Eq. (A.15) gives

$$\int_{-y_b}^{y_b} \frac{\partial q_y}{\partial y}\, dy = q_y|_{y_b} - q_y|_{-y_b}, \tag{A.18}$$

where $q_y|_{y_b}$ and $q_y|_{-y_b}$ represent the transverse bedload in the bed region close respectively to the left and the right bank regions. By continuity with the wall regions, one have the conditions that $q_y|_{y_b} = -q_y|_{-y_b} = |q_{wy}|$ where the absolute value insures that the transverse transport from both bank regions to bed region always gives a positive contribution to the bed. Eq. (A.18) is reduced to

$$\int_{-y_b}^{y_b} \frac{\partial q_y}{\partial y}\, dy = -2|q_{wy}|. \tag{A.19}$$

The integrated sediment continuity for the bed reads

$$(1-\phi)\frac{\partial z_b}{\partial t} = -\frac{\partial q_{bx}}{\partial x} + 2\frac{|q_{wy}|}{w_b}. \tag{A.20}$$

A.0.3.2 Sediment continuity for the submerged sidewall region

Integration of the Exner equation (A.14) over the submerged bank region yields

$$(1-\phi)\int_{y_b}^{y_s} \frac{\partial z}{\partial t}\, dy = -\int_{y_b}^{y_s} \frac{\partial q_x}{\partial x}\, dy - \int_{y_b}^{y_s} \frac{\partial q_y}{\partial y}\, dy. \tag{A.21}$$

The same relation apply for the left and the right bank so that it is only considered once. Between y_b and y_s, bed elevation z obeys the relation $z = z_s - S_s(y_s - y)$ (Fig. A.1), so that (at fixed y)

$$\frac{\partial z}{\partial t} = \frac{\partial z_s}{\partial t} - S_s \frac{\partial y_s}{\partial t}. \tag{A.22}$$

Using this relation, the first term in Eq. (A.21) becomes

$$(1-\phi)\int_{y_b}^{y_s}\frac{\partial z}{\partial t}\,dy = (1-\phi)(y_s-y_b)\left(\frac{\partial z_s}{\partial t} - S_s\frac{\partial y_s}{\partial t}\right), \tag{A.23}$$

which can be reduced with the following geometrical relations, $z_s = z_b + h$, $y_s - y_b = h/S_s$ and $y_s = (w_s - w_b)/2$ to

$$(1-\phi)\int_{y_b}^{y_s}\frac{\partial z}{\partial t}\,dy = -(1-\phi)h\left(\frac{1}{2}\frac{\partial w_b}{\partial t} - \frac{1}{S_s}\frac{\partial z_b}{\partial t}\right). \tag{A.24}$$

According to the Leibnitz rule and with the conditions,

$$q_x = \begin{cases} q_{bx} & 0 < y < y_b, \\ q_{wx} & y_b < y < y_s, \\ 0 & y \geq y_s. \end{cases} \tag{A.25}$$

the second term in Eq. (A.21) reduces to

$$-\int_{y_b}^{y_s}\frac{\partial q_x}{\partial x}\,dy = -\frac{1}{S_s}\frac{\partial h q_{wx}}{\partial x} - \frac{1}{2}q_{bx}\frac{\partial w_b}{\partial x}. \tag{A.26}$$

Integration of the last term in Eq. (A.21) gives

$$-\int_{y_b}^{y_s}\frac{\partial q_y}{\partial y}\,dy = q_y|_{y_b} - q_y|_{y_s}. \tag{A.27}$$

$q_y|_{y_b}$ represents the transverse transport in the submerged region close to the bed and $q_y|_{y_b} = -|q_{wy}|$. $q_y|_{y_s}$ represents the transverse transport in the submerged region close to the emerged region. If $|q_{ey}|$ denotes the positive load from the emerged region, one have by continuity $-q_y|_{y_s} = |q_{ey}|$. Thus Eq. (A.27) becomes

$$-\int_{y_b}^{y_s}\frac{\partial q_y}{\partial y}\,dy = -|q_{wy}| + |q_{ey}| \tag{A.28}$$

The integrated sediment continuity for the submerged sidewall region finally reads

$$(1-\phi)h\left(\frac{1}{2}\frac{\partial w_b}{\partial t} - \frac{1}{S_s}\frac{\partial z_b}{\partial t}\right) = \frac{1}{S_s}\frac{\partial h q_{wx}}{\partial x} + \frac{1}{2}q_{bx}\frac{\partial w_b}{\partial x} + |q_{wy}| - |q_{ey}|. \tag{A.29}$$

A.0.3.3 Sediment continuity for the emerged sidewall region

Exner equation (A.14) is integrated over the emerged bank region to yield

$$(1-\phi)\int_{y_s}^{y_e}\frac{\partial z}{\partial t}\,dy = -\int_{y_s}^{y_e}\frac{\partial q_x}{\partial x}\,dy - \int_{y_s}^{y_e}\frac{\partial q_y}{\partial y}\,dy, \tag{A.30}$$

which applies for the left and the right banks. In the emerged bank region, the relation $z = z_e - S_e(y_e - y)$ holds (Fig. A.1) and its differenciation with respect to time gives

$$\frac{\partial z}{\partial t} = -S_e\frac{\partial y_s}{\partial t} = -S_e\frac{\partial}{\partial t}\left(\frac{w_b}{2} + \frac{h}{S_s} + \frac{z_e - z_s}{S_e}\right), \tag{A.31}$$

with the alluvial plain height z_e being constant and using simple geometrical relations. Using this relation, the first terms integrates as

$$(1-\phi)\int_{y_s}^{y_e}\frac{\partial z}{\partial t}\,dy = -(1-\phi)(z_e - z_s)\left[\frac{1}{2}\frac{\partial w_b}{\partial t} + \left(\frac{1}{S_s} - \frac{1}{S_e}\right)\frac{\partial h}{\partial t} - \frac{1}{S_e}\frac{\partial z_b}{\partial t}\right]. \tag{A.32}$$

Since no flow occurs in the emerged bank region, q_x can be assumed to vanish so that the second term in Eq. (A.30) can be dropped. The third term in Eq. (A.30) integrates as

$$-\int_{y_s}^{y_e}\frac{\partial q_y}{\partial y}\,dy = q_y|_{y_s} - q_y|_{y_e}. \tag{A.33}$$

Here, $q_y|_{y_s}$ represents the transverse transport in the emerged region towards the submerged region and is negative since erosion only can occur and one have $q_y|_{y_s} = -|q_{ey}|$. $q_y|_{y_e}$ is assumed to vanish in the absence of earthflow from the alluvial plain. Eq. (A.33) becomes

$$-\int_{y_s}^{y_e}\frac{\partial q_y}{\partial y}\,dy = -|q_{ey}|. \tag{A.34}$$

Finally, with Eqs. (A.32) and (A.34), the integrated sediment continuity for the emerged sidewall region reads

$$(1-\phi)(z_e - z_s)\left[\frac{1}{2}\frac{\partial w_b}{\partial t} + \left(\frac{1}{S_s} - \frac{1}{S_e}\right)\frac{\partial h}{\partial t} - \frac{1}{S_e}\frac{\partial z_b}{\partial t}\right] = |q_{ey}|. \tag{A.35}$$

The equations (A.20), (A.29) and (A.35) are the equation for the channel geometry since they relate the geometry variation to the bedload transport and therefore to the shear stress. For the moment, no hypothesis has been made concerning the streamwise variations of the geometry and of the bedload; they are allowed.

A.0.4 Width variation equation

Equations (A.20), (A.29) and (A.35) can be reduced to an equation for the width:

$$(1-\phi)\left[\frac{z_e-z_b}{2}-r(z_e-z_b-h)\left(\frac{1}{S_s}-\frac{1}{S_e}\right)\right]\frac{\partial w_b}{\partial t}-\frac{1}{2}q_{bx}\frac{w_b}{\partial x}= \\ -\left[\frac{z_e-z_b}{S_e}+\left(\frac{1}{S_s}-\frac{1}{S_e}\right)h\right]\frac{\partial q_{bx}}{\partial x}+\frac{1}{S_s}\frac{\partial h q_{wx}}{\partial s} \\ +\left[1+2\frac{z_e-z_b}{w_s S_e}+\left(\frac{1}{S_s}-\frac{1}{S_e}\right)\right]|q_{wy}|, \quad \text{(A.36)}$$

in which r comes from the evaluation of $\partial h/\partial t = -r\partial w_b/\partial t$ with equation (A.6):

$$r=\frac{\frac{3}{5}+\frac{3}{10}\frac{C_n-1}{C_n}-\frac{9}{10}\frac{C_d-1}{C_d}}{1-\frac{3}{10}\frac{C_n-1}{C_n}-\frac{9}{10}\frac{C_d-1}{C_d}}\frac{h}{w_b} \quad \text{(A.37)}$$

The width variation equation (A.36) is therefore a non-linear equation.

Bibliography

Ackers, P. (1964). Experiments on small streams in alluvium. *J. Hydrol. Div. 90*, 1–37.

Ahnert, F. (1998). *Introduction to Geomorphology.* Arnold, London.

Andrews, E. D. (1984). Bed-material entrainment and hydraulic geometry of gravel-bed rivers in Colorado. *Geol. Soc. Am. Bull. 95*, 371–378.

Armstrong, L. et F. Métivier (2003a). Independence of sediment flux and width evolution through time in a microscale straight river channel. Part 1. scaling of microscale experiments and regime equations. *in prep.*.

Armstrong, L. et F. Métivier (2003b). Independence of sediment flux and width evolution through time in a microscale straight river channel. Part 2. Implications on the conservation of mass and stream section evolution. *in prep.*.

Avouac, J.-P. (1993). Analysis of scarp profiles: evaluation of errors in morphologic dating. *J. Geophys. Res. 98*, 6745–6754.

Avouac, J.-P., P. Tapponnier, M. Bai, H. You, et G. Wang (1993). Active thrusting and folding along the northern Tien Shan and late Cenozoic rotation of the Tarim relative to Dzungaria and Kazakhstan. *J. Geophys. Res. 98*, 6755–6804.

Bagnold, R. (1973). The nature of saltation and of bed load transport in water. *Proc. Roy. Soc. Ser. A 332*, 473–504.

Bagnold, R. A. (1977). Bed load transport by natural rivers. *Water. Resour. Res. 13*, 303–312.

Chang, H. H. (1988). *Fluvial processes in river engineering.* Kreiger Publishing Company.

Chow, V. T. (1959). *Open-channel hydraulics.* Mc Graw-Hill.

Dade, W. B. et P. F. Friend (1998). Grain-size, sediment-transport regime, and channel slope in alluvial rivers. *J. Geol. 106*, 661–675.

Dietrich, W. E. et J. D. Gallinatti (1991). Fluvial geomorphology. In O. Slaymaker (Ed.), *Fied experiments and measurement programs in geomorphology.* Balkema, Rotterdam.

Diplas, P. (1990). Characteristics of self-formed straight channels. *J. Hydr. Engrg. 116*, 707–728.

Gaudemer, Y., P. Tapponnier, B. Meyer, G. Pelzer, S. Guo, Z. Chen, H. Dai, et I. Cifuentes (1995). Partitioning of crustal slip between linked active faults in the eastern Qilian Shan, and evidence for a major seismic gap, the 'Tianzhu gap', on the wester Haiyuan fault, Gansu (China). *J. Int. 120*, 599–645.

Hack, J. T. (1960). Interpretation of erosion topography in humid temperate regions. *aam 258A*, 80–97.

Hinze, J. O. (1975). *Turbulence.* McGraw-Hill, New York.

Ikeda, S. (1981). Self-formed straight channels in sandy beds. *J. Hydrol. Div. 107*, 389–406.

Ikeda, S., G. Parker, et Y. Kimura (1988). Stable width and depth of straight gravel rivers with heterogeneous bed materials. *Water. Resour. Res. 24*, 713–722.

Johannesson, H. et G. Parker (1989). Linear theory of river meanders. In S. Ikeda et G. Parker (Eds.), *River meandering* (AGU Water Ressources Monograph ed.), Volume 12, pp. 181–214.

Julien, P. Y. (1994). *Erosion and sedimentation.* Cambridge University Press.

Kovacs, A. et G. Parker (1994). A new vectorial bedload formulation and its application to the time evolution of straight river channels. *J. Fluid Mech. 267*, 153–183.

Lacey, G. (1930). Stable channels in alluvium. *Proc. ICE 229*, 259–270.

Langbein, W. B. (1964). Geometry of stable channels. *J. Hydr. Div. 90*, 301–312.

Lasserre, C., P.-H. Morel, Y. Gaudemer, P. Tapponnier, F. J. Ryerson, G. C. P. King, F. Métivier, M. Kasser, M. Kashgarian, L. Baichi, L. Taiya, et Y. Daoyang (1999). Postglacial left slip rate and past occurence of $M \geq 8$ earthquakes on the western Haiyuan fault, Gansu, China. *J. Geophys. Res. 104*, 17633–17651.

Lavé, J. et J. P. Avouac (2000). Active folding of fluival terraces across the Siwaliks Hills, Himalayas of central Nepal. *J. Geophys. Res. 105*, 5735–5770.

Leopold, L. B. et T. J. Maddock (1953). The hydrolic geometry of stream channels and some physiographic implications. *U. S. Geol. Survey. Professional Paper 252.*

Mackin, J. H. (1948). Concept of the graded river. *Geol. Soc. Am. Bull. 59*, 463–512.

Macky, G. H. (1999). Large flume experiments on the stable straight gravel bed channel. *Water. Resour. Res. 35*, 2601–2603.

Merritts, D., K. R. Vincent, et E. E. Wohl (1994). Long river profiles, tectonism, and eustasy: a guide to interpreting fluvial terraces. *J. Geophys. Res. 99*, 14031–13050.

Métivier, F. et P. Meunier (2003). Input and output mass flux correlations in an experimental braided stream. Implications on the dynamics of bed load transport. *J. Hydrol. 271*, 22–38.

Meunier, P. et F. Métivier (2000). Permanence des flux de masse d'une rivière en tresse expérimentale. *C. R. Acad. Sci., Earth and Planetary Sciences 331*, 105–110.

Parker, G. (1978a). Self-formed straight rivers with equilibrium banks and mobile bed. Part 1. The sand-silt river. *J. Fluid Mech. 89*, 109–125.

Parker, G. (1978b). Self-formed straight rivers with equilibrium banks and mobile bed. Part 2. The gravel river. *J. Fluid Mech. 89*, 127–146.

Parker, G. (1979). Hydraulic geometry of active gravel rivers. *J. Hydrol. Div. 105*, 1185–1201.

Schumm, S. A. et R. W. Lichty (1965). Time, space and causality in geomorphology. *Am. Jour. Sci. 263*, 110–119.

Schumm, S. A., M. P. Mosley, et W. E. Weaver (1987). *Experimental fluvial geomorphology.* John Wiley & Sons.

Shields, A. (1936). Anwendung der aenlichkeitsmechanik und der turbulenzforschung auf die geschiebebewegung. *Mitt. Preuss. Versuchsanst. Wasserbau Schiffbau.* translated to English by W. P. Ott and J. C. van Uchelen, CalTech, Pasadena, CA.

Shvidchenko, A. B. et G. Pender (2000). Flume study of the effect of relative depth on the incipient motion of coarse uniform sediments. *Water. Resour. Res. 36*, 619–628.

Van der Woerd, J., F. J. Ryerson, P. Tapponnier, Y. Gaudemer, R. Finkel, A. S. Mériaux, M. Caffee, G. Zhao, et Q. He (1998). Holocene left-slipe rate determined by cosmogenic surface dating on the Xidatan segment of the Kunlun fault, (Qinghai, China. *Geology 26*, 695–698.

Wallis (1969). *One dimensional two-phase flow.* Mc Graw Hill.

Yalin, M. S. (1992). *River mechanics.* Pergamon Press.

Yalin, M. S. et A. M. Ferreira da Silva (2001). *Fluvial processes.* International Association of Hydraulic Engineering and Research, Delft, The Netherlands.

Appendix B

Variables and physical parameters

Table B.1 – *Variables and physical parameters.*

Symbol	Definition	Dimension
ϕ	Sediment porosity	–
μ	Dynamic viscosity of water	M L^{-1} T^{-1}
ρ	Density of water	M L^{-3}
ρ_s	Density of sediments	M L^{-3}
$\mathscr{R}$	Submerged specific density ($= \rho_s/\rho - 1$)	–
τ	Relaxation time of widenning	T
τ_b	Bed shear stress	M L^{-1} T^{-2}
τ_w	Shear stress on bank region	M L^{-1} T^{-2}
c	Chézy friction factor coefficient	–
d_{50}	Median diameter of sediments	L
g	Acceleration of gravity	L T^{-2}
h	Flow height	L
h_b	Bank height	L
L	Flume length	L
m	Cumulated mass	M

Table B.1 – *(continued)*

Symbol	Definition	Dimension
n	Manning roughness coefficient	$L^{-1/3}$ T
q_b	Sediment flux per unit width on the bed region	L^2 T^{-1}
q_w	Sediment flux per unit width on the bank region	L^2 T^{-1}
q_{bx}	Streamwise component of q_b	L^2 T^{-1}
q_{by}	Transverse component of q_b	L^2 T^{-1}
q_{wx}	Streamwise component of q_w	L^2 T^{-1}
q_{wy}	Transverse component of q_w	L^2 T^{-1}
Q_b	Sediment flux on the bed region	L^3 T^{-1}
Q_w	Sediment flux on the bank region	L^3 T^{-1}
Q	Water discharge	L^3 T^{-1}
ρQ	Water discharge	M T^{-1}
Q_s	Output flux of sediments ($= \rho_s(Q_b + Q_w)$)	M T^{-1}
Ro	Rouse number ($= v_s/(\kappa u_*)$)	–
S	Slope ($= -\partial z/\partial x$)	–
S_s	Slope of the submerged bank region	–
S_e	Slope of the emerged bank region	–
Sh	Shields number ($= \rho u_*^2/[(\rho_s - \rho)gd_{50}]$)	–
u_*	Shear velocity	L T^{-1}
U	Velocity of surface flow	L T^{-1}
$\overline{U}$	Reach averaged velocity	L T^{-1}
v_s	Stokes fall velocity	L T^{-1}
w	Free surface width ($= w_b + w_s \sim w_b$)	L
w_0	Initial channel width	L
w_b	Width of channel bed region	L
w_s	Width of submerged bank region	L

Table B.1 – *(continued)*

Symbol	Definition	Dimension
w_e	Width of emerged bank region	L
W_e	Equilibrium width	L
x, y, z	Longitudinal, transverse and vertical directions	L
z_0	Initial bed elevation	L
z_b	Bed elevation	L
z_e	Alluvial plain elevation	L
z_s	Water surface elevation	L

Bibliography

Ackers, P. (1964). Experiments on small streams in alluvium. *J. Hydrol. Div. 90*, 1–37.

Ahnert, F. (1998). *Introduction to Geomorphology.* Arnold, London.

Andrews, E. D. (1984). Bed-material entrainment and hydraulic geometry of gravel-bed rivers in Colorado. *Geol. Soc. Am. Bull. 95*, 371–378.

Armstrong, L. et F. Métivier (2003a). Independence of sediment flux and width evolution through time in a microscale straight river channel. Part 1. scaling of microscale experiments and regime equations. *in prep.*.

Armstrong, L. et F. Métivier (2003b). Independence of sediment flux and width evolution through time in a microscale straight river channel. Part 2. Implications on the conservation of mass and stream section evolution. *in prep.*.

Avouac, J.-P. (1993). Analysis of scarp profiles: evaluation of errors in morphologic dating. *J. Geophys. Res. 98*, 6745–6754.

Avouac, J.-P., P. Tapponnier, M. Bai, H. You, et G. Wang (1993). Active thrusting and folding along the northern Tien Shan and late Cenozoic rotation of the Tarim relative to Dzungaria and Kazakhstan. *J. Geophys. Res. 98*, 6755–6804.

Bagnold, R. (1973). The nature of saltation and of bed load transport in water. *Proc. Roy. Soc. Ser. A 332*, 473–504.

Bagnold, R. A. (1977). Bed load transport by natural rivers. *Water. Resour. Res. 13*, 303–312.

Chang, H. H. (1988). *Fluvial processes in river engineering.* Kreiger Publishing Company.

Chow, V. T. (1959). *Open-channel hydraulics.* Mc Graw-Hill.

Dade, W. B. et P. F. Friend (1998). Grain-size, sediment-transport regime, and channel slope in alluvial rivers. *J. Geol. 106*, 661–675.

Dietrich, W. E. et J. D. Gallinatti (1991). Fluvial geomorphology. In O. Slaymaker (Ed.), *Fied experiments and measurement programs in geomorphology.* Balkema, Rotterdam.

Diplas, P. (1990). Characteristics of self-formed straight channels. *J. Hydr. Engrg. 116*, 707–728.

Gaudemer, Y., P. Tapponnier, B. Meyer, G. Pelzer, S. Guo, Z. Chen, H. Dai, et I. Cifuentes (1995). Partitioning of crustal slip between linked active faults in the eastern Qilian Shan, and evidence for a major seismic gap, the 'Tianzhu gap', on the wester Haiyuan fault, Gansu (China). *J. Int. 120*, 599–645.

Hack, J. T. (1960). Interpretation of erosion topography in humid temperate regions. *aam 258A*, 80–97.

Hinze, J. O. (1975). *Turbulence.* McGraw-Hill, New York.

Ikeda, S. (1981). Self-formed straight channels in sandy beds. *J. Hydrol. Div. 107*, 389–406.

Ikeda, S., G. Parker, et Y. Kimura (1988). Stable width and depth of straight gravel rivers with heterogeneous bed materials. *Water. Resour. Res. 24*, 713–722.

Johannesson, H. et G. Parker (1989). Linear theory of river meanders. In S. Ikeda et G. Parker (Eds.), *River meandering* (AGU Water Ressources Monograph ed.), Volume 12, pp. 181–214.

Julien, P. Y. (1994). *Erosion and sedimentation.* Cambridge University Press.

Kovacs, A. et G. Parker (1994). A new vectorial bedload formulation and its application to the time evolution of straight river channels. *J. Fluid Mech. 267*, 153–183.

Lacey, G. (1930). Stable channels in alluvium. *Proc. ICE 229*, 259–270.

Langbein, W. B. (1964). Geometry of stable channels. *J. Hydr. Div. 90*, 301–312.

Lasserre, C., P.-H. Morel, Y. Gaudemer, P. Tapponnier, F. J. Ryerson, G. C. P. King, F. Métivier, M. Kasser, M. Kashgarian, L. Baichi, L. Taiya, et Y. Daoyang (1999). Postglacial left slip rate and past occurence of $M \geq 8$ earthquakes on the western Haiyuan fault, Gansu, China. *J. Geophys. Res. 104*, 17633–17651.

Lavé, J. et J. P. Avouac (2000). Active folding of fluival terraces across the Siwaliks Hills, Himalayas of central Nepal. *J. Geophys. Res. 105*, 5735–5770.

Leopold, L. B. et T. J. Maddock (1953). The hydrolic geometry of stream channels and some physiographic implications. *U. S. Geol. Survey. Professional Paper 252.*

Mackin, J. H. (1948). Concept of the graded river. *Geol. Soc. Am. Bull. 59*, 463–512.

Macky, G. H. (1999). Large flume experiments on the stable straight gravel bed channel. *Water. Resour. Res. 35*, 2601–2603.

Merritts, D., K. R. Vincent, et E. E. Wohl (1994). Long river profiles, tectonism, and eustasy: a guide to interpreting fluvial terraces. *J. Geophys. Res. 99*, 14031–13050.

Métivier, F. et P. Meunier (2003). Input and output mass flux correlations in an experimental braided stream. Implications on the dynamics of bed load transport. *J. Hydrol. 271*, 22–38.

Meunier, P. et F. Métivier (2000). Permanence des flux de masse d'une rivière en tresse expérimentale. *C. R. Acad. Sci., Earth and Planetary Sciences 331*, 105–110.

Parker, G. (1978a). Self-formed straight rivers with equilibrium banks and mobile bed. Part 1. The sand-silt river. *J. Fluid Mech. 89*, 109–125.

Parker, G. (1978b). Self-formed straight rivers with equilibrium banks and mobile bed. Part 2. The gravel river. *J. Fluid Mech. 89*, 127–146.

Parker, G. (1979). Hydraulic geometry of active gravel rivers. *J. Hydrol. Div. 105*, 1185–1201.

Schumm, S. A. et R. W. Lichty (1965). Time, space and causality in geomorphology. *Am. Jour. Sci. 263*, 110–119.

Schumm, S. A., M. P. Mosley, et W. E. Weaver (1987). *Experimental fluvial geomorphology.* John Wiley & Sons.

Shields, A. (1936). Anwendung der aenlichkeitsmechanik und der turbulenzforschung auf die geschiebebewegung. *Mitt. Preuss. Versuchsanst. Wasserbau Schiffbau.* translated to English by W. P. Ott and J. C. van Uchelen, CalTech, Pasadena, CA.

Shvidchenko, A. B. et G. Pender (2000). Flume study of the effect of relative depth on the incipient motion of coarse uniform sediments. *Water. Resour. Res. 36*, 619–628.

Van der Woerd, J., F. J. Ryerson, P. Tapponnier, Y. Gaudemer, R. Finkel, A. S. Mériaux, M. Caffee, G. Zhao, et Q. He (1998). Holocene left-slipe rate determined by cosmogenic surface dating on the Xidatan segment of the Kunlun fault, (Qinghai, China. *Geology 26*, 695–698.

Wallis (1969). *One dimensional two-phase flow.* Mc Graw Hill.

Yalin, M. S. (1992). *River mechanics.* Pergamon Press.

Yalin, M. S. et A. M. Ferreira da Silva (2001). *Fluvial processes.* International Association of Hydraulic Engineering and Research, Delft, The Netherlands.